KU LEUVEN

FACULTEIT INGENIEURSWETENSCHAPPEN

Advanced Techniques for Robust Dynamic Optimization of Chemical Reactors

Lorenzo Cabianca
Matricola n. 783577

POLITECNICO DI MILANO

Sucola di Ingegneria Industriale e dell'Informazione

Corso di Laurea Magistrale in Ingegneria Chimica

Relatore:
Prof. Dr. Ing. Flavio Manenti

Correlatori:
Prof. Dr. Ir. Jan Van Impe
Prof. Dr. Ir. Filip Logist

Mentori:
Ing. Mattia Vallerio
Ir. Dries Telen

Anno Accademico 2013 – 2014

KU LEUVEN

FACULTEIT INGENIEURSWETENSCHAPPEN

POLITECNICO MILANO

Advanced Techniques for Robust Dynamic Optimization of Chemical Reactors

Lorenzo Cabianca

Thesis submitted for the degree of
Master of Science in
Chemical Engineering, option
Chemical and biochemical process
engineering

Thesis supervisors:

Prof. Dr. Ir. Jan Van Impe
Prof. Dr. Ir. Filip Logist
Prof. Dr. Ing. Flavio Manenti

Assessors:

Prof. Dr. Ir. Peter Van Puyvelde
Prof. Dr. Ing. Sauro Pierucci

Mentors:

Ing. Mattia Vallerio
Ir. Dries Telen

Academic year 2013 – 2014

Preface

Finally, as all the adventures a man undertakes, this one has also come to an end. But more than for having reached the end, I am happy for everything that such an adventure has offered me. I went through many emotions, from happiness and satisfaction to sadness and demoralisation, being put to the test several times, most of them by myself and by my ambition, and I learnt to face unforeseen and undeserved defeats. I worked as never before but I was able to, at least partially, satisfy my deep curiosity. I met many people in my same situation and I am glad I could spend some of my time with them, establishing long-lasting relationships. There are then many people I would like to thank for having reached the end of this adventure.

Thank you Marta, for being there to celebrate my successes with me, but also to support and sustain me in all the dire situations I went through. Thank you for being always at my side in these years, even when we were both wishing not to be so far apart. Lastly, thank you for the real and tangible love you offer me everyday.

I also would like to thank my mentors and promoters, who helped me during these months of hard work, and other people of the CIT department who were ready to give me their assistance when needed. Thank you Mattia for being so willing to offer me your hand every time I was bound to fall and for being such an open person also outside the office hours. Thank you Dries for your kindness and your capability of always making people feel at ease. Thank you Prof. Filip Logist for your professional enthusiasm concerning our research and Prof. Jan Van Impe for having allowed me to work on the topic I desired. Thank you Prof. Flavio Manenti for your willingness to support me in this thesis at any time, even from Milan. Thanks also to those who shared their office with me in these months, Joost and Dominique, the latter also for his support with Pomodoro. Thanks also to the head of the CIT department, Prof. Peter Van Puyvelde, for being so kind in welcoming me in KULeuven and so willing to help me with all the international exchange related problems.

However, I should not forget the support I got from people I already knew before leaving. Thus, I would like to thank my family for its continuous support. Thanks to my father Luciano and my mother Paola for having always been ready to listen to my doubts and to advise me in the hard choices I had to take. Thank you Leonardo for your immeasurable strength and for being always willing to ask or give advice to me, irrespectively of the physical distance. I am really glad you could make it to my proclamation. Thanks also to the rest of my family, to my grandparents, aunts,

uncles and cousins, because in our meetings, despite their rarity, I always feel at home.

A special thanks should also go to my good old friends. Thank you Michele for being such a good friend when drinking and playing, but also when a deep reflection is needed. Thank you Dario for all the support you gave me at the beginning of this thesis and for being a good friend I can always count on. Thank you Elena, Francesco, Giacomo, Giovanni and Matteo. Although we only meet few times a year, those are always good moments that I look for. Thanks also to my friends Alberto, Cristina, Federica, Laura, Luca, Marco, Michelangelo, Valentina for the good times we spend together. Thanks to my staff colleagues Carlo, Giulio, Marianna, Giulia, Francesca, Francesco for having shared so many thoughts and unforgettable adventures with me. Thank you to the rest of my Scout community Alberto, Andrea, Anna, Antonella, Camilla, Camilla, Federica, Francesca, Guelfo, Marco, Matteo, Michele, Mimmo, Sergio, Tommaso, Valeria for having been part of my life outside the University. Thank you to my Milanese friends Andrea, Bruno, Edoardo, Giovanna, Marco, Mattia, Paola, Rafaella, Stefano, Stefano for all the days we spent smiling in Politecnico and for all the exams we faced together.

There are many more people I would like to thank. Old friends, as Prof. Roberto Masiero, my high school class-mates and my Scout companions, as well as new ones, who I only met in Leuven. That will take too much time, space and effort, but do not worry, I did not forget you.

Thanks to all of you again, because, although in different moments, you have all shared a part of my University adventure. However, now that this is over I am looking forward to set out for a new challenging one. I do not know what the future has in store for me, but I really hope that many of you could still share with me even just a fraction of this new journey.

Lorenzo Cabianca

Prefazione

Come tutte le avventure che un uomo intraprende, anche questa è giunta alla sua fine. Ma più che per l'aver raggiunto la fine, sono felice per tutto ciò che quest'avventura ha avuto da offrirmi. Ho provato molte emozioni, da felicità e soddisfazione a tristezza e demoralizzazione, essendo stato messo alla prova molte volte, la maggior parte delle quali da me stesso e dalla mia ambizione, e ho imparato ad affrontare sconfitte impreviste e immeritate. Ho lavorato come non mai ma sono stato in grado, almeno in parte, di soddisfare la mia sterminata curiosità. Ho incontrato molte persone nella mia stessa situazione e sono davvero contento di aver potuto spendere un po' del mio tempo con loro, creando relazioni durevoli e profonde. Ci sono quindi molte persone che desidero ringraziare per essere riuscito a terminare questa avventura.

Grazie Marta per esserci sempre stata per celebrare i miei successi con me, ma anche per sostenermi in tutti i momenti bui che ho attraversato. Grazie per essere sempre stata al mio fianco questi anni, anche quando entrambi desideravamo non essere così lontani. Grazie, infine, per l'amore concreto ed autentico che mi doni ogni giorno.

Desidero anche ringraziare i miei mentori e relatori, che mi hanno aiutato in questi mesi di duro lavoro, e altre persone del dipartimento di ingegneria chimica (CIT) della KULeuven, sempre pronte ad assistermi quando ne avessi avuto bisogno. Grazie Mattia per essere stato così disponibile a tendermi la mano ogniqualvolta stessi per cadere e per essere una persona così disponibile e aperta anche al di fuori dell'orario di lavoro. Grazie Dries, per la tua gentilezza e la tua capacità di mettere sempre chiunque a suo agio. Grazie Prof. Filip Logist per il suo entusiasmo professionale per la nostra ricerca e grazie Prof. Jan Van Impe per avermi permesso di lavorare sul tema che desideravo. Grazie Prof. Falvio Manenti per la sua disponibilità a supportarmi in questa tesi in ogni momento, anche da Milano. Ringrazio anche coloro che hanno condiviso il loro ufficio con me in questi mesi, Joost e Dominique, quest'ultimo anche per la sua assistenza con Pomodoro. Grazie anche al Prof. Peter Van Puyvelde, per avermi così gentilmente accolto nella KULeuven e per essere sempre stato disposto ad aiutarmi con con tutti i problemi relativi allo scambio internazionale.

Non posso però dimenticare il supporto ricevuto da tutte le persone che conoscevo prima di partire. Per questa ragione, vorrei ringraziare la mia famiglia, per il suo supporto continuo. Grazie a mio papà Luciano e a mia mamma Paola per essere sempre stati pronti ad ascoltare i miei dubbi e consigliami nelle scelte difficili che ho

dovuto fare. Grazie Leonardo per la tua forza incommensurabile e per essere sempre disponibile a chiedere o dare consigli, indipendentemente dalla nostra distanza fisica. Sono davvero felice che tu sia riuscito ad esserci alla mia proclamazione. Grazie anche a tutto il resto della mia famiglia, ai miei nonni, zie, zii e cugini perché durante i nostri incontri, anche se rari, mi sento sempre a casa.

Un grazie speciale anche ai miei vecchi amici. Grazie Michele, per essere un così buon amico, quando si gioca o si beve, ma anche quando c'è bisogno di fare riflessioni importanti. Grazie Dario per l'aiuto che mi hai dato all'inizio di questa tesi e per essere un amico su cui posso sempre contare. Grazie Elena, Francesco, Giacomo, Giovanni e Matteo. Anche se riusciamo a vederci poche volte all'anno, sono sempre momenti che apprezzo e che cerco. Grazie anche ai miei amici Alberto, Cristina, Federica, Laura, Luca, Marco, Michelangelo, Valentina per tutti i bei momenti che passiamo insieme. Grazie alle miei compagni di staff Carlo, Giulio, Marianna, Giulia, Francesca, Francesco per aver condiviso con me così tante idee e avventure indimenticabili. Grazie a tutto il resto della mia Comunità Capi Alberto, Andrea, Anna, Antonella, Camilla, Camilla, Federica, Francesca, Guelfo, Marco, Matteo, Michele, Mimmo, Sergio, Tommaso, Valeria per essere stati parte della mia vita extra-universitaria. Grazie ai miei amici milanesi Andrea, Bruno, Edoardo, Giovanna, Marco, Mattia, Paola, Rafaella, Stefano, Stefano per tutti i giorni passati sorridendo al Politecnico e per tutti gli esami che abbiamo affrontato insieme.

Ci sono molte altre persone che vorrei ringraziare. Vecchi amici, come il Prof. Roberto Masiero, i miei compagni del liceo e i miei compagni Scout, ma anche nuovi amici, che ho incontrato a Leuven. Questo prenderebbe parecchio tempo, spazio ed energie, ma non preoccupatevi, non vi ho dimenticato.

Grazie a tutti voi ancora perché, anche se in momenti diversi, avete tutti condiviso con me una parte della mia avventura universitaria. Ma ora che questa avventura è finita, sono già pronto a partire per una nuova. Non so cosa il futuro abbia in serbo per me, ma spero davvero che molti di voi possano condividere con me anche solo una frazione di questo nuovo viaggio.

Lorenzo Cabianca

Contents

Abstract

This thesis will focus on the application of optimal control theory to (bio-)chemical processes, where it can be applied to shift towards more sustainable production routes. It should be stressed, however, that the solution of highly non-linear systems, as those involved in (bio-)chemical processes, is not always easy to obtain and that it can lead to computational problems.

Two variations of optimal control will also be analised, namely robust optimal control and multi-objective optimal control, which deal respectively with uncertain parameters and multiple objectives. These two features can be combined in a robust multi-objective optimal control problem, which will also be investigated.

Two mathematical formulations to solve robust optimal control problems, the linear and sigma points approximations, will be exploited for the solution of different case studies for a number of uncertain parameters varying from one to four. The obtained results are compared and the sigma points will prove itself to be more effective than the linear approximation when dealing with highly non-linear systems. Generally, the sigma points approximation will also require lower computational time. The application of such approximations introduces an additional safety margin to account for uncertainties. Nevertheless, a loss in terms of performances is to be expected for both approaches.

The multi-objective optimisation of a Siemens reactor will be faced. The results will present a clear trade-off between the production and the energy consumption and multiple optimal solutions will be found. This last problem is also solved when two uncertain parameters are present in the model equations. Despite the higher complexity of the system treated, and the high amount of solutions demanded, the sigma points will prove once more its efficiency in terms of computational time.

All the results shown suggest that optimal control should be regarded at as an interesting field for additional research in the frame-works of sustainable development and sustainable production models for the (bio-)chemical industry.

Estratto

Sebbene la teoria del controllo ottimale e dell'ottimizzazione dinamica siano stati studiati da secoli, oggigiorno stanno acquisendo interesse crescente anche in applicazioni industriali. In particolare, questa tesi si focalizzerà sulla loro applicazione in processi (bio)chimici, dove possono essere un ottimo strumento per procedere verso modelli di produzione più sostenibili. Sono infatti strumenti per operare diversi processi al più elevato livello di efficienza. È comunque importante sottolineare che ottenere la soluzione di problemi che presentano equazioni ad alto grado di non linearità, quali i sistemi coinvolti in applicazioni (bio)chimiche, non è sempre facile, con il rischio concreto di incorrere in problemi di calcolo.

In questa tesi, la teoria del controllo ottimale verrà analizzata considerando due variazioni: controllo ottimale robusto e controllo ottimale multiobiettivo. La prima delle due variazioni permette la soluzione di problemi di ottimizzazione anche in presenza di parametri incerti nelle equazioni del modello. Spesso infatti, nelle equazioni che descrivono i sistemi considerati, ci sono parametri che non possono essere identificati correttamente o che sono stimati con un certo grado di incertezza. Il controllo ottimale robusto permette di ottenere una soluzione ottimale nonostante questa difficoltà, grazie all'introduzione di un margine di sicurezza aggiuntivo, a costo di una perdita di prestazioni del sistema.

La seconda variazione, invece, permette di considerare più di una singola funzione obiettivo nel problema di ottimizzazione. Un chiaro esempio potrebbe essere il desiderio di massimizzare la produzione ed allo stesso tempo minimizzare i consumi energetici. In aggiunta, queste due caratteristiche possono essere combinate in un problema di controllo ottimale multiobiettivo e robusto, il quale verrà a sua volta studiato in questa tesi.

Due formulazioni matematiche per la soluzione di problemi di controllo ottimale con parametri incerti verranno utilizzate per la soluzione di due diversi esempi con un numero di parametri incerti compreso tra uno e quattro. I due approcci utilizzati possono essere definiti approssimazione lineare e approssimazione sigma points. I risultati ottenuti con i due approcci saranno poi confrontati e il metodo sigma points si dimosterà più efficace dell'approssimazione lineare, quando il problema coinvolge equazioni altamente non lineari. Verrà anche dimostrato che il metodo sigma points richiede meno tempo per la risoluzione dei casi analizzati.

Successivamente verrà affrontata l'ottimizzazione multiobiettivo di un reattore Siemens per la produzione di silicio policristallino. I risultati ottenuti, mostreranno un chiaro compromesso tra la produzione e il consumo energetico, portando a diverse soluzioni ottimali. Sebbene matematicalmente equivalenti, queste soluzioni presenteranno diversi valori per le funzioni obiettivo. In casi reali, il decision-maker è dunque chiamato a scegliere una di queste soluzioni equivalenti ed a metterla in pratica.

Infine, due parametri verranno considerati come incerti nell'ottimizzazione multiobiettivo del reattore Siemens. Il metodo sigma points verrà utilizzato, e le conseguenze sulle soluzioni ottimali precedentemente ottenute verranno discusse. Nonostante il caso trattato sia più complesso dei precedenti, il metodo sigma points dimostrerà nuovamente la sua efficienza in termini di tempo di calcolo, necessitando di solamente un'ora per la soluzione di un problema di controllo ottimale multiobiettivo e robusto, che modella il comportamento del reattore per tre giorni.

Attraverso tutti i casi teorici e pratici trattati, il controllo ottimale si è dimostrato altamente efficace nell'ottimizzazione di reattori (bio)chimici, anche se le sue applicazioni non si limitano a questo unico campo. Inoltre, l'utilizzo di algoritmi numerici efficienti e formulazioni matematiche adeguate porta ad ottenere risultati in tempi rapidi, anche quando sono coinvolti sistemi di equazioni altamente non lineari. Tutti questi risultati suggeriscono che la teoria del controllo ottimale può essere ritenuta un campo di ricerca interessante nell'ambito dello sviluppo sostenibile e di modelli di produzione sostenibili per l'industria (bio)chimica.

List of Figures

List of Tables

List of Abbreviations

ACADO	Automatic Control And Dynamic Optimization
BVP	Boundary Value Problem
CasADi	Computer algebra system Automatic Differentiation
CHIM	Convex Hull of Individual Minima
CVD	Chemical Vapour Deposition
ENNC	Enhanced Normalised Normal Constraint
HJB	Hamilton-Jacobi-Bellman
IPOPT	Interior Point OPTimizer
KKT	Karush-Kuhn-Tucker
LQP	Linear-Quadratic Programming
MOOC	Multi-Objective Optimal Control
MOOCP	Multi-Objective Optimal Control Problem
NBI	Normal Boundary Intersection
NLP	Non-Linear Programming
NNC	Normalised Normal Constraint
OC	Optimal Control
OCP	Optimal Control Problem
ODE	Ordinary Differential Equation
PV	Photo-Voltaic
SP	Sigma Points
WO	Williams-Otto
WS	Weighted Sum

Introduction and theoretical concepts

Chapter 1

Introduction

This thesis will focus on the theory of *optimal control problems* (OCPs) applied to (bio)chemical processes. Although with different names, OCP has been of interest also in the past. In fact, famous past scientists as Galileo Galilei and Johann Bernouilli already approached the problem in the 17^{th} century. Galilei dealt with finding the shape of a heavy chain hanged at the extremes, called the catenary problem, while Bernouilli challenged his contemporary colleagues with the brachystochrone problem (Sussmann and Willems, 1997) (Sargent, 2000). This last problem involved the investigation of the trajectory that minimises the time a ball needs to fall from a point A to a point B under the influence of its own weight (Sussmann and Willems, 1997) (Sargent, 2000). Nevertheless, the widely accepted start of the modern OCP theory is the development of *Pontryagin's maximum principle* (1958), which has been widely exploited in the aerospace industry and during the space missions of the 1960s (Sussmann and Willems, 1997) (Diehl, 2011).

In more recent years, *optimal control* (OC) has become a very useful tool in industry. It is mainly exploited to facilitate decision-making, either when planning and taking strategic future decisions, or during real-time optimisation (Logist and Van Impe, 2013) (Manenti et al., 2013). OCP involves the optimisation of a single objective function, usually chosen depending on the market situation. This gives rise to a function that determines the inputs to the system, to make it as efficient as possible. By doing that, the chosen objective is minimised or maximised, depending on its formulation.

OCP in industry can be applied to single unit operations but also to complete processes. Examples can be maximising the productivity or the yield of a reactor, as in Logist et al. (2009), but also minimising energy consumption of a whole plant or the raw materials cost. Many other examples can be thought of, depending on the individual process considered. Although this work will focus mainly on chemical engineering applications, this does not restrict the field of application of optimal control. Different examples can be found in Diehl et al. (2006) and Houska and Diehl (2009), where OC theory is applied to a robot arm and a crane.

In the chemical industry, the need for this tool arises from different problems that have to be faced by European companies in order to be competitive on the global scale. Raw materials often have to be imported and many of them are depleting in the world, leading to increase in their price. Together with that, energy prices in Europe are higher than they were few decades ago, but also higher with respect to other parts of the world. A clear example of this point are the Middle-East countries, that can exploit oil at very low prices, or the USA that can do the same with methane, by using unconventional natural gas sources, as shale-gas. Thus the need of operating processes in the most efficient ways is evident, although the definition of efficient is not univocal since it highly depends on what should be optimised.

Nowadays, though, interest has been developed in trying to optimise more than one objective function. For instance, a decision-maker might be interested in maximising the productivity of a reactor and minimising energy consumption at the same time, being faced with a so-called *multi-objective optimal control problem* (MOOCP). This is due to several factors of global concern:

1. increase in energy prices, following the oil crisis of the past century;
2. increase in raw materials and resource prices, due to progressive depletion and political choices of the producing countries;
3. social and political awareness of environmental issues, as global warming or waste emissions, which brought to stricter regulations and attempts to decrease emissions, like the European Union tradable permits system.

All these factors, together with those described in the previous paragraph, are putting pressure on the (bio)chemical industry. Optimal control and *multi-objective optimal control* (MOOC) can be a suitable tool for sustainable development. Indeed, the objective functions can be based on economic considerations, as the maximisation of the productivity, but also on environmental or social basis. Examples can be the minimisation of the raw material consumption or of the waste production. MOOCP deals with the simultaneous optimisation of more than one objective, giving a set of possible and mathematically equivalent solutions, called Pareto set. From all these possible solutions, the decision-maker can pick the best one according to her or his choice criteria. Several examples are already available in the literature, e.g. (Logist et al., 2009) (Logist et al., 2012). MOOCP will also be treated in this master thesis.

The solution of OCPs and MOOCPs is nowadays obtained through the exploitation of numeric computation. Several algorithms are present in the literature, e.g. in Houska et al. (2011). For this thesis, those of *Pomodoro*, a package developed within the BioTeC division of KULeuven to solve optimal control problems, will be employed.

OCP and MOOCP usually rely on the system dynamics of the process, which have to be carefully modelled. This implies a perfect knowledge of all parameters involved in the system equations. However, this is not always guaranteed. In fact, very often, parameters are introduced in model equations to simplify them and avoid taking

care of quantities that can only be estimated, or that are difficult to measure with good precision. Examples can be the scaling factor on a heat exchanger wall (Logist et al., 2011) (Houska et al., 2012) or the inlet substrate concentration of a fed-batch bio-reactor (Logist et al., 2011). Usually, the presence of uncertain parameters leads to lower performances of the system, as it will be more clearly explained in the text. In order to deal with these uncertainties, robust OCP has been developed. In particular, two approaches will be considered in this thesis: the *linear approximation* (Srinivasan et al., 2003) and the *sigma points approximation* (Julier and Uhlmann, 1996) (Recker et al., 2012).

Finally, uncertainties on parameters will be considered also when dealing with multiple objectives. This problem, that can be renamed robust MOOCP, will combine the robustification approach together with the concept of Pareto set. Again a set of equivalent solutions is obtained, but they will not be as performing as they were in the original MOOCP (Logist et al., 2011).

Although whole plants can also be optimised, only (bio-)chemical reactors are considered in this work. In particular, four models of different complexity will be used. The two simplest cases will be a fed-batch bio-reactor for the lysine production (Logist et al., 2009) and a jacketed tubular reactor (Logist et al., 2011) (Houska et al., 2012). The *Williams-Otto* (WO) reactor (Williams and Otto, 1960) (Forbes, 1994) and, in particular, the *chemical vapour deposition* (CVD) reactor (Viganò et al., 2010) will, instead, present higher complexity. This last reactor, in particular, will present a highly complex model, being a real industrial reactor for the production of polycrystalline silicon rods (Viganò et al., 2010).

The objectives of this thesis are the followings:

1. assess the reliability and efficiency of the newly developed computational algorithms implemented in Pomodoro;

2. evaluate the performances on small and medium-scale models of two different approaches for robust OC, namely the linear and sigma points approximations;

3. solve the multi-objective and robust multi-objective optimal control problem of a real industrial case, the chemical vapour deposition reactor.

The thesis structure can be summarised as follows. In Chapter 2, a literature study about optimal control is made. This will be comprehensive of the most important theoretical background needed to deal with the practical cases of this thesis. The methods available for the solution of OCPs will also be presented and briefly described.

Afterwards, Chapter 3 will present the materials and methods. The software adopted for the solution of OCPs are described. Additionally, the model equations of three of the reactors introduced before are given. These will be the fed-batch bio-reactor, the jacketed tubular reactor and the WO reactor. These examples will be useful to assess the algorithms and the methodologies exploited during the thesis. This

will be done in Chapters 4 and 5. In particular, Chapter 4 deals with the simultaneous maximisation of the productivity and the yield of the fed-batch bio-reactor. Thus a multi-objective optimisation problem will be solved. The results obtained are then compared with the literature (Logist et al., 2009), in order to assess the algorithms exploited in this thesis. In Chapter 5 the conversion in the jacketed tubular reactor and the productivity of the WO reactor are maximised. These OCPs, however, will also take into consideration several uncertain parameters. Thus Chapter 5 will deal with robust OC. As in Chapter 4, the results obtained for the jacketed tubular reactor case will be compared with the literature (Logist et al., 2011).

Finally, a real industrial problem will be treated in Chapter 6. Indeed, this will be the CVD reactor, often referred to as *Siemens* reactor (Viganò et al., 2010), for the production of polycrystalline silicon rods (Viganò et al., 2010). The rods obtained are mostly required for their semi-conductive properties and are of vital importance for the photo-voltaic and micro-electronics industries (del Coso et al., 2011). The aim of the Chapter will be to maximise the production of the reactor, while minimising its energy consumption. While doing so, uncertainties on two different model parameters will also be taken in consideration. In Chapter 6, then, a robust multi-objective optimal control problem will be solved for a real industrial case.

Lastly, Chapter 7 will conclude the thesis, finalising and summarising the results attained.

Chapter 2

Literature Study

2.1 Introduction

The definition of an optimal control problem together with its general formulation and the explanation of the involved terms will be given in Section 2.2. Due to the high complexity of the systems treated, nowadays the solution of optimal control problems is exploited by efficient numerical algorithms. The basic approaches to numerically solve an OCP will be treated in Section 2.3. In particular, already mentioned Pontryagin's maximum principle will be explained in Section 2.3.2, while the approach exploited throughout all this thesis will be explained in Section 2.3.3.

Moreover, in recent years, two particular variations of OC are gaining more importance, namely *multi-objective optimal control* (MOOC) and robust OC. The first one handles the simultaneous optimisation of more than one objective function. The second one deals with optimal control of systems where uncertainties over some parameters are present. Again, the solution methodology and algorithms will be a relevant matter. They will also be discussed in this Chapter.

Section 2.4 introduces the MOOCP formulation, while its solution methodologies are addressed in Section 2.5. Section 2.6 instead explains the theory behind robust OC and its solution approaches.

Section 2.7 will then conclude and summarise this first review Chapter.

2.2 Optimal control problem formulation

Optimal control is an optimisation strategy that allows to evaluate the control trajectories needed to exploit a process at its optimum. A control trajectory, can be defined as a function that regulates the behaviour of the control inputs of the analysed system. The control inputs depend on the objective that has to be optimised. For the purpose of this thesis, the general formulation of an optimal control problem is the following (Logist et al., 2009) (Logist et al., 2012):

$$\underset{\mathbf{x}(\xi),\mathbf{u}(\xi),\mathbf{p},\xi_\mathrm{f}}{\text{minimise}} \quad J(\mathbf{x}(\xi),\mathbf{u}(\xi),\mathbf{p},\xi_\mathrm{f}) \tag{2.1a}$$

$$\text{subject to} \quad \frac{d\mathbf{x}}{d\xi} = \mathbf{f}(\mathbf{x}(\xi),\mathbf{u}(\xi),\mathbf{p},\xi) \qquad \xi \in [0,\xi_\mathrm{f}] \tag{2.1b}$$

$$0 = \mathbf{b}_\mathrm{i}(\mathbf{x}(0),\mathbf{p}) \tag{2.1c}$$

$$0 = \mathbf{b}_\mathrm{t}(\mathbf{x}(\xi_\mathrm{f}),\mathbf{p}) \tag{2.1d}$$

$$0 \geq \mathbf{c}_\mathrm{p}(\mathbf{x}(\xi),\mathbf{u}(\xi),\mathbf{p},\xi) \tag{2.1e}$$

$$0 \geq \mathbf{c}_\mathrm{t}(\mathbf{x}(\xi_\mathrm{f}),\mathbf{u}(\xi_\mathrm{f}),\mathbf{p},\xi_\mathrm{f}) \tag{2.1f}$$

In these equations, ξ is the independent variable, usually the time, $\mathbf{x}(\xi)$ are the differential states of the system such that $\mathbf{x}(\xi) : \Re \longrightarrow \Re^{n_\mathrm{x}}$, $\mathbf{u}(\xi)$ are the control variables of the system $\mathbf{u}(\xi) : \Re \longrightarrow \Re^{n_\mathrm{u}}$, $\mathbf{p}$ are the parameters of the system of dynamic equations and they are usually considered as constant $\mathbf{p} : \Re \longrightarrow \Re^{n_\mathrm{p}}$ (Houska et al., 2011). The inputs $\mathbf{u}(\xi)$ are those variables that can be manipulated in order to achieve the optimal trajectory required. J represents the objective function, $\mathbf{f}$ the system dynamics equations, $\mathbf{b}_\mathrm{i}$ and $\mathbf{b}_\mathrm{t}$ the boundary conditions at respectively the initial and final time, $\mathbf{c}_\mathrm{p}$ and $\mathbf{c}_\mathrm{t}$ the path and terminal inequality constraints to which the system is subjected. Equations 2.1b-f represent the constraints to which the system is subjected. It is important to highlight that the model equation itself is a very important constraint for the OCP 2.1, since it is the only constraint that must always be present.

The general Formulation 2.1 can be extended by considering the dependency of the system not only on the differential states $\mathbf{x}(\xi)$, but also on some algebraic states $\mathbf{a}(\xi)$ (Houska et al., 2011).

2.2.1 Objective function

It is important to know that, although J is called objective function, it is not a function, but a functional. A functional is defined as a function from a vector space to a scalar space. In fact, it is possible to see that the inputs of J are functions of several vectors, but the output is only a scalar value. From here on, as it is done in most of the literature, the functional J will be called objective function, although this feature should always be kept in mind. For standard OCPs, the functional J is expressed in the formulation (Logist et al., 2009) (Logist et al., 2012):

$$J(\mathbf{x}(\xi),\mathbf{u}(\xi),\mathbf{p},\xi_\mathrm{f}) = h(\mathbf{x}(\xi_\mathrm{f}),\mathbf{p},\xi_\mathrm{f}) + \int_{t_0}^{\xi_\mathrm{f}} g(\mathbf{x}(\xi),\mathbf{u}(\xi),\mathbf{p},\xi)d\xi \tag{2.2}$$

The first term in Equation 2.2 is called the *Mayer* term, or terminal cost, and it only considers conditions at the end of the time horizon ξ_f, while the second term in Equation 2.2 is called the *Lagrange* term, or integral cost, and it considers the path followed $\forall \xi \in [0,\xi_\mathrm{f}]$. As stated in Logist et al. (2011), a Lagrange term can always be rewritten in a Mayer form. This is done by including a new cost state $\frac{dx_\mathrm{c}}{d\xi} = \mathbf{g}(\mathbf{x}(\xi),\mathbf{u}(\xi),\mathbf{p},\xi)$ with initial condition $x_\mathrm{c}(0) = 0$.

2.2.2 Constraints

Usually, in real processes, it is not allowed to change the inputs without taking into account several constraints on both states and inputs themselves. Examples can be that the feeding rate to a certain reactor cannot exceed the pump capacity, or that the liquid level in that same reactor has to remain between a lower and an upper bound. A general formulation for the constraints has been presented in Equations 2.1b-f. Important to notice is that the indipendent variable ξ has been limited to a lower and upper bound $[0, \xi_\mathrm{f}]$, in Problem 2.1. Usually, the lower bound for this variable is known also in practical cases, but its upper bound is not known for all OCPs and there are frequent cases when this value is free and has to be determined. In this formulation, the dynamic model that the system is following is represented in Constraint 2.1b. The boundary conditions to the model equation, for $\xi = 0$ and $\xi = \xi_\mathrm{f}$ are given in Constraints 2.1c and 2.1d, while the Lagrange and Mayer constraints on both states and inputs are assessed in Equations 2.1e and 2.1f, respectively.

In conclusion, it is important to define the feasible set Ω as the set containing all the points that satisfy the dynamic Equation 2.1b, together with all the other Constraints 2.1c-f (Logist et al., 2012) (Diehl, 2013).

Definition 1. $\Omega = \{\boldsymbol{y} = (\boldsymbol{x}(\xi), \boldsymbol{u}(\xi), \boldsymbol{p}, \xi_\mathrm{f}) | (\{\boldsymbol{b}_\mathrm{i}, \boldsymbol{b}_\mathrm{t}\} = 0), \boldsymbol{c}_\mathrm{p} \leq 0, \boldsymbol{c}_\mathrm{t} \leq 0\}$.

2.3 Optimal control problem solution

All the previous formulations of OCP have been posed in a continuous-time form. For simple OCPs, often the exploitation of an analytical solution is possible, as it was for Galilei's catenary problem (Sussmann and Willems, 1997). Anyway, chemical industry is often dealing with dynamic systems of high complexity. For this reason, most of the times solutions are found by using computer programmes and numerical techniques. The general Problem 2.1 can then be rewritten in a discrete-time form, of which good example is provided by Diehl (2011):

$$\underset{\mathbf{x}_0,\mathbf{u}_0,\mathbf{x}_1,\mathbf{u}_1,\ldots,\mathbf{x}_{\mathrm{N}-1},\mathbf{u}_{\mathrm{N}-1},\mathbf{x}_\mathrm{N},\mathbf{p}}{\text{minimise}} \quad \sum_{\mathrm{k}=0}^{\mathrm{N}-1} L(\mathbf{x}_\mathrm{k}, \mathbf{u}_\mathrm{k}, \mathbf{p}) + E(\mathbf{x}_\mathrm{N}, \mathbf{p}) \tag{2.3a}$$

$$\text{subject to} \quad \mathbf{x}_{\mathrm{k}+1} - \mathbf{f}_\mathrm{k}(\mathbf{x}_\mathrm{k}, \mathbf{u}_\mathrm{k}, \mathbf{p}) = 0 \quad \forall \mathrm{k} = 0, \ldots, \mathrm{N}-1 \tag{2.3b}$$

$$\sum_{\mathrm{k}=0}^{\mathrm{N}-1} \mathbf{r}_\mathrm{k}(\mathbf{x}_\mathrm{k}, \mathbf{u}_\mathrm{k}, \mathbf{p}) + \mathbf{r}_\mathrm{N}(\mathbf{x}_\mathrm{N}, \mathbf{p}) = 0 \tag{2.3c}$$

$$\mathbf{h}_\mathrm{k}(\mathbf{x}_\mathrm{k}, \mathbf{u}_\mathrm{k}, \mathbf{p}) \leq 0 \quad \forall \mathrm{k} = 0, \ldots, \mathrm{N}-1 \tag{2.3d}$$

$$\mathbf{h}_\mathrm{N}(\mathbf{x}_\mathrm{N}, \mathbf{p}) \leq 0 \tag{2.3e}$$

In this formulation, the independent variable ξ has disappeared. The time horizon $[0, \xi_\mathrm{f}]$ has been discretised in N intervals with index k. Although different from

Equation 2.2, in Equation 2.3a it is still possible to identify the Mayer and Lagrange term of the objective function. The latter has no more an integral form, but it has become a sum. Also the constraints have been rearranged. The model constraint Equation 2.1b has been replaced with the discretised form 2.3b. The same happened to the path and terminal inequality Constraints 2.1e and 2.1f that have been replaced with 2.3d and 2.3e. The boundary Conditions 2.1c and 2.1d, instead have been rearranged in a less intuitive formulation. In the discretised form, in principle, every interval k has its own initial and terminal boundary conditions. In practical applications, this does not happen and usually only $\mathbf{r}_0(\mathbf{x}_0, \mathbf{u}_0, \mathbf{p})$ and $\mathbf{r}_\mathrm{N}(\mathbf{x}_\mathrm{N}, \mathbf{u}_\mathrm{N}, \mathbf{p})$ are given, but the expression in Equation 2.3c is the most general formulation (Diehl, 2011).

The solution to this problem must satisfy the so-called *Karush-Kuhn-Tucker* (KKT) condition, which in the discretised-time formulation can be expressed as (Diehl, 2011)

$$\nabla_\mathbf{x} \mathcal{L}(\mathbf{x}, \lambda, \mu) = 0 \tag{2.4a}$$
$$\mathbf{G}(\mathbf{x}) = 0 \tag{2.4b}$$
$$\mathbf{H}(\mathbf{x}) \leq 0 \tag{2.4c}$$

where

$$\mathcal{L}(\mathbf{x}, \lambda, \mu) = J(\mathbf{x}) + \lambda^\top \mathbf{G}(\mathbf{x}) + \mu^\top \mathbf{H}(\mathbf{x}) \tag{2.5a}$$
$$\mathbf{G}(\mathbf{x}) = \begin{pmatrix} \mathbf{f}_0(\mathbf{x}_0, \mathbf{u}_0, \mathbf{p}) - \mathbf{x}_1 \\ \mathbf{f}_1(\mathbf{x}_1, \mathbf{u}_1, \mathbf{p}) - \mathbf{x}_2 \\ \vdots \\ \mathbf{f}_{\mathrm{N}-1}(\mathbf{x}_{\mathrm{N}-1}, \mathbf{u}_{\mathrm{N}-1}, \mathbf{p}) - \mathbf{x}_\mathrm{N} \\ \sum_{\mathrm{k}=0}^{\mathrm{N}-1} \mathbf{r}_\mathrm{k}(\mathbf{x}_\mathrm{k}, \mathbf{u}_\mathrm{k}, \mathbf{p}) + \mathbf{r}_\mathrm{N}(\mathbf{x}_\mathrm{N}, \mathbf{p}) = 0 \end{pmatrix} \tag{2.5b}$$
$$\mathbf{H}(\mathbf{x}) = \begin{pmatrix} \mathbf{h}_\mathrm{k}(\mathbf{x}_\mathrm{k}, \mathbf{u}_\mathrm{k}, \mathbf{p}) \\ \mathbf{h}_\mathrm{N}(\mathbf{x}_\mathrm{N}, \mathbf{p}) \end{pmatrix} \tag{2.5c}$$

These necessary first-order conditions will be taken into account also by the software used for this work. Problem 2.3 can be classified as a *non-linear programming* (NLP) problem. In the literature, several NLP solvers are available. Throughout all this work, the *interior point method* will be the one adopted to solve the NLPs within the optimisation problems. Not being the general aim and topic of this thesis, the interior point method will not be explained here. Interested readers can find further informations in Wächter and Biegler (2006).

According to Diehl et al. (2006) and Diehl (2011), there exist three main families of methods to solve and discretise OCPs, which are: (*i*) state space approaches, (*ii*) indirect methods, (*iii*) direct methods. An explanation of all of them will be given in the following Sections.

Finally, it is worth to remark that, although the problem has now been posed in a discrete-time form and all the presented methods deal with discretisation of states

and controls, real processes follow continuous-time laws. The discretisation itself will then cause the solution to be approximated.

2.3.1 State space approaches

The *state space* approaches are based on the *principle of optimality*: each sub-trajectory of an optimal trajectory is an optimal trajectory (Bertsekas, 2005) (Diehl et al., 2006) (Diehl, 2011). There are two methods based on this principle, *dynamic programming* and the *Hamilton-Jacobi-Bellman* (HJB) equation.

In dynamic programming, a cost-to-go function is defined as the optimal cost obtained if at any time $\mathrm{k} = 0, \ldots, \mathrm{N}-1$ the following OCP is solved (Diehl, 2011):

$$J_{\mathrm{k}}(\bar{\mathbf{x}}_{\mathrm{k}}) = \underset{\mathbf{x}_{\mathrm{k}},\mathbf{u}_{\mathrm{k}},\ldots,\mathbf{x}_{\mathrm{N}-1},\mathbf{u}_{\mathrm{N}-1},\mathbf{x}_{\mathrm{N}},\mathbf{p}}{\text{minimise}} \quad \sum_{\mathrm{i}=\mathrm{k}}^{\mathrm{N}-1} L(\mathbf{x}_{\mathrm{i}}, \mathbf{u}_{\mathrm{i}}, \mathbf{p}) + E(\mathbf{x}_{\mathrm{N}}, \mathbf{p}) \tag{2.6a}$$

$$\text{subject to} \qquad \mathbf{x}_{\mathrm{i}+1} - \mathbf{f}_{\mathrm{i}}(\mathbf{x}_{\mathrm{i}}, \mathbf{u}_{\mathrm{i}}, \mathbf{p}) = 0 \quad \forall \mathrm{i} = \mathrm{k}, \ldots, \mathrm{N}-1 \tag{2.6b}$$

$$\bar{\mathbf{x}}_{\mathrm{k}} - \mathbf{x}_{\mathrm{k}} = 0 \tag{2.6c}$$

$\bar{\mathbf{x}}_{\mathrm{k}}$ is the initial value for the k^{th} shortened OCP. This OCP is said to be shortened since the time horizon investigated is no more $\xi \in [0, \xi_{\mathrm{f}}]$ but $\xi \in [\xi_{\mathrm{k}}, \xi_{\mathrm{f}}]$. Otherwise said, not all intervals are considered when solving this problem, but the firsts $\mathrm{k}-1$ are excluded. Of course this will lead to the solution of only a fraction of the initial problem, the sub-optimal trajectory introduced with the principle of optimality. For this reason, the solution of the initial problem is obtained by the so-called dynamic programming recursion (Diehl, 2011). This means that first the cost-to-go function for $\mathrm{k} = \mathrm{N}$ is found, as (Diehl, 2011)

$$J_{\mathrm{N}}(\mathbf{x}) = E(\mathbf{x}) \tag{2.7}$$

and then all cost-to-go functions are calculated backwards following the law

$$J_{\mathrm{k}}(\bar{\mathbf{x}}_{\mathrm{k}}) = \min_{\mathbf{u}} L(\bar{\mathbf{x}}_{\mathrm{k}}, \mathbf{u}, \mathbf{p}) + J_{\mathrm{k}+1}(\mathbf{f}(\bar{\mathbf{x}}_{\mathrm{k}}, \mathbf{u}, \mathbf{p})) \tag{2.8}$$

which is a direct consequence of the principle of optimality (Diehl, 2011). From this both the optimal control values and the optimal trajectory can be calculated $\forall \mathrm{k} \in [0, \mathrm{N}-1]$:

$$\mathbf{u}_{\mathrm{k}}^{*}(\mathbf{x}_{\mathrm{k}}) = \arg\min_{\mathbf{u}} L(\mathbf{x}_{\mathrm{k}}, \mathbf{u}, \mathbf{p}) + J_{\mathrm{k}+1}(\mathbf{f}(\mathbf{x}_{\mathrm{k}}, \mathbf{u}, \mathbf{p})) \tag{2.9}$$

$$\mathbf{x}_{\mathrm{k}+1} = \mathbf{f}(\mathbf{x}_{\mathrm{k}}, \mathbf{u}_{\mathrm{k}}^{*}(\mathbf{x}_{\mathrm{k}}), \mathbf{p}) \tag{2.10}$$

By choosing infinitely small time steps in dynamic programming for $\xi \in [0, \xi_{\mathrm{f}}]$, and thus approaching the continuous time case, the HJB equation is obtained (Diehl, 2011) (Diehl, 2012):

$$-\frac{\partial J}{\partial \xi}(\mathbf{x}, \xi) = \min_{\mathbf{u}} L(\mathbf{x}, \mathbf{u}) + \nabla_{\mathbf{x}} J(\mathbf{x}, \xi)^{\top} f(\mathbf{x}, \mathbf{u}) \tag{2.11}$$

and

$$J(\mathbf{x}, \xi_{\mathrm{f}}) = E(\mathbf{x}) \tag{2.12}$$

In the HJB equation, the cost-to-go function $J(\mathbf{x}, \xi)$ is assumed to be continuous and differentiable with respect to $\mathbf{x}$, which might not be always the case and which is often not known a priori. Nevertheless, if it is possible to solve the HJB equation, as it is for example in a *linear-quadratic programming* (LQP), the optimal control trajectory can be obtained from Equation 2.11 (Bertsekas, 2005).

It is important to stress that both dynamic programming and the HJB equation suffer of the Bellman curse of dimensionality. In fact, the continuous state space of the real process needs to be discretised and put in a grid in state space. If the number of states is large, the computational effort to obtain the numerical solution might be expensive (Diehl, 2011) (Diehl, 2012). For this reason the state approaches are considered as possible methods only for problems with low state dimensionality.

2.3.2 Indirect methods

Indirect methods are developed from the HJB equation and are mainly due to the work of Pontryagin. In 1958 he developed the Pontryagin's maximum principle, which states the necessary conditions that an optimal trajectory must satisfy. These methods are often referred to as *first optimise, then discretise* (Diehl et al., 2006) (Diehl, 2011).

Equation 2.11, can be rewritten in terms of the hamiltonian as (Diehl, 2011):

$$-\frac{\partial J}{\partial \xi}(\mathbf{x}, \xi) = \min_{\mathbf{u}} H(\mathbf{x}, \nabla_{\mathbf{x}} J(\mathbf{x}, \xi)) \tag{2.13a}$$

$$H(\mathbf{x}, \nabla_{\mathbf{x}} J(\mathbf{x}, \xi), \mathbf{u}) = L(\mathbf{x}, \mathbf{u}) + \nabla_{\mathbf{x}} J(\mathbf{x}, \xi)^{\top} f(\mathbf{x}, \mathbf{u}) \tag{2.13b}$$

where usually $\nabla_{\mathbf{x}} J(\mathbf{x}, \xi)$ is substituted by the ad-joint variables $\lambda(\xi) = \nabla_{\mathbf{x}} J(\mathbf{x}, \xi)$. The idea of the indirect approach is to find explicitly the optimal controls by assuming that the states $\mathbf{x}^*(\xi)$ and the co-states $\lambda^*(\xi)$ are known and then differentiate the HJB equation along the optimal trajectory (Diehl, 2011). Once the explicit optimal controls are known, they can be eliminated. The problem results then in a *boundary value problem* (BVP) in *ordinary differential equations* (ODE) in the states $\mathbf{x}$ and the co-states λ and needs to be solved numerically. This method is also referred to as *two point boundary problem method* (Bertsekas, 2005).

The explicit formulation of the optimal controls $\mathbf{u}^*_{\text{explicit}}(\mathbf{x}, \lambda)$ is obtained from (Bertsekas, 2005) (Diehl, 2011)

$$\mathbf{u}^*_{\text{explicit}}(\mathbf{x}^*, \lambda^*) = \arg\min_{\mathbf{u}} H(\mathbf{x}, \lambda, \mathbf{u}) \tag{2.14a}$$

$$\text{subject to} \qquad h(\mathbf{x}, u) \leq 0 \tag{2.14b}$$

by putting the derivative $\frac{\partial H}{\partial \mathbf{u}}(\mathbf{x}^*, \lambda^*, \mathbf{u}^*) = 0$. The boundary conditions depend on the kind of problem. If the terminal value of the states $\mathbf{x}$ are fixed, the values of

$\mathbf{x}(0)$ and $\mathbf{x}(\xi_f)$ should be taken as boundary conditions. If $\mathbf{x}(\xi_f)$ are not available, conditions on the ad-joints λ are to be taken in consideration. (Bertsekas, 2005).

If the dependence of the hamiltonian on the optimal control is explicit, the expression of $\mathbf{u}^*_{\text{explicit}}(\mathbf{x}^*, \lambda^*)$ is easily obtained. If this is not the case, there is the presence of a singular arc. This happens when the minimum of the hamiltonian is not unique. In this case, the derivative $\frac{d}{d\xi}\frac{\partial H}{\partial \mathbf{u}}(\mathbf{x}, \lambda, \mathbf{u}) = 0$ is taken and it is looked for explicit dependence on $\mathbf{u}$. If it is not the case, higher order derivatives with respect to ξ are calculated, until an explicit dependence on $\mathbf{u}$ is found for the relation (Diehl, 2011):

$$\left(\frac{d}{d\xi}\right)^{\mathrm{n}} \frac{\partial H}{\partial \mathbf{u}}(\mathbf{x}, \lambda, \mathbf{u}) = 0 \tag{2.15}$$

Solution of the BVP is obtained numerically and three possible methods are used: single shooting, collocation, multiple shooting (Diehl et al., 2006) (Diehl, 2011). All three of them will be explained in Section 2.3.3.

2.3.3 Direct methods

Direct methods are often described as *first discretise, then optimise* (Diehl et al., 2006) (Diehl, 2011), in contrast with indirect methods. They are the most widely used and, in particular, the orthogonal collocation method will also be applied in the simulations presented in the next Chapters of this work. Direct methods are direct single shooting, direct multiple shooting and direct orthogonal collocation. All three of them will be described in this Section.

2.3.3.1 Direct single shooting

In direct single shooting (Sargent and Sullivan, 1978) (Vassiliadis et al., 1994a) (Vassiliadis et al., 1994b), a time grid is chosen and the controls $\mathbf{u}(t)$ are parameterised as piecewise constant functions in each interval of the grid. These constant values $\mathbf{u}_{\mathrm{i}}$ can be gathered in a vector which is the variable manipulated by the NLP solver to reach the optimal solution. Only the intial value of the states $\mathbf{x}$ is given and the states profiles are considered implicitly depending on the controls vector $\mathbf{u}(t)$ (Diehl et al., 2006). Once a vector of controls $\mathbf{u}_{\mathrm{i}}$ is obtained, the ODE system is solved and the objective function is computed. After that, the NLP solver updates the control parmeterisation and the objective function is computed again. The simulation and optimisation recur at each iteration. For this reason, direct single shooting is considered a sequential approach (Diehl et al., 2006) (Logist and Van Impe, 2013). From Figure 2.1a it is possible to have an idea of the control parameterisation, $\mathbf{u}_{\mathrm{i}}$.

Drawbacks of direct single shooting are the impossibility to use background knowledge to initialize the states $\mathbf{x}$ (Diehl et al., 2006) and being a time consuming method, due to the sequential integrations (Logist and Van Impe, 2013). Moreover, the constraints on the states $\mathbf{x}$ cannot be directly enforced in an easy and efficient manner, due to the fact that the states are not discretised (Logist and Van Impe, 2013).

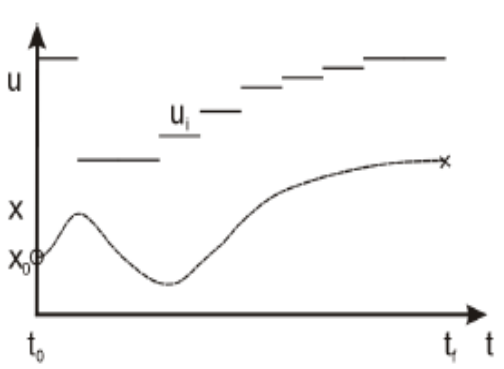

(a) *Direct single shooting: discretised controls and continuous states.*

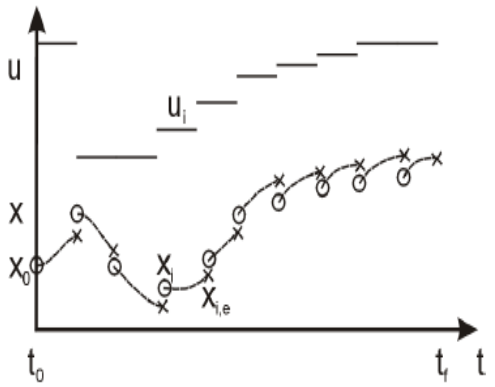

(b) *Direct multiple shooting: discretised controls and states.*

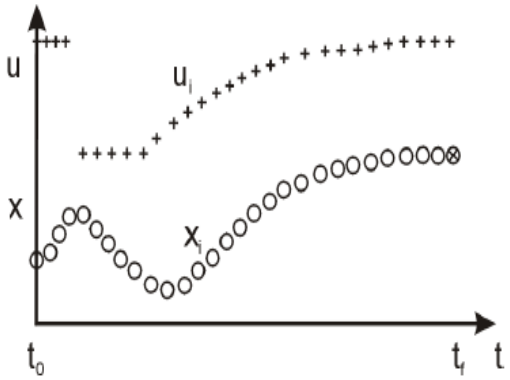

(c) *Direct orthogonal collocation: discretised controls and states, with intermediate points.*

Figure 2.1: *Direct single shooting, direct multiple shooting and direct orthogonal collocation. Gentle courtesy of Logist and Van Impe (2013)*

2.3.3.2 Direct multiple shooting

In direct multiple shooting (Bock and Plitt, 1984) (Leineweber et al., 2003a) (Leineweber et al., 2003b), the controls $\mathbf{u}(t)$ are again parameterised in piecewise constant functions, as it was in direct single shooting. In this case, though, the initial values of the states $\mathbf{x}(t)$ at the beginning of each interval are given to the solver as degrees of freedom. Figure 2.1b shows this feature. Through this peculiarity it is possible to exploit initialisation of the states $\mathbf{x}$ when previous knowledge is present (Diehl et al., 2006) (Diehl, 2011). Additional continuity conditions are added, such that, for the states $\mathbf{x}(t)$ of the optimal trajectory, the final value of each interval $\mathbf{x}_{\mathrm{i,e}}$ coincides with the initial value of the following one $\mathbf{x}_{\mathrm{i+1,e}}$ (Diehl et al., 2006) (Logist and Van Impe, 2013). In multiple shooting, the simulation and optimisation problems are not treated sequentially as it was in direct single shooting, but simultaneously (Leineweber et al., 2003b) (Diehl et al., 2006). This allows to save computational time, while avoiding

repeated integrations (Logist and Van Impe, 2013).

2.3.3.3 Direct orthogonal collocation

Direct orthogonal collocation (Biegler, 1984) is also considered a simultaneous approach as direct multiple shooting (Diehl et al., 2006). The controls $\mathbf{u}(t)$ are parameterised and states $\mathbf{x}(t)$ are given as degrees of freedom as it was in the multiple shooting case. The continuity of the states $\mathbf{x}(t)$ is also assured as it was in the multiple shooting case. Anyway, additional conditions are that in each interval $[t_\mathrm{i}, t_{\mathrm{i}+1}]$, n collocation points are placed and the trajectory is approximated by a polynomial passing through those points (Biegler, 1984) (Diehl, 2011) (Logist and Van Impe, 2013). For each of the collocation points, the Constraints 2.1b-f must be satisfied. This allows to solve an optimal control problem as if more discretisation points were chosen (Biegler, 1984).

Direct orthogonal collocation will be the method exploited in this master thesis in order to solve OCPs. For each interval, the number of interpolating points is $\mathrm{n} = 3$. Thus, a 4^{th} degree polynomial is chosen to interpolate the states profiles between the initial, collocation and final points of each discretised interval. The main advantages of this approach are that background knowledge on the states $\mathbf{x}$ can be exploited as initialisation, it can easily deal with unstable systems, constraints on the states $\mathbf{x}$ are directly imposed and it shows fast local convergence (Diehl et al., 2006).

2.4 Multi-objective optimal control problem formulation

Historically in the chemical industry only one objective function, usually the productivity, was to be optimised through optimal control. However, as already anticipated, a decision-maker can be interested in optimising more than a single objective. More and more often, production processes can then be faced with a multi-objective optimal control problem. A simple bi-objective example can be the maximisation of the top purity in a distillation column, together with the minimisation of the energy consumption. Nevertheless, also more than two objectives can be chosen, depending on the decision-maker preferences. For the purpose of this thesis, the general formulation for a MOOCP is (Logist et al., 2009) (Logist et al., 2012):

$$\underset{\mathbf{x}(\xi),\mathbf{u}(\xi),\mathbf{p},\xi_\mathrm{f}}{\text{minimise}} \quad \{J_1, J_2, \ldots, J_\mathrm{m}\} \tag{2.16a}$$

$$\text{subject to} \quad \frac{d\mathbf{x}}{d\xi} = \mathbf{f}(\mathbf{x}(\xi), \mathbf{u}(\xi), \mathbf{p}, \xi) \qquad \xi \in [0, \xi_\mathrm{f}] \tag{2.16b}$$

$$0 = \mathbf{b}_\mathrm{i}(\mathbf{x}(0), \mathbf{p}) \tag{2.16c}$$

$$0 = \mathbf{b}_\mathrm{t}(\mathbf{x}(\xi_\mathrm{f}), \mathbf{p}) \tag{2.16d}$$

$$0 \geq \mathbf{c}_\mathrm{p}(\mathbf{x}(\xi), \mathbf{u}(\xi), \mathbf{p}, \xi) \tag{2.16e}$$

$$0 \geq \mathbf{c}_\mathrm{t}(\mathbf{x}(\xi_\mathrm{f}), \mathbf{u}(\xi_\mathrm{f}), \mathbf{p}, \xi_\mathrm{f}) \tag{2.16f}$$

Often, in a multi-objective optimal control problem the objectives $[J_1, \ldots, J_\mathrm{m}]$ are in contrast with each other, as it is the case of maximising the top purity in a distillation column, while minimising energy consumption. For this reason, it is not possible to find a single optimal solution for such a problem. A set of optimal solutions is instead obtained, which is called Pareto set. Before explaining what a Pareto set is, it is better to recall the definition of feasible set, from Section 2.2.2:

Definition 1. $\Omega = \{\boldsymbol{y} = (\boldsymbol{x}(\xi), \boldsymbol{u}(\xi), \boldsymbol{p}, \xi_\mathrm{f}) | (\{\boldsymbol{b}_\mathrm{i}, \boldsymbol{b}_\mathrm{t}\} = 0), \boldsymbol{c}_\mathrm{p} \leq 0, \boldsymbol{c}_\mathrm{t} \leq 0\}$.

The Pareto set comprehends all the possible solutions of the MOOCP 2.16. These points are often called Pareto optimal points or Pareto optimals and are defined as follows (Logist et al., 2012):

Definition 2. A point $\boldsymbol{y}_\mathrm{a} \in \Omega$ is Pareto optimal if and only if there is no other point $\boldsymbol{y}_\mathrm{b} \in \Omega$ with $J_\mathrm{i}(\boldsymbol{y}_\mathrm{b}) \leq J_\mathrm{i}(\boldsymbol{y}_\mathrm{a}), \forall \mathrm{i} \in \{1 \ldots \mathrm{m}\}$ and $J_\mathrm{i}(\boldsymbol{y}_\mathrm{b}) < J_\mathrm{i}(\boldsymbol{y}_\mathrm{a})$ for at least one $\mathrm{i} \in \{1, \ldots, \mathrm{m}\}$

This definition can be explained as follows: for each Pareto optimal, it is not possible to improve one of the objective functions without worsening at least one of the others. Definition 2 can be additionally expanded in two additional definitions of global and local Pareto optimal points.

Definition 3. A point $\boldsymbol{y}_\mathrm{a} \in \Omega$ is global Pareto optimal if there is no other point $\boldsymbol{y}_\mathrm{b} \in \Omega$ with $J_\mathrm{i}(\boldsymbol{y}_\mathrm{b}) \leq J_\mathrm{i}(\boldsymbol{y}_\mathrm{a}), \forall \mathrm{i} \in \{1 \ldots \mathrm{m}\}$ and $J_\mathrm{i}(\boldsymbol{y}_\mathrm{b}) < J_\mathrm{i}(\boldsymbol{y}_\mathrm{a})$ for at least one $\mathrm{i} \in \{1, \ldots, \mathrm{m}\}$ in all the feasible design space.

Definition 4. A point $\boldsymbol{y}_\mathrm{a} \in \Omega$ is local Pareto optimal if there is no other point $\boldsymbol{y}_\mathrm{b} \in \Omega$ with $J_\mathrm{i}(\boldsymbol{y}_\mathrm{b}) \leq J_\mathrm{i}(\boldsymbol{y}_\mathrm{a}), \forall \mathrm{i} \in \{1 \ldots \mathrm{m}\}$ and $J_\mathrm{i}(\boldsymbol{y}_\mathrm{b}) < J_\mathrm{i}(\boldsymbol{y}_\mathrm{a})$ for at least one $\mathrm{i} \in \{1, \ldots, \mathrm{m}\}$ in a neighbourhood of $\boldsymbol{y}_\mathrm{a}$.

Different algorithms exist to exploit a multi-objective optimisation problem. In the following Section they will be introduced.

2.5 Multi-objective optimal control problem solution

According to Logist et al. (2009), the solution methodologies for a multi-objective problem are divided in two classes: scalarisation and stochastic methods. The first class involves the partition of the original problem into several parametric single objective problems (Logist et al., 2012). The Pareto set is then obtained by solving all these problems with different parameter values each time. The parameters, as will be seen in the following sections, are often referred to as weights. The second class, instead, allows to obtain the Pareto set without changing the formulation of the problem. This is done by repeatedly calculating the cost functions and updating the solutions (Logist et al., 2009). Stochastic methods are considered as global optimisation methods, although a rigorous proof has not been developed yet (Logist et al., 2009). Unfortunately several drawbacks are present, mainly their time-consuming feature, due to the repeated simulations that have to be performed,

their difficulty in handling constraints exactly and their limitation to low dimensional search spaces (Logist et al., 2009) (Logist et al., 2012).

In this work only scalarisation methods will be exploited. For this reason the stochastic techniques will not be explained further. In the following sections a deeper elucidation of the most used scalarisation techniques will be given.

2.5.1 Weighted sum

This section presents the oldest and more intuitive method for solving a MOOCP, the *weighted sum* (WS).

A very practical method for solving Problem 2.16 is to minimise a combination of all the objectives J_i, which can be expressed as follows:

$$\underset{\mathbf{x}(\xi),\mathbf{u}(\xi),\mathbf{p},\xi_\mathrm{f}}{\text{minimise}} \quad \left\{\sum_{\mathrm{i}=1}^{\mathrm{m}} w_\mathrm{i} J_\mathrm{i}\right\} \tag{2.17a}$$

$$\text{subject to} \quad \frac{d\mathbf{x}}{d\xi} = \mathbf{f}(\mathbf{x}(\xi),\mathbf{u}(\xi),\mathbf{p},\xi) \qquad \xi \in [0,\xi_\mathrm{f}] \tag{2.17b}$$

$$0 = \mathbf{b}_\mathrm{i}(\mathbf{x}(0),\mathbf{p}) \tag{2.17c}$$

$$0 = \mathbf{b}_\mathrm{t}(\mathbf{x}(\xi_\mathrm{f}),\mathbf{p}) \tag{2.17d}$$

$$0 \geq \mathbf{c}_\mathrm{p}(\mathbf{x}(\xi),\mathbf{u}(\xi),\mathbf{p},\xi) \tag{2.17e}$$

$$0 \geq \mathbf{c}_\mathrm{t}(\mathbf{x}(\xi_\mathrm{f}),\mathbf{u}(\xi_\mathrm{f}),\mathbf{p},\xi_\mathrm{f}) \tag{2.17f}$$

$$\sum_{\mathrm{i}=1}^{\mathrm{m}} w_\mathrm{i} = 1 \tag{2.17g}$$

$$w_\mathrm{i} \geq 0 \tag{2.17h}$$

where the vector $\mathbf{w} = [w_1, w_2, \ldots, w_\mathrm{m}]^\top \in \Re^\mathrm{m}$ is the so-called weight vector.

Despite its intuitive and practical formulation, the WS method is subjected to important drawbacks (Das and Dennis, 1997) (Logist et al., 2012):

1. It fails to obtain Pareto optimal points in the non-convex region of the Pareto set;

2. A uniform spread of the weights w_i does not guarantee a uniform spread of optimal points on the Pareto curve;

3. The solutions obtained through the optimisation routines are highly dependent on the scaling of the objective functions themselves.

These important drawbacks will be better explained in Section 4.2. In order to overcome these features of the WS method, other scalarisation methods have been developed and they will be explained in the two following Sections.

2.5.2 Normal boundary intersection

Normal boundary intersection (NBI) method arises from the need of overcoming the drawbacks of the WS. It was first described in Das and Dennis (1998) and it is based on the concepts of *utopia point* and *convex hull of individual minima* (CHIM). The utopia point J^* for Problem 2.16 is defined as the vector containing the global minima of all the objective functions J_i. Usually a transformation is applied, in order to define J^* as coincident with the origin of the system. The CHIM is the set of points with all possible convex combinations of the individual minima. From this, the m $\times$ m pay off matrix Φ, whose i^{th} column is $J_\mathrm{i}^* - J^*$, is constructed (Das and Dennis, 1998) (Logist et al., 2009).

Considering the feasible set Ω, the NBI is a technique which basically comes down to find the portion of the boundary of the feasible set itself that contains the Pareto optimal points (Das and Dennis, 1998). This is done by considering the intersection between the part of the boundary of Ω closest to the origin and the quasi-normal of any point on the CHIM (Logist et al., 2009). Figure 2.2 shows a geometric representation of this method (Logist et al., 2009). There, the CHIM is the line connecting the minima of the normalised objective functions $\bar{J}_1 = 1$ $\bar{J}_2 = 1$. Problem 2.16 can then be rewritten as (Logist et al., 2009):

$$\underset{\mathbf{u}(\xi),\xi_\mathrm{f},\lambda}{\text{maximise}} \quad \lambda \tag{2.18a}$$

$$\text{subject to} \quad \frac{d\mathbf{x}}{d\xi} = \mathbf{f}(\mathbf{x}(\xi),\mathbf{u}(\xi),\mathbf{p},\xi) \qquad \xi \in [0,\xi_\mathrm{f}] \tag{2.18b}$$

$$0 = \mathbf{b}_\mathrm{i}(\mathbf{x}(0),\mathbf{p}) \tag{2.18c}$$

$$0 = \mathbf{b}_\mathrm{t}(\mathbf{x}(\xi_\mathrm{f}),\mathbf{p}) \tag{2.18d}$$

$$0 \geq \mathbf{c}_\mathrm{p}(\mathbf{x}(\xi),\mathbf{u}(\xi),\mathbf{p},\xi) \tag{2.18e}$$

$$0 \geq \mathbf{c}_\mathrm{t}(\mathbf{x}(\xi_\mathrm{f}),\mathbf{u}(\xi_\mathrm{f}),\mathbf{p},\xi_\mathrm{f}) \tag{2.18f}$$

$$\Phi\mathbf{w} - \lambda\Phi\mathbf{e} = J - J^* \tag{2.18g}$$

Problem 2.16 has been reformulated in a maximisation problem, that looks for the maximum distance from any point $\bar{J}_\mathrm{p}$ in the CHIM along the quasi-normal towards the utopia point (Logist et al., 2009) (Logist et al., 2012). In Figure 2.2, these quasi-normal lines to the CHIM are clearly visible and the their intersections with the CHIM itself are the equally spread points $\bar{J}_\mathrm{p}$ (Logist et al., 2009).

With respect to the MOOCP 2.16, the additional Constraint 2.18g has been added: the vector $\mathbf{w}$ contains weights such that $\sum_{\mathrm{i}=1}^{\mathrm{m}} w_\mathrm{i} = 1$ and $w_\mathrm{i} \geq 0$. This last condition only holds for bi-objective optimisation problems, while for m ≥ 3, there is the possibility to have some $w_\mathrm{i} \leq 0$ (Das and Dennis, 1998). However, this will not be the case for this work, so from now on, it can be assumed that $w_\mathrm{i} \geq 0, \forall \mathrm{i}$. The vector $\mathbf{e}$ is a column vector of all one. Being negative, it is used to let all the quasi-normals, obtained by an equally weighted linear combination of the columns of Φ, pointing towards the origin (Das and Dennis, 1998).

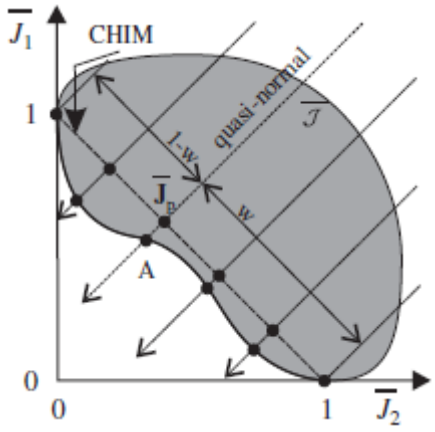

Figure 2.2: *Normal boundary intersection: geometric interpretation of the method. Gentle courtesy of Logist et al. (2009).*

The NBI method allows to find Pareto optimal points also in the concave part of the Pareto set and an even spread of weights **w** returns an even spread of Pareto points (Das and Dennis, 1998). A drawback anyway is still present: with the NBI method some non-Pareto optimal points might be found (Das and Dennis, 1998).

2.5.3 (Enhanced) Normalised normal constraint

Normalised normal constraint (NNC) (Messac et al., 2003) is the third and last scalarisation method for multi-objective opitmisation that will be discussed. Together with that, also its variant *enhanced NNC* (ENNC) (Sanchis et al., 2008) will be explained in this Section.

As for NBI, it is based on the definition of utopia point and *utopia hyperplane*, that can be assimilated to the CHIM. Anyway procedure and rationale for finding Pareto points, are different. The main idea, is to normalise each objective function J_i into a normalised form $\bar{J}_\mathrm{i}$. This normalisation for the ENNC case is explained later in this Section, in Equation 2.20. Important to know is that the main difference between ENNC and NNC is how the normalised objective functions $\bar{J}_\mathrm{i}$ are obtained (Logist et al., 2012). Since NNC will not be exploited for the practical work of this master thesis, only the ENNC normalised objective functions will be explained. The global minima of $\bar{J}_\mathrm{i}$, called *anchor points*, are all connected together forming the utopia hyperplane (Messac et al., 2003). This plane contains the evenly distributed points $\bar{J}_\mathrm{p}$, from which the Pareto optimals are obtained through successive optimisations (Messac et al., 2003) (Logist et al., 2009).

These optimisation problems can be rewritten as an optimal control problem where the goal is optimising only one of the multiple objectives, usually the most important one, while all other objective functions are considered by the addition of

m − 1 inequality constraints (Logist et al., 2009):

$$\underset{\mathbf{u}(\xi),\xi_\mathrm{f}}{\text{minimise}} \quad \bar{J}_\mathrm{k} \tag{2.19a}$$

$$\text{subject to} \quad \frac{d\mathbf{x}}{d\xi} = \mathbf{f}(\mathbf{x}(\xi), \mathbf{u}(\xi), \mathbf{p}, \xi) \qquad \xi \in [0, \xi_\mathrm{f}] \tag{2.19b}$$

$$0 = \mathbf{b}_\mathrm{i}(\mathbf{x}(0), \mathbf{p}) \tag{2.19c}$$

$$0 = \mathbf{b}_\mathrm{t}(\mathbf{x}(\xi_\mathrm{f}), , \mathbf{p}) \tag{2.19d}$$

$$0 \geq \mathbf{c}_\mathrm{p}(\mathbf{x}(\xi), \mathbf{u}(\xi), \mathbf{p}, \xi) \tag{2.19e}$$

$$0 \geq \mathbf{c}_\mathrm{t}(\mathbf{x}(\xi_\mathrm{f}), \mathbf{u}(\xi_\mathrm{f}), \mathbf{p}, \xi_\mathrm{f}) \tag{2.19f}$$

$$(\bar{J}(\mathbf{u}^*_\mathrm{k}, \xi^*_{\mathrm{f,k}}) - \bar{J}(\mathbf{u}^*_\mathrm{i}, \xi^*_{\mathrm{f,i}}))^\top (\bar{J}(\mathbf{u}, \xi_\mathrm{f}) - \bar{J}_\mathrm{p}) \leq 0 \qquad \mathrm{i} = 1 \ldots \mathrm{m}, \mathrm{i} \neq \mathrm{k} \tag{2.19g}$$

where the general term $\bar{J}_\mathrm{k}$ refers to the normalised objective function. Equation 2.19g represents the m − 1 additional inequality constraints, which are hyperplanes chosen through the beforehand selected points $\bar{J}_\mathrm{p}$, and orthogonal to the vectors connecting the anchor point of $\bar{J}_\mathrm{k}$ with all other anchor points.

In general, the normalisation of the objective functions is obtained by shifting the utopia point J^* in the origin of the system and multiply the shifted objectives with a matrix $\mathbf{T}$ (Logist et al., 2012):

$$\bar{J}(\mathbf{u}, \xi_\mathrm{f}) = \mathbf{T}(J(\mathbf{u}, \xi_\mathrm{f}) - J^*) \tag{2.20}$$

The matrix $\mathbf{T}$ is defined in different ways in NNC and ENNC. Throughout this work only the ENNC method will be exploited. It defines $\mathbf{T}$ as:

$$\mathbf{T} = \mathbf{E}(J(\mathbf{u}^*_\mathrm{i}, \xi^*_\mathrm{i}) - J^*) \tag{2.21}$$

with $\mathbf{E}$ a squared matrix having all zeros on the diagonal and all ones on the off-diagonal elements (Logist et al., 2009) (Logist et al., 2012).

In Figure 2.3 the geometric representation of the ENNC method is provided (Logist et al., 2009). The utopia hyperplane is represented by a single line, called *utopia line*, since only two normalised objective functions $\bar{J}_1$ and $\bar{J}_2$ are present. The additional inequality constraint is depicted as the line normal to the utopia line passing through the point $\bar{J}_\mathrm{p}$, while the restricted feasible set is depicted with the lighter colour.

As NBI, also the ENNC method is able to overcome the disadvantages of the WS. Unfortunately, also the same drawback of NBI, the possibility to return non-Pareto optimal points, is present. In order to overcome this drawback, a Pareto filter is often applied (Messac et al., 2003). This will be explained in the following Section.

2.5.4 Pareto filter

In order to remove non-Pareto optimal points from the Pareto set, a Pareto filter is applied (Messac et al., 2003). This is an algorithm based on Definition 3 and Definition 4 of global and local Pareto optimal points, respectively.

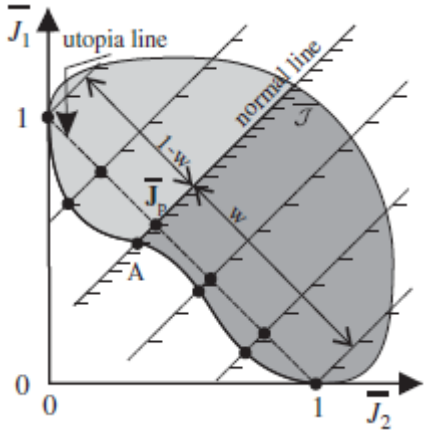

Figure 2.3: *(Enhanced) Normalized normal constraint: geometric interpretation of the method. Gentle courtesy of Logist et al. (2009).*

The Pareto filter algorithm compares each point generated by Problem 2.19 with all the others, discarding the non-global Pareto optimal. By doing this, the drawback of NBI and ENNC is circumvented (Messac et al., 2003). Interested readers can find more informations in Messac et al. (2003).

2.6 Robust optimal control formulation and solution

In the previous sections, it has been seen that, for both an OCP and a MOOCP, it is important to know the model equations describing the system. This is clear when looking at Equations 2.1b for an OCP and 2.16b for a MOOCP. In those equations, the dependence on the vector of parameters $\mathbf{p}$ is evident. Unfortunately, in some cases, these parameters are known with a degree of uncertainty. In real situations, this can be a problem when the calculated optimal trajectory for the OCP is close to one of the constraints of the system. In fact, even a small uncertainty over one of the parameters present in the model equation can cause the violation of that constraint, leading to problems in the real application.

Several examples can be found in the literature. In Houska et al. (2012) the maximisation of the conversion in a jacketed tubular reactor with an uncertainty on the heat transfer coefficient due to fouling was discussed. In Logist et al. (2011), a fed-batch bio-reactor is considered. In this last example, a MOOCP was solved, maximising the conflicting objectives yield and productivity, when considering an uncertainty over the substrate concentration in the feed.

In this work, three different solution methodologies for robust OCPs will be presented. It is, nevertheless, worth highlighting that all of them are approximations.

2.6.1 Worst-case approach

The general formulation of a robust OCP can be derived from Equation 2.1. From that, Equation 2.1b can be rewritten as (Logist et al., 2011) (Houska et al., 2012):

$$\frac{d\mathbf{x}}{d\xi} = \mathbf{f}(\mathbf{x}(\xi), \mathbf{u}(\xi), \mathbf{p}, \xi, \mathbf{w}(\xi)) \tag{2.22}$$

where an additional dependency $\mathbf{w}(\xi)$ is added. This represents the vector of uncertainties on the parameters of the model (Logist et al., 2011) (Houska et al., 2012). For the explanation of all other variables and terms in the equation, the reader is invited to go back to Section 2.2 and Equation 2.1. Moreover in order to simplify the following explanation, also the boundary conditions and the inequality constraints will be rearranged. Equation 2.1c, representing the boundary condition at $\xi = 0$ will be simply rewritten in the form (Houska et al., 2012) (Logist et al., 2011):

$$\mathbf{x}(0) = \mathbf{x}_0 \tag{2.23}$$

Equations 2.1e and 2.1f, instead are merged in a single inequality constraint defined as (Logist et al., 2011):

$$0 \geq \mathbf{h}_\mathrm{i}(\mathbf{x}(\xi), \mathbf{u}(\xi), \mathbf{p}, \xi) \qquad \forall \xi \in \Xi_\mathrm{i}(\xi_\mathrm{f}) \tag{2.24}$$

Here the inequality constraints $\mathbf{h}_\mathrm{i}$ are considered as path or terminal constraints depending on the definition of $\Xi_\mathrm{i}(\xi_\mathrm{f}) \subseteq [0, \xi_\mathrm{f}]$ (Logist et al., 2011).

Often, as it was in Logist et al. (2011), uncertainties can be present also on the initial values $\mathbf{x}_0$. For this reason, usually all possible uncertainties are described by the set $(\mathbf{x}_0, \mathbf{w}) \in \mathbf{W}$. This set is usually considered bounded and given (Logist et al., 2011).

Assuming that the solution of Equation 2.22 has a unique solution, the state $\mathbf{x}(\xi)$ can be rewritten as

$$\mathbf{x}(\xi) = \zeta[\xi, \mathbf{x}_0, \mathbf{u}(\xi), \mathbf{p}, \mathbf{w}(\xi)] \qquad \forall \xi \in [0, \xi_\mathrm{f}] \tag{2.25}$$

The robust OCP can then be written with a min-max or worst-case formulation (Logist et al., 2011):

$$\underset{\mathbf{x}(\xi), \mathbf{u}(\xi), \mathbf{p}, \xi_\mathrm{f}}{\text{minimise}} \quad J(\mathbf{x}(\xi), \mathbf{u}(\xi), \mathbf{p}, \xi_\mathrm{f}) \tag{2.26a}$$

$$\text{subject to} \quad \max_{(\mathbf{x}_0, \mathbf{w}) \in \mathbf{W}} \quad \mathbf{h}_\mathrm{i}(\mathbf{u}(\xi), \mathbf{p}, \xi, \zeta[\xi, \mathbf{x}_0, \mathbf{u}(\xi), \mathbf{p}, \mathbf{w}(\xi)]) \tag{2.26b}$$

where all constraints in Equation 2.26b are called robust counterpart functions. For this reason, Equation 2.26 is also called the robust counterpart problem. Note that all constraints of Problem 2.26 are not dependent from the differential states $\mathbf{x}$.

This problem can be solved with different methodologies, but only linearisation strategies will be explained here. In this approach, a higher order Taylor expansion of

the model functions is computed with respect to the uncertainties. Of this expansion, only the first term is taken in consideration, while all the higher order terms are neglected. This approximation is legitimate in the case of small uncertainties with respect to the model curvature (Ma and Braatz, 2001) (Logist et al., 2011). Other solution methods for the robust counterpart Problem 2.26 are presented in Houska and Diehl (2009) and will not be discussed here.

Following the linearisation strategy, Equation 2.22 can be split in a reference and a deviation model equation as follows (Logist et al., 2011):

$$\frac{d}{d\xi}\mathbf{x}_{\text{ref}}(\xi) = \mathbf{f}(\mathbf{x}_{\text{ref}}(\xi), \mathbf{u}(\xi), \mathbf{p}, \xi, \mathbf{w}_{\text{ref}}) \qquad \mathbf{x}_{\text{ref}}(0) = \mathbf{x}_0^{\text{ref}} \tag{2.27a}$$

$$\frac{d}{d\xi}\delta\mathbf{x}(\xi) = \mathbf{A}(\xi)\delta\mathbf{x}(\xi) + \mathbf{B}(\xi)\delta\mathbf{w}(\xi) \qquad \delta\mathbf{x}(0) = \mathbf{B}_0\delta\mathbf{w}_0 \tag{2.27b}$$

where $\mathbf{x}_{\text{ref}}$ and $\delta\mathbf{x}$ are respectively the reference trajectory and deviation defined such that $\mathbf{x} = \mathbf{x}_{\text{ref}} + \delta\mathbf{x}$. It is important to be aware that the linear Approximation 2.27 is valid only for small uncertainties $\mathbf{w}(\xi)$ (Logist et al., 2011). The terms $\mathbf{A}(\xi)$ and $\mathbf{B}(\xi)$ are introduced, together with two other short notations used in Logist et al. (2011), $\mathbf{C}_{\text{i}}(\xi)$ and $\mathbf{d}_{\text{i}}(\xi)$ as follows:

$$\mathbf{A}(\xi) = \frac{\partial}{\partial\mathbf{x}}\mathbf{f}(\mathbf{x}_{\text{ref}}(\xi), \mathbf{u}(\xi), \mathbf{p}, \xi, \mathbf{w}_{\text{ref}}) \tag{2.28a}$$

$$\mathbf{B}(\xi) = \frac{\partial}{\partial\mathbf{w}}\mathbf{f}(\mathbf{x}_{\text{ref}}(\xi), \mathbf{u}(\xi), \mathbf{p}, \xi, \mathbf{w}_{\text{ref}}) \tag{2.28b}$$

$$\mathbf{C}_{\text{i}}(\xi) = \frac{\partial}{\partial\mathbf{x}}\mathbf{h}_{\text{i}}(\mathbf{x}_{\text{ref}}(\xi), \mathbf{u}(\xi), \mathbf{p}, \xi, \mathbf{w}_{\text{ref}}) \tag{2.28c}$$

$$\mathbf{d}_{\text{i}}(\xi) = \mathbf{h}_{\text{i}}(\mathbf{x}_{\text{ref}}(\xi), \mathbf{u}(\xi), \mathbf{p}, \xi) \tag{2.28d}$$

These terms will be used in the linear approximation of the robust counterpart problem. This approximation can be obtained through the use of *Lyapunov function* (Kalman, 1963) when the uncertainty set $\mathbf{W}$ is modelled as a *ball* of size $\Gamma \in \Re^+$ (Houska et al., 2012). This is proven in Houska and Diehl (2009). What is important is that, through this approximation, the robust counterpart Problem 2.26 can be approximated as follows:

$$\underset{\mathbf{x}_{\text{ref}}(\xi),\mathbf{u}(\xi),\mathbf{p},\xi_{\text{f}},\mathbf{P}(\xi)}{\text{minimise}} \quad J(\mathbf{x}(\xi), \mathbf{u}(\xi), \mathbf{p}, \xi_{\text{f}}) \tag{2.29a}$$

$$\text{subject to} \quad \frac{d}{d\xi}\mathbf{f}(\mathbf{x}_{\text{ref}}(\xi), \mathbf{u}(\xi), \mathbf{p}, \xi, \mathbf{w}_{\text{ref}}) \qquad \forall\xi \in [0, \xi_{\text{f}}] \tag{2.29b}$$

$$\mathbf{x}_{\text{ref}}(0) = \mathbf{x}_0 \tag{2.29c}$$

$$\frac{d}{d\xi}\mathbf{P}(\xi) = \mathbf{A}(\xi)\mathbf{P}(\xi) + \mathbf{P}(\xi)\mathbf{A}(\xi)^\top + \mathbf{B}(\xi)\mathbf{B}(\xi)^\top \tag{2.29d}$$

$$\mathbf{P}(0) = \mathbf{B}(0)\mathbf{B}(0)^\top \tag{2.29e}$$

$$0 \geq \mathbf{d}_{\text{i}}(\xi) + \Gamma\sqrt{\mathbf{C}_{\text{i}}(\xi)\mathbf{P}(\xi)\mathbf{C}_{\text{i}}(\xi)^\top} \qquad \forall\xi \in \Xi_{\text{i}}(\xi_{\text{f}}) \tag{2.29f}$$

In Problem 2.29, $\mathbf{P}$ is a matrix valued function that satisfies a Lyapunov differential Equation 2.29d with initial Conditions 2.29e for all $\xi \in [0, \xi_f]$ (Logist et al., 2011). This matrix, introduces a significant amount of additional differential states to the system. In fact, the number of total states in Problem 2.29 increases quadratically with the number of original states, due to the matrix $\mathbf{P}$. Being the matrix $\mathbf{P}$ symmetric, the total amount of additional states is $\frac{N_x(N_x+1)}{2}$ with N_x the number of states present in the original OCP. This will also lead to much higher computational efforts in order to solve the robust OCP, with respect to the non-robustified original OCP.

A last important thing to notice is that Equation 2.29f describes inequality constraints for the linear approximated problem. With respect to the original ones of Equations 2.24 and 2.28d, the new constraints are stricter, due to the presence of an additional term. This term introduces a supplementary back-off value or safety margin, related to the size Γ of the set $\mathbf{W}$, which is needed to meet the constraints without exceeding them (Logist et al., 2011).

2.6.2 Sigma points approximation

As already said, also other methods for taking into account uncertainties on the system parameters exist. In this Section, a second approach will be investigated. From here on, it will be referred to this method as the *sigma points approach* (Julier and Uhlmann, 1996) (Recker et al., 2012). Before applying the sigma points approach, it is necessary to know the distribution of the uncertain parameters (Julier and Uhlmann, 1996). In this work, these parameters will be considered to have a gaussian distribution with mean values equal to the nominal values $\mathbf{p}$, used for the non-robustified Problem 2.1. The variance-covariance matrix $\mathbf{V}$ of those distributions will be assumed and decided by the user. In this thesis, the matrix $\mathbf{V}$ will always be assumed as diagonal.

The method can be easily implemented and the explanation given will be based on Julier and Uhlmann (1996). At first, the sigma points have to be established. For each uncertain parameter j, two sigma points are identified through (Julier and Uhlmann, 1996):

$$\sigma_{j,i} = \pm\sqrt{(n_p + k)V_{pp}} \qquad \forall i = 1,2 \qquad \forall j \in [1, n_p] \tag{2.30}$$

where n_p is the number of uncertain parameters and $k = 3 - n_p$. This factor allows the exploitation of the knowledge on higher order moments of the parameters distributions (Julier and Uhlmann, 1996). However, for the purpose of this work only the first two moments, namely the mean and the variance-covariance matrix will be of relevance. Any further explanation can be found in Julier and Uhlmann (1996).

From Equation 2.30, $2n_p + 1$ sets of parameters are constructed:

$$\mathbf{p}_0 = \mathbf{p} \tag{2.31a}$$

$$\mathbf{p}_{j,i} = \left[p_1,\ p_2,\ \ldots,\ p_j + \sigma_{j,i},\ \ldots,\ p_{n_p}\right] \qquad \forall i = 1,2 \qquad \forall j \in [1, n_p] \tag{2.31b}$$

where Equation 2.31b represents $2n_\mathrm{p}$ parameters set where, in turn, each parameter j is modified by adding the terms $\sigma_{\mathrm{j,i}}$ of Equation 2.30. The factor 2 is present because on each parameter there can be either a positive or negative uncertainty, as shown by the values of sigma in Equation 2.30. Equation 2.31a represents the nominal case, when no manipulation are made on the parameters values. After this, $2n_\mathrm{p}+1$ dynamic systems are solved. Each of the $2n_\mathrm{p}$ systems is referring to a system where the uncertainty over one single parameter is taken, according to Equation 2.31b. These problems will give raise to $2n_\mathrm{p}$ solutions, that will be called $\mathbf{Y}_\mathrm{i}$, with $\mathrm{i} \in [1, 2n_\mathrm{p}]$ (Julier and Uhlmann, 1996). The remaining dynamic system is the nominal one, where all parameters are assumed to be known and correct, as in Equation 2.31a, and its solution will be called $\mathbf{Y}_0$ (Julier and Uhlmann, 1996).

Next is the evaluation of the expected values of the states, based on the results of the previous systems. They can be calculated as

$$\bar{\mathbf{y}} = \frac{1}{n_\mathrm{p}+\kappa}\left(\kappa\mathbf{Y}_0 + \frac{1}{2}\sum_{\mathrm{i}=1}^{2n_\mathrm{p}}\mathbf{Y}_\mathrm{i}\right) \tag{2.32}$$

Once the expected values are calculated, their own variance-covariance matrix needs to be found. This is computed through the following relation (Julier and Uhlmann, 1996):

$$\mathbf{P} = \frac{1}{n_\mathrm{p}+\kappa}\left(\kappa[\mathbf{Y}_0-\bar{\mathbf{y}}][\mathbf{Y}_0-\bar{\mathbf{y}}]^\top + \frac{1}{2}\sum_{\mathrm{i}=1}^{2n_\mathrm{p}}[\mathbf{Y}_\mathrm{i}-\bar{\mathbf{y}}][\mathbf{Y}_\mathrm{i}-\bar{\mathbf{y}}]^\top\right) \tag{2.33}$$

$\mathbf{P}$ is a squared matrix with dimension equal to the number of states involved in the system. From the squared matrix $\mathbf{P}$, new constraints are built for the expected values $\bar{\mathbf{y}}$. For each expected state, $\bar{y}_\mathrm{i}$, it is asked for the quantity

$$\bar{y}_\mathrm{i} \pm q\sqrt{\mathrm{P_{ii}}} \tag{2.34}$$

to be, at every time, within the upper and lower bounds given for the state i. The factor q depends on the confidence required and, in turn, on the decision of the user.

In this case, the estimated objective function $\bar{J}(\bar{\mathbf{y}}(\xi), \mathbf{u}(\xi), \mathbf{p}, \xi_\mathrm{f})$ will be a function of the expected values $\bar{\mathbf{y}}$. However, an alternative formulation to this one is present in the literature (Logist et al., 2011). The problem, in fact, might also account for the uncertainty over the objective itself, which can be reformulated as

$$\bar{J}(\bar{\mathbf{y}}(\xi), \mathbf{u}(\xi), \mathbf{p}, \xi_\mathrm{f}) + \tau\sqrt{\mathrm{P_{JJ}}} \tag{2.35}$$

where τ depends on the confidence required from the user, as it is for q. The roles of the factors q and τ will be better explained in the course of this text.

Finally, it is important to highlight that, although the methodology for the sigma points approach has been presented in a sequential way, the steps presented must be

done together in the optimisation problem. This means that the solution of the $2n_\mathrm{p}+1$ dynamic systems, the computation of the estimate and of the variance-covariance matrix and the addition of the new constraints are all implemented in the same optimisation problem.

This simultaneous implementation will increase the computational effort with respect to the non-robustified problem. The totality of states involved in such approximation is in fact $(2n_\mathrm{p}+1)N_\mathrm{x}$. However, it should be highlighted that the amount of additional states is linear with respect to the original number of states in the sigma points approach and quadratic in the linearisation approach. The direct consequence is that, in the case of a single uncertain parameter, the sigma points approximation leads to a final robust OCP smaller than the linear approximation. Nevertheless, due to the fact that several uncertainties can be dealt with, the overall amount of states for the sigma points approximation is also linearly depending on n_p. At this stage, however, the linear approximation with respect to more than one uncertain parameter is rather complicated. For this reason, a revision of the linear approximation, where also more than one uncertain parameter can be dealt with in a clear procedure, will be given in Section 2.6.3.

2.6.3 A new linear approximation

In Sections 2.6.1 and 2.6.2, two robustification approaches were introduced. Unfortunately, at this stage, it is not yet possible to make a fair comparison between them. In this Section, a new formulation for the linearisation approach, based on Srinivasan et al. (2003), Houska and Diehl (2009) and Logist et al. (2011) is presented. The development of this new linearisation method is given in Srinivasan et al. (2003). What is important to remark is that this new formulation allows a comparison between the sigma points and the linearisation approaches for robust OC.

The main difference with the approach described in Section 2.6.1 is that, with this new approximation approach, the variance-covariance matrix $\mathbf{V}$ of the uncertain parameters is directly entering the robust OCP. With the old approach, this was not possible and the user had to introduce a robustification parameter Γ, which was related to the size of the uncertainty set $\mathbf{W}$ (Houska and Diehl, 2009) (Houska et al., 2012). Equations 2.29d and 2.29e are rewritten in the following formulation (Srinivasan et al., 2003):

$$\frac{d}{d\xi}\mathbf{P}(\xi) = \mathbf{A}(\xi)\mathbf{P}(\xi) + \mathbf{P}(\xi)\mathbf{A}(\xi)^\top + \mathbf{B}(\xi)\mathbf{V}\mathbf{B}(\xi)^\top \tag{2.36a}$$

$$\mathbf{P}(0) = \mathbf{B}(0)\mathbf{V}\mathbf{B}(0)^\top \tag{2.36b}$$

By changing the formulation of the Lyapunov states, also the additional Constraint 2.29f has to be rewritten. The new formulation is similar to Equation 2.34:

$$0 \geq \mathbf{d}_\mathrm{i}(\xi) + q\sqrt{\mathbf{C}_\mathrm{i}(\xi)\mathbf{P}(\xi)\mathbf{C}_\mathrm{i}(\xi)^\top} \tag{2.37}$$

The matrices $\mathbf{A}$, $\mathbf{B}$, $\mathbf{C}_\mathrm{i}$ and the vector $\mathbf{d}_\mathrm{i}$ are expressed as in Equation 2.28 where the term $\mathbf{p}$ now represents the row vector with the mean values of all the uncertain parameters considered.

The new OCP can then be rewritten as

$$\underset{\mathbf{x}_\mathrm{ref}(\xi),\mathbf{u}(\xi),\mathbf{p},\xi_\mathrm{f},\mathbf{P}(\xi)}{\text{minimise}} \quad J(\mathbf{x}(\xi),\mathbf{u}(\xi),\mathbf{p},\xi_\mathrm{f}) \tag{2.38a}$$

$$\text{subject to} \quad \frac{d}{d\xi}\mathbf{f}(\mathbf{x}_\mathrm{ref}(\xi),\mathbf{u}(\xi),\mathbf{p},\xi,\mathbf{w}_\mathrm{ref}) \qquad \forall \xi \in [0,\xi_\mathrm{f}] \tag{2.38b}$$

$$\mathbf{x}_\mathrm{ref}(0) = \mathbf{x}_0 \tag{2.38c}$$

$$\frac{d}{d\xi}\mathbf{P}(\xi) = \mathbf{A}(\xi)\mathbf{P}(\xi) + \mathbf{P}(\xi)\mathbf{A}(\xi)^\top + \mathbf{B}(\xi)\mathbf{V}\mathbf{B}(\xi)^\top \tag{2.38d}$$

$$\mathbf{P}(0) = \mathbf{B}(0)\mathbf{V}\mathbf{B}(0)^\top \tag{2.38e}$$

$$0 \geq \mathbf{d}_\mathrm{i}(\xi) + q\sqrt{\mathbf{C}_\mathrm{i}(\xi)\mathbf{P}(\xi)\mathbf{C}_\mathrm{i}(\xi)^\top} \qquad \forall \xi \in \Xi_\mathrm{i}(\xi_\mathrm{f}) \tag{2.38f}$$

It is important to notice the improvements of the linear approximation introduced in this Section with respect to that one given in Section 2.6.1.

First of all, a comparison between the linear approximation and the sigma points approximation is now possible. This can be done by choosing the same factor q, which depends on the confidence required from the user, for the additional Constraints 2.34 and 2.37.

Moreover, the mean values and the variance-covariance matrix of the uncertain parameters are now directly entering the problem, making it possible to exploit knowledge available from parameter estimation.

Lastly, with the old linear approximation given in Section 2.6.1, handling more than one uncertain parameter was not straight-forward. With the introduction of the variance-covariance matrix $\mathbf{V}$ into the OCP 2.38, the investigation of more than one uncertain parameter is made definitely easier.

This last point also allows to make an additional observation. In fact, the size of the robust OCP for the linear approximation does not depend on the number of uncertain parameters. Once the Lyapunov expansion and the additional states have entered the OCP, the amount of uncertain parameters will only influence the size of the matrices $\mathbf{V}$ and $\mathbf{B}$, but the additional Lyapunov states remain $\frac{N_\mathrm{x}(N_\mathrm{x}+1)}{2}$, as in Section 2.6.1. However, this is not true for the sigma points approximation where, as explained in Section 2.6.2, $2n_\mathrm{p}+1$ dynamic systems have to be solved, leading to $(2n_\mathrm{p}+1)N_\mathrm{x}$ states. Thus, it can be concluded that the sizes of the OCPs solved through the sigma points approach grow linearly with the number of uncertain parameters, while they are fixed for the linearisation approach. This is of course

expected to influence heavily the computational time and effort for the solution of the robust OCPs.

2.7 Conclusion

Optimal control was presented in this Chapter. Together with that, the theory background necessary to handle and solve optimal control problems was presented.

Due to the high dimensionality of the systems that will be handled throughout this work, direct approaches will be preferred over state space and indirect ones in order to solve OCPs. In particular the orthogonal collocation method is adopted.

Moreover, two recent variations of OC were addressed. These are multi-objective optimal control problem and robust OCP. MOOCP in particular arises from the need of chemical industries to still achieve high productivities while trying to minimise costs related to energy or raw material consumption, or pollutant emissions. All methods presented for solving MOOCP, namely WS, NBI and ENNC, will be exploited for generating the Pareto sets of the case studies that will be investigated. Robust optimal control, instead, comes from the necessity to cope with uncertainties in the process model equations, to still ensure safe operations. As anticipated, this will lead to lower performances of the investigated system and higher computational effort, due to the increased number of differential states. In this work, both the linearisation approach and the sigma points approach will be exploited and a comparison between the two will be made.

Materials and methods

Chapter 3

Materials and Methods

3.1 Introduction

The aim of this chapter is three-fold. First of all, in Section 3.2, the software exploited in all this thesis will be introduced and described.

Afterwards, in Section 3.3, the model equations and the OCPs of three investigated case studies will be presented. These are a fed-batch bio-reactor (Logist et al., 2009), a jacketed tubular reactor (Logist et al., 2011) (Houska et al., 2012) and the Williams-Otto reactor (Williams and Otto, 1960) (Forbes, 1994). In this Chapter only the systems dynamics of these problems will be given, with the aim to introduce them to the reader. The results of the optimisation problems and the conclusions that can be drawn based on them will be reported in Chapters 4 and 5. Moreover, the results presented in Chapter 5, will deal with the comparison between the linear and the sigma points approximations for robust OC. Before that, however, it is necessary to explain in detail the procedure that will be followed. This will be given and explained in Section 3.4.

Section 3.5 will then conclude this Chapter, highlighting the main issues that will arise in the following sections.

3.2 Software

In order to solve the optimisation problems encountered during this thesis, the exploitation of numeric computation is fundamental. In fact, all the models of the systems considered in this master thesis work involve highly non-linear expressions. For this reason specific programmes and algorithms for optimisation are used together, exploiting their features at best.

The first and most important tool-kit used is *Pomodoro*. This new software tool has been developed within the BioTeC division of KULeuven, in order to solve optimal control problems. It allows the solution of numerical optimisation problems by exploiting the orthogonal collocation method. Together with that, also MOOCP

can be solved. The WS, NBI and ENNC method are available as a choice for the user. As it was seen in the previous Chapter, all these methods imply a partition of MOOCPs into parametric single objective problems. Thus, the same algorithm for single optimisation can be exploited for the solution of both OCPs and MOOCPs. The major difference is that for MOOCPs, the problem is solved several times, depending on the number of Pareto optimals required from the user. This of course means, in general, that higher computational times are needed for solving MOOCPs than OCPs.

However, Pomodoro is not meant to calculate also gradients of the functions involved in the problem. These functions are the objectives and the equality and inequality constraints. In order to calculate the Jacobians and Hessians, *CasADi* is called (Andersson et al., 2012). The gradients of the functions are then calculated through automatic differentiation.

As anticipated in Section 2.3 the NLP within the optimisation problems are solved using the interior point method. This is done through *IPOPT* (Interior Point OPTimizer) (Wächter and Biegler, 2006). This package is already implemented in *CasADi*. The interior point method is not explained in this work, but interested readers can find more information in Wächter and Biegler (2006).

Finally, *ACADO Toolkit* is employed. This tool for optimisation and optimal control does not come into play when solving OCPs with Pomodoro. However, being a tool-kit which has already been assessed in the literature, it can be used as a bench-mark to verify the solutions obtained with Pomodoro. It is important to highlight that this tool-kit allows to solve OCPs by exploiting direct single shooting and direct multiple shooting, while, as already stated, Pomodoro is exploiting direct orthogonal collocation.

Lastly, information about the computational power available should be provided. All the optimisation problems presented in this thesis have been solved exploiting a 8×3.40 GHz processor and 15.6 GiB RAM computer.

3.3 Case Studies

In this section, the systems dynamics of three case studies taken from the literature are presented. These examples are only introduced in this Chapter, but will be deeply investigated in Chapters 4 and 5. Together with the equation models, also the optimal control problems that need to be solved will be given, in their nominal formulation.

3.3.1 Fed-batch bio-reactor

The first case presented is the multi-objective optimal control problem of a fed-batch bio-reactor for lysine production (Logist et al., 2009) which is already present in the ACADO Toolkit database. The system dynamics which are optimised are slightly

different from the ones present in the original reference (Logist et al., 2009). In fact, they are taken from the ACADO Toolkit library, where an additional state is present. This choice has been taken due to the fact that, as already anticipated in Section 3.2, the results obtained with Pomodoro need to be validated through a comparison with those obtained with ACADO Toolkit. This can be done, of course, only if the system dynamics are the same for both implementations.

Problem 3.1 shows the differential equations governing this system:

$$\frac{dx_1}{dt} = +\mu x_1 \tag{3.1a}$$
$$\frac{dx_2}{dt} = -\sigma x_1 + uC_{\mathrm{s,f}} \tag{3.1b}$$
$$\frac{dx_3}{dt} = +\pi x_1 \tag{3.1c}$$
$$\frac{dx_4}{dt} = +u \tag{3.1d}$$
$$\frac{dx_5}{dt} = 0.001\left(u^2 + 0.01t_{\mathrm{f}}\right)^2 \tag{3.1e}$$

where x_1[g] represents the amount of biomass in the bio-reactor, x_2[g] the amount of substrate available for the biomass growth, x_3[g], the amount of product lysine, x_4[L] the liquid volume in the bio-reactor. x_5 is an artificial state which has been introduced to reduce control fluctuations. The control of the system is in fact the inlet feed $u\left[\frac{\mathrm{L}}{\mathrm{s}}\right]$ and too many rapid fluctuations can cause damages to the feed pump. t_{f}[s] is the time needed for the reaction. It is kept as an additional degree of freedom to the system, although it can only vary between two fixed values, as seen from Equations 3.3f and 3.4g. $C_{\mathrm{s,f}}\left[\frac{\mathrm{mol}}{\mathrm{L}}\right]$ is the substrate concentration at the inlet feed u and its value is taken constant and equal to $2.8\left[\frac{\mathrm{mol}}{\mathrm{L}}\right]$.

Some intermediate states are present and defined as follows

$$\mu = \frac{0.125x_1}{x_3} \tag{3.2a}$$
$$\sigma = \frac{\mu}{0.135} \tag{3.2b}$$
$$\pi = -384\mu^2 + 134\mu \tag{3.2c}$$

These states represent the biomass growth rate $\mu\left[\frac{1}{\mathrm{h}}\right]$, the substrate consumption for both growth and maintenance of the biomass $\sigma\left[\frac{\mathrm{g_{substrate}}}{\mathrm{g_{biomass}\ h}}\right]$ and the lysine production rate $\pi\left[\frac{\mathrm{g_{lysine}}}{\mathrm{g_{biomass}\ h}}\right]$ (Logist et al., 2009).

The problem requires an investigation of the Pareto set for the two conflicting objectives of maximising productivity and maximising yield. This is done in two separate cases, each of them with a different definition of the two objective functions.

3.3.1.1 Fed-batch bio-reactor 1

In the first case, no regularisation term is considered in the objective functions and, following the general formulation for a multi-objective optimal control Problem 2.16, the problem is implemented as

$$\underset{\mathbf{x}(t),u(t),\mathbf{p},t_\mathrm{f}}{\text{minimise}} \quad \left\{ J_1 = -\frac{x_3\left(t_\mathrm{f}\right)}{t_\mathrm{f}}, J_2 = -\frac{x_3\left(t_\mathrm{f}\right)}{\left(C_{\mathrm{s,f}} x_4\left(t_\mathrm{f}\right) - x_2\left(t_\mathrm{f}\right)\right)} \right\} \tag{3.3a}$$

$$\text{subject to} \quad \frac{d\mathbf{x}}{dt} = \mathbf{f}(\mathbf{x}(t), u(t), \mathbf{p}, t_\mathrm{f}) \tag{3.3b}$$

$$\mathbf{x}(0) = [0.1,\ 14,\ 5,\ 0,\ 0] \tag{3.3c}$$

$$[0,\ 0,\ 0,\ 5] \leq [x_1(t),\ x_2(t),\ x_3(t),\ x_4(t)] \leq [15,\ 30,\ 1000,\ 20] \tag{3.3d}$$

$$0 \leq u(t) \leq 2 \tag{3.3e}$$

$$20\mathrm{h} \leq t_\mathrm{f} \leq 40\mathrm{h} \tag{3.3f}$$

with J_1 the productivity and J_2 the yield. Equation 3.3b accounts for the model constraints described in Equations 3.1 and 3.2.

It is important to notice that, although the objective functions are both maximisations, in the OCP formulation, they are presented as minimisations, by adding a minus sign in front of both expressions. This is done due to the fact that only minimisation problems can be treated with Pomodoro and ACADO Toolkit.

3.3.1.2 Fed-batch bio-reactor 2

In the second case, a small regularisation term is taken into account and an additional constraint on the liquid volume in the reactor at the final time, $x_4(t_\mathrm{f})$, is imposed:

$$\underset{\mathbf{x}(t),u(t),\mathbf{p},t_\mathrm{f}}{\text{minimise}} \quad \left\{ J_1 = -\frac{x_3\left(t_\mathrm{f}\right)}{t_\mathrm{f}} + 0.01 x_5\left(t_\mathrm{f}\right), J_2 = -\frac{x_3\left(t_\mathrm{f}\right)}{\left(C_{\mathrm{s,f}}(x_4\left(t_\mathrm{f}\right) - 5)\right)} + 0.01 x_5\left(t_\mathrm{f}\right) \right\} \tag{3.4a}$$

$$\text{subject to} \quad \frac{d\mathbf{x}}{dt} = \mathbf{f}(\mathbf{x}(t), u(t), \mathbf{p}, t_\mathrm{f}) \tag{3.4b}$$

$$\mathbf{x}(0) = [0.1,\ 14,\ 5,\ 0,\ 0] \tag{3.4c}$$

$$[0,\ 0,\ 0,\ 5] \leq [x_1(t),\ x_2(t),\ x_3(t),\ x_4(t)] \leq [15,\ 30,\ 1000,\ 20] \tag{3.4d}$$

$$x_4(t_\mathrm{f}) \geq 5 + \frac{20}{C_{\mathrm{s,f}}} \tag{3.4e}$$

$$0 \leq u(t) \leq 2 \tag{3.4f}$$

$$20\mathrm{h} \leq t_\mathrm{f} \leq 40\mathrm{h} \tag{3.4g}$$

Again J_1 and J_2 are respectively the productivity and the yield, although they are defined differently from the case fed-batch 1. As for the case fed-batch 1, Equation 3.4b is a short-cut notation representing the model Constraints 3.1 and 3.2.

3.3.2 Jacketed tubular reactor

In this section, a second case study is presented. The system investigated is a jacketed tubular reactor (Logist et al., 2011) (Houska et al., 2012) where an irreversible and exothermic reaction A $\longrightarrow$ B is taking place. The reactor is working in steady state conditions and heat removal or supply are possible by controlling the temperature of the jacket fluid (Logist et al., 2011) (Houska et al., 2012).

The system dynamics consist of 3 differential equations in the spatial coordinate z, which are represented in Problem 3.5. These are dimensionless equations. Readers further interested in the original differential system and how the dimensionless parameters α, β, γ and δ are calculated are referred to Logist et al. (2011) and Houska et al. (2012).

$$\frac{dx_1(z)}{dz} = \frac{\alpha}{v}\left(1 - x_1\left(z\right)\right) e^{\frac{\gamma x_2(z)}{1+x_2(z)}} \tag{3.5a}$$

$$\frac{dx_2(z)}{dz} = \frac{\alpha\delta}{v}\left(1 - x_1\left(z\right)\right) e^{\frac{\gamma x_2(z)}{1+x_2(z)}} + \frac{\beta}{v}(u(z) - x_2(z)) \tag{3.5b}$$

$$\frac{dx_3(z)}{dz} = \frac{\beta}{z_\mathrm{f}}(u(z) - x_2(z)) \tag{3.5c}$$

$x_1(z)$, $x_2(z)$ and $x_3(z)$ respectively represent the product molar fraction, the dimensionless reactor temperature and the scaled heat exchanged with the jacket. The manipulated variable $u(z)$, is the dimensionless jacket fluid temperature. For the sake of completeness, the values of $C_{\mathrm{A,in}}$, T_{in} and of the fluid velocity v are given as $0.02\left[\frac{\mathrm{mol}}{\mathrm{L}}\right]$, $340\,[\mathrm{K}]$ and $0.1\left[\frac{\mathrm{m}}{\mathrm{s}}\right]$ respectively.

Equations 3.5 will enter as model constraints for the optimal control Problem 3.6.

$$\underset{\mathbf{x}(z),u(z),\mathbf{p},z_\mathrm{f}}{\text{minimise}} \quad 100 \cdot C_{\mathrm{A,in}}\left(1 - x_1(z_\mathrm{f})\right) \tag{3.6a}$$

$$\text{subject to} \quad \frac{d\mathbf{x}}{dz} = \mathbf{f}(\mathbf{x}(z), u(z), \mathbf{p}, z_\mathrm{f}) \tag{3.6b}$$

$$\mathbf{x}(0) = [0,\ 0,\ 0] \tag{3.6c}$$

$$\left[0,\ \frac{280 - T_{\mathrm{in}}}{T_{\mathrm{in}}}\right] \leq [x_1(z),\ x_2(z)] \leq \left[1,\ \frac{400 - T_{\mathrm{in}}}{T_{\mathrm{in}}}\right] \tag{3.6d}$$

$$\frac{280 - T_{\mathrm{in}}}{T_{\mathrm{in}}} \leq u(z) \leq \frac{400 - T_{\mathrm{in}}}{T_{\mathrm{in}}} \tag{3.6e}$$

$$C_{\mathrm{A,in}}\left(1 - x_1(z_\mathrm{f})\right) \leq 0.002 \tag{3.6f}$$

$$0.5 \leq z_\mathrm{f} \leq 1 \tag{3.6g}$$

The objective function of Problem 3.6 is the minimisation of the concentration of reactant A at the end of the reactor. This objective can be interpreted as the maximisation of the reactant conversion. Some constraints are present both on the states and on the control. Equation 3.6d gives the upper and lower bounds for the states $x_1(z)$ and $x_2(z)$. The state $x_3(z)$ is unbounded. Equations 3.6e and 3.6f

respectively demand the control action to be always within an upper and lower boundaries and a final conversion of at least 90%. Equation 3.6g gives boundaries for the total length of the reactor, which is taken as additional degree of freedom.

3.3.3 Williams-Otto reactor

The third and last case study that is described in this Chapter, is the Williams-Otto fed-batch reactor, originally introduced by Williams and Otto (1960) and then modified by, e.g. Forbes (1994), Hannemann and Marquardt (2010) and Logist et al. (2012). The formulation considered for this master thesis is taken from Hannemann and Marquardt (2010) and Logist et al. (2012).

The system dynamics are more complicated than those of the previous cases. As a matter of fact, more than one reaction are taking place inside the reactor, with the following reaction scheme:

$$A + B \rightarrow C \tag{3.7a}$$
$$C + B \rightarrow P + E \tag{3.7b}$$
$$P + C \rightarrow G \tag{3.7c}$$

A and B are the reagents of the system, C is an intermediate in the formation of the products P and E, while G is a side product. The reagent A is initially present in the reactor, while B is continuously added through the control action $u_1(t) = \mathrm{F_{B,in}}(t)$, which represents the feed rate of B. Together with $\mathrm{F_{B,in}}(t)$, another control action is present, $u_2(t) = \mathrm{T_W}(t)$, where $\mathrm{T_W}$ is the dimensionless cooling water temperature (Hannemann and Marquardt, 2010) (Logist et al., 2012).

The dynamic model describing the system is shown in Equation 3.8:

$$\frac{dx_\mathrm{A}}{dt} = \frac{x_\mathrm{A} u_1}{1000 V_\mathrm{R}} - k_1 \eta_1 x_\mathrm{A} x_\mathrm{B} \tag{3.8a}$$
$$\frac{dx_\mathrm{B}}{dt} = \frac{(1 - x_\mathrm{B}) u_1}{1000 V_\mathrm{R}} + k_1 \eta_1 x_\mathrm{A} x_\mathrm{B} - k_2 \eta_2 x_\mathrm{B} x_\mathrm{C} \tag{3.8b}$$
$$\frac{dx_\mathrm{C}}{dt} = \frac{-x_\mathrm{C} u_1}{1000 V_\mathrm{R}} + k_7 \eta_1 x_\mathrm{A} x_\mathrm{B} - k_3 \eta_2 x_\mathrm{B} x_\mathrm{C} - k_6 \eta_3 x_\mathrm{C} x_\mathrm{P} \tag{3.8c}$$
$$\frac{dx_\mathrm{P}}{dt} = \frac{-x_\mathrm{P} u_1}{1000 V_\mathrm{R}} + k_2 \eta_2 x_\mathrm{B} x_\mathrm{C} - k_4 \eta_3 x_\mathrm{C} x_\mathrm{P} \tag{3.8d}$$
$$\frac{dx_\mathrm{E}}{dt} = \frac{-x_\mathrm{E} u_1}{1000 V_\mathrm{R}} + k_3 \eta_2 x_\mathrm{B} x_\mathrm{C} \tag{3.8e}$$
$$\frac{dx_\mathrm{G}}{dt} = \frac{-x_\mathrm{G} u_1}{1000 V_\mathrm{R}} + k_5 \eta_3 x_\mathrm{C} x_\mathrm{P} \tag{3.8f}$$
$$\frac{dT}{dt} = \frac{(T_\mathrm{F} - T) u_1}{1000 V_\mathrm{R}} + k_8 \eta_1 x_\mathrm{A} x_\mathrm{B} + k_9 \eta_2 x_\mathrm{B} x_\mathrm{C} + k_{10} \eta_3 x_\mathrm{C} x_\mathrm{P} - l_1 (T - 1000 u_2) \tag{3.8g}$$
$$\frac{dV_\mathrm{R}}{dt} = \frac{u_1}{1000} \tag{3.8h}$$

where all the time-dependencies are removed, not to overload the equations. The states $x_\mathrm{i}(t), \forall \mathrm{i} = A,\ B,\ C,\ E,\ G,\ P$ represent the molar fraction of each components

Table 3.1: *Williams-Otto reactor: k_i and η_j values, after Hannemann and Marquardt (2010).*

Constant	Value	Constant	Value
k_1	$1.6599 \cdot 10^6\ \mathrm{s}^{-1}$	k_9	$2.728518427 \cdot 10^{10}$
k_2	$7.2117 \cdot 10^8\ \mathrm{s}^{-1}$	k_{10}	$1.446556764 \cdot 10^{14}$
k_3	$1.44234 \cdot 10^9$	k_{11}	$1.816050294 \cdot 10^{11}$
k_4	$1.33725 \cdot 10^{12}$	η_1	$\exp(\frac{-6666.7}{T+273.15})$
k_5	$4.01175 \cdot 10^{12}$	η_2	$\exp(\frac{-8333.3}{T+273.15})$
k_6	$2.6745 \cdot 10^{12}\ \mathrm{s}^{-1}$	η_3	$\exp(\frac{-11111}{T+273.15})$
k_7	$3.3198 \cdot 10^6$	T_F	35°C
k_8	$1.046562189 \cdot 10^8$	l_1	$2.434546857 \cdot 10^{-4}$

i present in the reaction Scheme 3.7, $T(t)$ is the reactor temperature and $V_\mathrm{R}(t)$ is the volume of liquid present in the reactor itself. T_F represents the temperature at which the reagent B is added and l_1 is a heat exchange coefficient. The terms $k_\mathrm{i}\eta_\mathrm{j}(t)$ represent the kinetics constants for the three reactions in the Scheme 3.7a-c. In particular, k_i are the pre-exponential factors related to the collision frequency, and $\eta_\mathrm{j}(t)$ the Arrhenius terms accounting for the temperature-dependencies of the kinetics constants. For the sake of completeness, they are all given in Table 3.1 (Forbes, 1994) (Hannemann and Marquardt, 2010).

As in Sections 3.3.2 and 3.3.1 an OCP is formulated, where Equation 3.8 is the model constraint.

$$\underset{\mathbf{x}(t),\mathbf{u}(t),\mathbf{p},t_\mathrm{f}}{\text{minimise}} \quad -5554.1x_\mathrm{P}(t_\mathrm{f})V_\mathrm{R}(t_\mathrm{f}) - 125.9x_\mathrm{E}(t_\mathrm{f})V_\mathrm{R}(t_\mathrm{f}) \tag{3.9a}$$

$$\text{subject to} \quad \frac{d\mathbf{x}}{dt} = \mathbf{f}(\mathbf{x}(t), \mathbf{u}(t), \mathbf{p}, t_\mathrm{f}) \tag{3.9b}$$

$$\mathbf{x}(0) = [1,\ 0,\ 0,\ 0,\ 0,\ 0,\ 65,\ 2] \tag{3.9c}$$

$$[0,\ 0,\ 0,\ 0,\ 0,\ 0,\ 60,\ 2] \leq \mathbf{x}(t) \leq [1,\ 1,\ 1,\ 1,\ 1,\ 1,\ 90,\ 5] \tag{3.9d}$$

$$[0,\ 0.02] \leq \mathbf{u}(t) \leq [5.784,\ 0.1] \tag{3.9e}$$

The objective function of Equation 3.9a is representing the maximisation of the productivity of the two products P and E. Again, as in the previous cases, it is introduced as a minimisation objective function.

The solutions of all the case studies presented in this section will be reported in the following Chapters. However, as already stated, the jacketed tubular reactor and the Williams-Otto reactor will serve to assess the two robustification approximations. For this reason, the methodology which will be performed to accomplish this comparison will be explained in the following Section.

3.4 Comparison of the two robustification approaches

In this Section, the methodology used to assess and compare the sigma points and linear approximations, respectively explained in Sections 2.6.2 and 2.6.3, will be given. In Chapter 5, the following procedure will be applied to two case studies, the jacketed tubular reactor (Logist et al., 2011) (Houska et al., 2012) and the Williams-Otto reactor (Williams and Otto, 1960) (Forbes, 1994) (Hannemann and Marquardt, 2010):

1. the nominal OCP is solved with all parameters considered to be certainly known;
2. one or more parameters are then considered as uncertain, with mean values equal to those used in the nominal OCP, and variance-covariance matrix defined by the user and diagonal;
3. the optimal control profile obtained at Point 1 is then fixed and integrated over time for 600 Monte-Carlo realisations. For each of these realisations, the values of the uncertain parameters are randomly drawn, following the parameters distributions defined at Point 2;
4. for each of the realisations executed at Point 3, it is checked if they still satisfy the constraints of the original problem or they violate them;
5. the robust OCP is solved with both robustification approaches and uncertain parameters as given at Point 2;
6. Points 3 and 4 are repeated for both the optimal control profiles obtained at Point 5.

The number of violations is counted for two main reasons. From Point 4, it is possible to have an idea about the sensitivity of the nominal OCP with respect to the uncertain parameters. From Point 6, the reliability of the two robustification approaches can be assessed, by checking whether the number of violations is effectively lower than the predicted ones. The predicted violations are determined by the factor q in Equations 2.34 and 2.37, as it was already explained in Sections 2.6.2 and 2.6.3.

3.5 Conclusion

In this chapter, the tools exploited in all the thesis are introduced, together with the procedure that will be followed in the next Chapters. In Section 3.2, the numerical tool-kits were presented and briefly described.

In Section 3.3, three case studies were presented. Each of them was given with its dynamic equations and the OCP or the MOOCP that has to be solved.

Lastly, in Section 3.4, the procedure that will be followed in Chapter 5 was described. This will be used in order to assess the reliability of the two robustification approximations and to compare them.

Results and conclusion

Chapter 4

Multi-objective optimal control of a literature case study

4.1 Introduction

In this chapter, the algorithms implemented in Pomodoro are verified through the solution of the MOOCP presented in Section 3.3.1. The fed-batch bio-reactor multi-objective optimisation is in fact solved with both Pomodoro and ACADO Toolkit. The results obtained with the two software tools are then compared, in Section 4.2, in order to verify that the same solution is attained.

4.2 Fed-batch bio-reactor results

In this Section, the results obtained for the problem presented in Section 3.3.1 are depicted and discussed. In order to reach these results, both Pomodoro and ACADO Toolkit were adopted.

From Figure 4.1 it can be seen that for both cases fed-batch 1 and fed-batch 2, the Pareto optimals obtained with Pomodoro are perfectly overlapping those of ACADO Toolkit. These are fundamental results, since they give a first indication of the reliability of the Pomodoro software. An additional comparison between the two software will be made in Chapter 5, based on the jacketed tubular reactor case study.

Moreover, also the time required to solve the MOOCPs described in Sections 3.3.1.1 and 3.3.1.2 is discussed. For all the problems, 21 Pareto points were calculated. In order to do that, the tolerances required for the solution of the NLP problems involved were set equal for each solver and case. Unfortunately, Pomodoro and ACADO Toolkit are exploiting different NLP solvers, making it difficult to compare precisely the tolerances. However, for the purpose of this comparison the tolerances of both solvers were set equal to 10^{-8}, which is the default tolerance value for Pomodoro. The MOOCPs fed-batch 1 and fed-batch 2 were solved with the WS, NBI and ENNC methods with Pomodoro and ACADO Toolkit. Unfortunately each of these problems

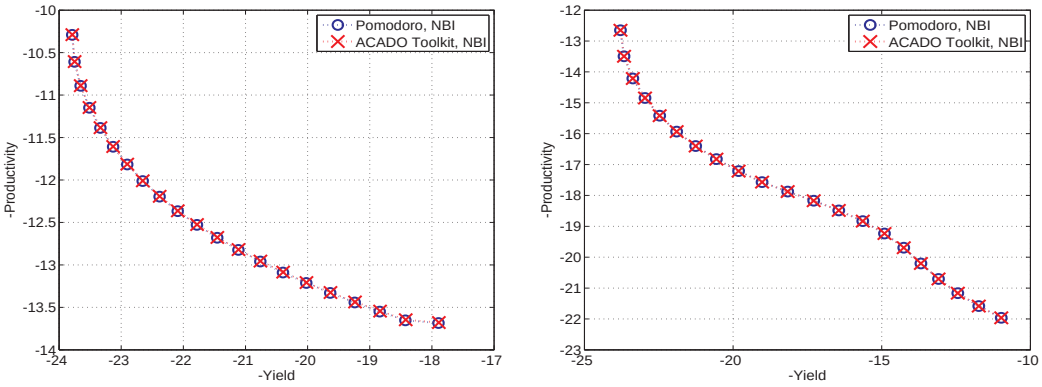

(a) *Fed-batch bio-reactor 1.* **(b)** *Fed-batch bio-reactor 2.*

Figure 4.1: *Fed-Batch bio-reactor 1 and 2: Pareto sets obtained with the NBI method with Pomodoro and ACADO Toolkit, after Logist et al. (2009)*

was only solved once. However, not being a statistically valid analysis, the results obtained can only be used for a qualitative description. Nevertheless, for all cases, Pomodoro proved to be faster than ACADO Toolkit, even if the differences were just fractions of second.

This case study can also be useful to show the main drawbacks of the WS method for multi-objective optimisation. These can be seen in Figure 4.2. It is clear from Figure 4.2a that the WS method fails to identify the Pareto optimals where the Pareto set becomes non-convex. Moreover, although the weights for the 21 points were chosen as equally spaced between 0 and 1, it is possible to see that the optimal points are definitely not equally spaced for the WS method. In fact, they tend to accumulate in the proximity of the yield optimum. These drawbacks, as it was already

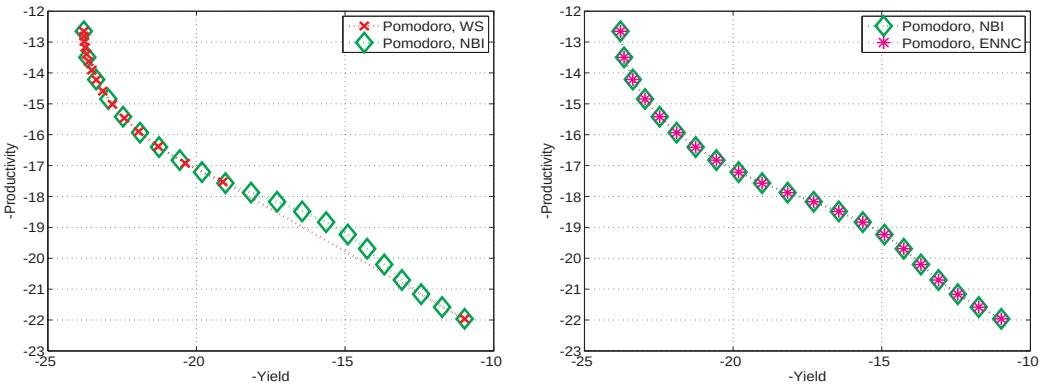

(a) *WS and NBI.* **(b)** *NBI and ENNC.*

Figure 4.2: *Fed-bacth bio-reactor 2: Pareto sets obtained with WS, NBI and ENNC methods.*

anticipated in Section 2.5.2, are not present when the NBI method is applied.

Additionally, a comparison between the methods NBI and ENNC is done in Figure 4.2b, leading to exactly the same results for the problem fed-batch bio-reactor 2.

4.3 Conclusion

In Section 4.2 the multi-objective optimisation of a fed-batch bio-reactor was accomplished. Four different formulations of the objective functions were investigated in couples, leading to two bi-objective optimisation problems. For both Problems 3.3.1.1 and 3.3.1.2, the results obtained with Pomodoro were found to be equal to those obtained with ACADO Toolkit in Logist et al. (2009).

Additionally, the drawbacks of the WS method, which were already presented in Section 2.5.1, were shown on a practical case study. It was also shown that the NBI and ENNC methods are instead able to overcome these drawbacks, as it was anticipated in Sections 2.5.2 and 2.5.3.

Chapter 5

Robust optimal control of literature case studies

5.1 Introduction

In this chapter, the solutions of robust OCPs for two case studies are reported. Firstly, the jacketed tubular reactor problem (Logist et al., 2011) (Houska et al., 2012) is solved with the linear approach reported in Section 2.6.1. As this case study was already solved in the literature (Logist et al., 2011), it can be used as a second bench-mark example, after the fed-batch bio-reactor, to assess the algorithms implemented in Pomodoro. This is accomplished in Section 5.2.1.

After that, a comparison is made between the linear and sigma points approximations for robust optimal control. As already mentioned, the linear approximation can be compared with the sigma points only if it is considered in the formulation given in Section 2.6.3. Results for the comparison of the two robust approximations are provided for the jacketed tubular reactor in Sections 5.2.2 and 5.2.3 and for the Williams-Otto reactor (Williams and Otto, 1960) (Forbes, 1994) (Hannemann and Marquardt, 2010) (Logist et al., 2012) in Sections 5.3.1 and 5.3.2. The number of uncertain parameters investigated is varying between one and four and the procedure which will be carried out was provided in Section 3.4.

The comparison between the two robustification approaches will focus on the reliability of the methods themselves and the loss in terms of performance of the considered objective function. Additionally, the size of the problems and the time required to solve them will also be considered when comparing and assessing the two approximations.

The Chapter is then concluded in Section 5.4, where the main results are highlighted and summarised.

5.2 Jacketed tubular reactor results

A complete description of the model is reported in Section 3.3.2. Additionally, two uncertain parameters are assumed. These are α and β, respectively representing a kinetics-related factor and the dimensionless heat exchange factor at the wall of the reactor. Their nominal values are $\alpha = 0.0581$ and $\beta = 0.2$.

It is also necessary to highlight that, for this case study, the most critical state is the internal reactor temperature. In fact, while it is desirable to keep it as high as possible in order to enhance the kinetics of the reaction, for safety issues it is necessary to always keep it below its upper bound, meaning $x_2(z) \leq \frac{400-T_{\text{in}}}{T_{\text{in}}}$. However, for the solution of the robust OCP, an additional constraint needs to be introduced in Problem 3.6, as explained in Section 2.6. The formulation of this additional constraint depends on the robust approximation that is considered and will be presented in Sections 5.2.1 and 5.2.2.

5.2.1 Comparison with ACADO Toolkit

In order to allow a fair comparison with the literature (Logist et al., 2011), only the uncertainty over the parameter β is considered in this section. Moreover, as already anticipated, an additional constraint needs to be included in the OCP of Section 3.3.2:

$$x_2(z) + \gamma\beta\sqrt{P_{22}(z)} \leq \frac{400 - T_{\text{in}}}{T_{\text{in}}} \tag{5.1}$$

where $\gamma\beta = \Gamma$ (Logist et al., 2011).

The problem is then solved for different values of the robustification factor γ and the results obtained with 20 discretisation points are shown in Figures 5.1 and 5.2. The results obtained with the two optimisation programmes show some differences, especially when looking at the control profiles, in Figure 5.1. In particular, the most striking differences are found in the control actions for the case $\gamma = 0.2$. While in Figure 5.1a the control profile for $\gamma = 0.2$ is monotonically decreasing for $0 \leq z \leq 0.5$, in Figure 5.1b a minimum and a maximum are encountered at $z = 0.2$ and $z = 0.25$. Some additional but less evident differences are also present in the control profiles calculated for $\gamma = 0$ and $\gamma = 0.1$.

However, it is surely more interesting to look at the consequences that these slightly different control profiles have on the states behaviours and on the objective function. The states profiles depicted in Figure 5.2 show that no excessive deviation are present, especially in the conversion profiles. The temperature profiles of Figure 5.2c and 5.2d still show some differences for the case with $\gamma = 0.2$, as a direct consequence of the different control profiles.

Nevertheless, in Table 5.1 it can be seen that the objective function values obtained with ACADO Toolkit and Pomodoro are really close one to each other, for all the investigated cases. This allows to state that the results obtained with the two

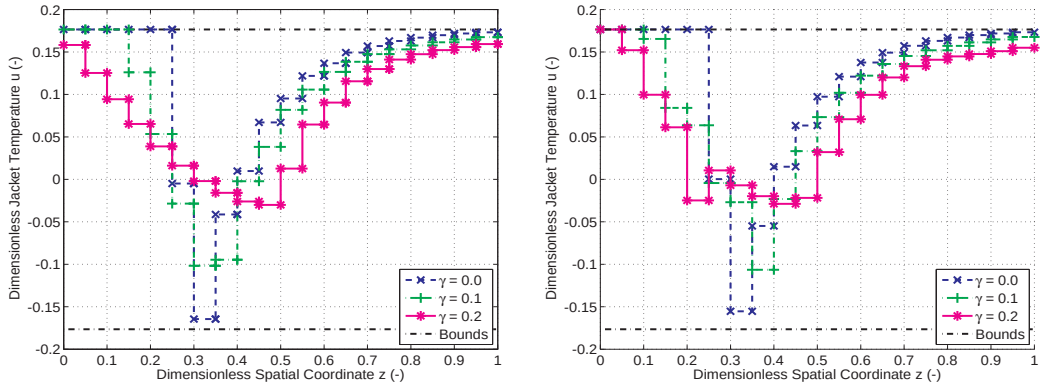

(a) *Pomodoro.* **(b)** *ACADO Toolkit after Logist et al. (2011).*

Figure 5.1: *Jacketed tubular reactor: control profiles obtained with different dynamic optimisation programmes.*

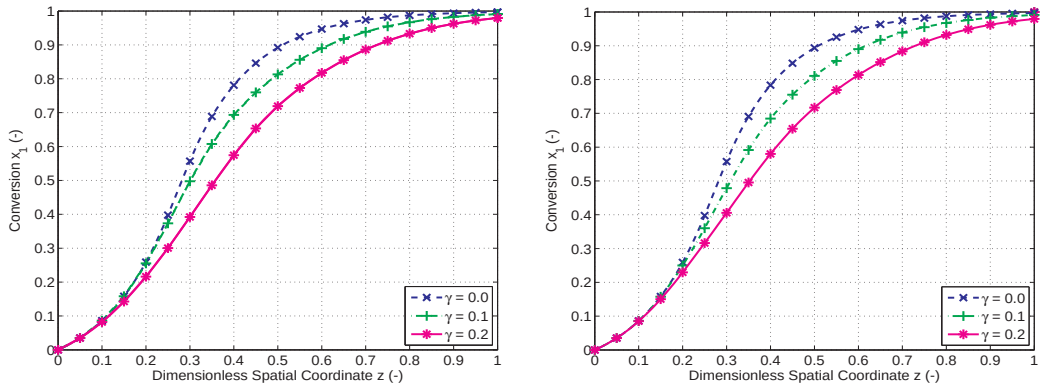

(a) *Pomodoro.* **(b)** *ACADO Toolkit after Logist et al. (2011).*

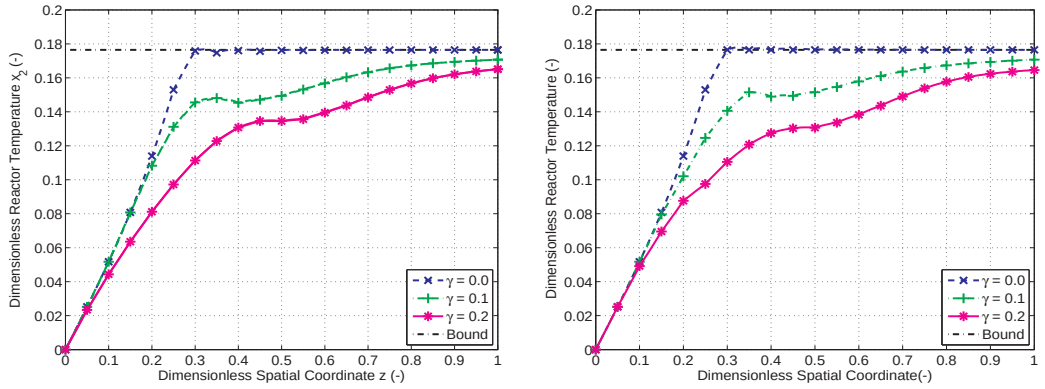

(c) *Pomodoro.* **(d)** *ACADO Toolkit after Logist et al. (2011).*

Figure 5.2: *Jacketed tubular reactor: conversion and reactor temperature profiles obtained with different dynamic optimisation programmes.*

Table 5.1: *Jacketed tubular reactor: conversion attained with different dynamic optimisation programmes.*

	ACADO Toolkit	Pomodoro
Final conversion, $\gamma = 0.0$	0.996915	0.996852
Final conversion, $\gamma = 0.1$	0.991018	0.990978
Final conversion, $\gamma = 0.2$	0.979212	0.979479

optimisation programmes are surely comparable and, as in Section 4.2, this can serve as a good indication for the reliability of Pomodoro.

5.2.2 Jacketed tubular reactor with uncertainty on β

In this section, the jacketed tubular reactor case study is used to assess and compare the linear and sigma points approximation for robust OC. As already said, to allow a fair comparison between the two methods, the linear approximation that needs to be used is the one given in Section 2.6.3. From here on, unless explicitly said otherwise, when referring to the linearisation approach or linear approximation it will always be referred to the formulation developed in that Section.

Again, one single parameter, β is taken as uncertainty. With respect to Section 5.2.1, it is important to notice that for this comparison the parameter β is assumed as normally distributed around its mean value $\beta = 0.2$ with a variance of 0.0004. This means that a standard deviation of 10% over the parameter β is taken into account.

In order to consider the uncertainty, in each of the robustified approaches, some additional constraints are imposed, as in Equation 5.1. However, the formulation of these additional constraints is different than that of Section 5.2.1. For the linear approximation, they are in fact built following the formulation presented in Equation 2.37. They can be seen in Equation 5.2, where $\mathrm{P}_{22}(z)$ is the variance on the reactor temperature $x_2(z)$ and q is a factor depending on the confidence level required from the user. For Problem 3.3.2, this required confidence level is 95%, thus, on the assumption that the states profiles are normally distributed, a factor $q = 1.96$ is taken. This value is taken according to the two-sided normal distribution function, since the variation in $x_2(z)$ can be in both directions. Such a confidence level requires that no more than 30 violations occur out of the 600 Monte-Carlo simulations that will be performed.

$$x_2(z) + q\sqrt{\mathrm{P}_{22}(z)} \leq \frac{400 - T_{\mathrm{in}}}{T_{\mathrm{in}}} \tag{5.2a}$$

$$x_2(z) - q\sqrt{\mathrm{P}_{22}(z)} \geq \frac{280 - T_{\mathrm{in}}}{T_{\mathrm{in}}} \tag{5.2b}$$

The sigma points approximation also requires two additional constraints which

are built following the formulation of Equation 2.34:

$$\bar{y}_2(z) + q\sqrt{\mathrm{P}_{22}(z)} \leq \frac{400 - T_{\mathrm{in}}}{T_{\mathrm{in}}} \tag{5.3a}$$

$$\bar{y}_2(z) - q\sqrt{\mathrm{P}_{22}(z)} \geq \frac{280 - T_{\mathrm{in}}}{T_{\mathrm{in}}} \tag{5.3b}$$

where $\bar{y}_2(z)$ is the expected value of the reactor temperature, calculated as in Equation 2.32 and $q = 1.96$ as in Equation 5.2. The two approaches differ in the way the term $\mathrm{P}_{22}(z)$ is calculated. The linear approximation, in fact, calculates it following Equation 2.36, while the sigma points approximation calculates it based on Equation 2.33.

Figure 5.3 shows the profiles of the manipulated variable for the nominal and the two robustified OCPs, solved with 100 discretisation points. Figure 5.4 shows the temperature profiles for the nominal and the two robustified OCPs together with their predicted 95% confidence regions. From here on, unless explicitly said otherwise, the states profiles calculated with the sigma points approach will be identified with their related estimates $\bar{y}_{\mathrm{i}}$, which are calculated by means of Equation 2.32.

From Figure 5.4 it is possible to see that the confidence regions predicted by the different robustification methods have similar size for $z = 1$, but that they differ substantially for lower values of z, in particular at the point $z = 0.4$. At this point, in fact, while the linearisation approach predicts a considerable confidence region, the sigma points approach predicts a pinch, where the confidence region is so small that the reactor temperature equals the upper bound.

For a better comprehension, the original sigma points temperature profiles are depicted in Figure 5.5. These actually represent the temperature profiles of the terms $\mathbf{Y}_0$ and $\mathbf{Y}_{\mathrm{i}}$ from which the mean temperature $\bar{y}_2$ is calculated, according to

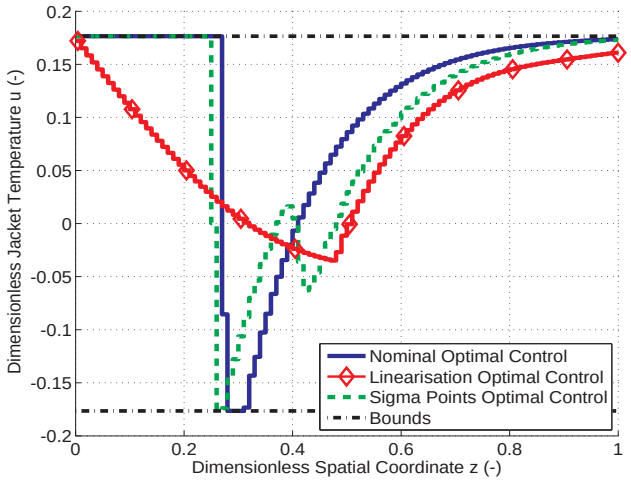

Figure 5.3: *Jacketed tubular reactor: optimal control profiles with β as uncertain parameter.*

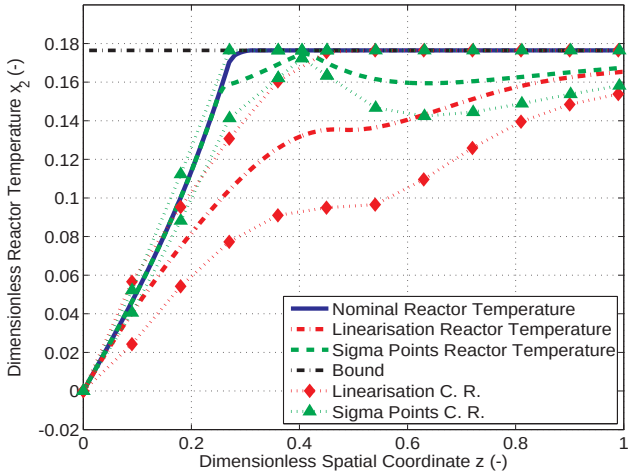

Figure 5.4: *Jacketed tubular reactor: temperature profiles and their predicted* 95% *confidence regions with* β *as uncertain parameter.*

Equation 2.32. Looking at their actual profiles it is possible to understand the origin of the pinch: at $z = 0.4$, all the profiles are crossing each other, leading then to a very small predicted confidence region. It is also important to notice that at least one of the sigma points profiles is approaching the upper bound for each $z \geq 0.3$, forcing the others, and consequently the estimate $\bar{y}_2$, to be pushed below the nominal temperature profile, as depicted in Figure 5.4.

The Monte-Carlo realisations are accomplished for the nominal OCP as described in Section 3.4 and are depicted in Figure 5.6. Figure 5.6a presents the β sample used for the Monte-Carlo realisations, while Figure 5.6b shows the reactor temperature profiles for each Monte-Carlo realisation. These profiles were calculated by applying

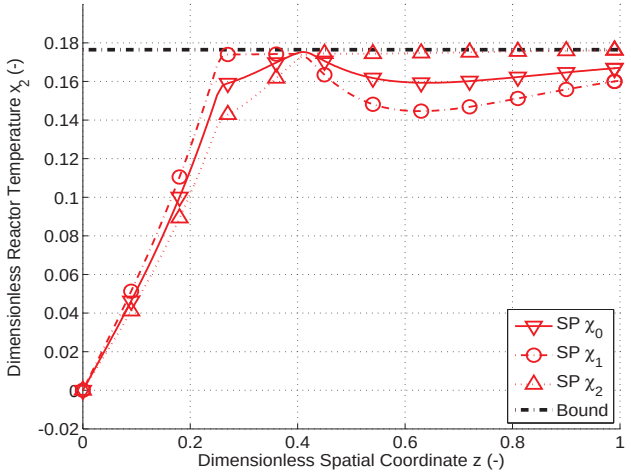

Figure 5.5: *Jacketed tubular reactor: sigma points with* β *as uncertain parameter.*

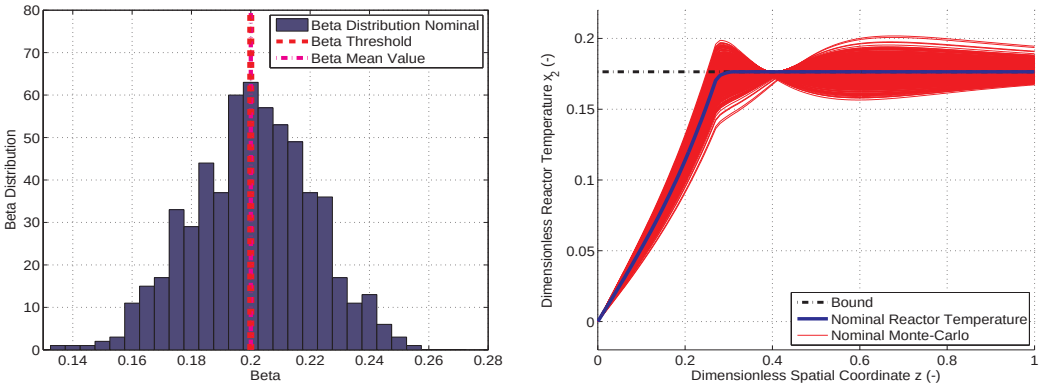

(a) *β distribution.*

(b) *Temperature profiles for each Monte-Carlo realisation.*

Figure 5.6: *Jacketed tubular reactor: Monte-Carlo realisations for the nominal OCP.*

the already known nominal optimal control to the system and considering a randomly sampled β.

It can be seen that many of the realisations are exceeding the upper temperature bound. In particular, as it can be seen from Table 5.2, 589 violations out of 600 Monte-Carlo simulations occur. The system is thus extremely unsafe and also values of β lying close to the mean value $\beta = 0.2$ cause violation of the temperature upper bound. In particular, the threshold values that mark the separation between the safe and unsafe process for the depicted β sample are $\beta_1 = 0.199533$ and $\beta_2 = 0.200458$. All randomly drawn $\beta_\text{i} \leq \beta_1$ or $\beta_\text{i} \geq \beta_2$ lead to violations. The crossings of the upper bound happen either around the point $z = 0.3$ when $\beta_\text{i} \geq \beta_2$, either at $z \geq 0.4$, when $\beta_\text{i} \leq \beta_1$. High values of β, in fact, imply better heat transfer coefficients. When this is the case, more heat is provided by the control in order to initiate the reaction, leading to violation of the bound at the beginning of the process. Low values of β, instead, mean worse heat transfer coefficients. In this case, once the reaction has started, the reaction heat is not removed fast enough and the inner reactor temperature rises above its upper bound.

The problem is also solved with the two robustification approximations, with the aim of reducing the number of violations, thus improving the safety of the system. The same β sample is used to assess the reliability of the two robust optimal controls. The results obtained are shown in Figures 5.7 and 5.8. For both approximations, the number of realisations which exceed the temperature bound are shown in Table 5.2. From Figures 5.7b and 5.8b, it is possible to calculate the empirical 95% confidence regions for the two approaches and then draw a comparison with the predicted ones of Figure 5.4. In Figure 5.9 it is possible to see that the linearisation approach clearly overestimates the empirical confidence region. However, due to this fact, the linear approach has proven to satisfy the additional Constraints 5.2 of the system for more than 99% of the realisations, while the sigma points satisfy its additional Constraints

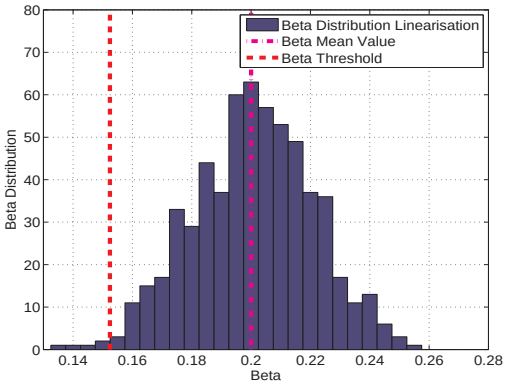

(a) *β distribution.*

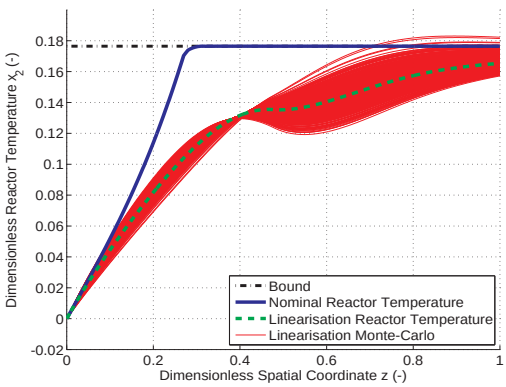

(b) *Temperature profiles for each Monte-Carlo realisation.*

Figure 5.7: *Jacketed tubular reactor: Monte-Carlo realisations for the linearisation approach robust OCP.*

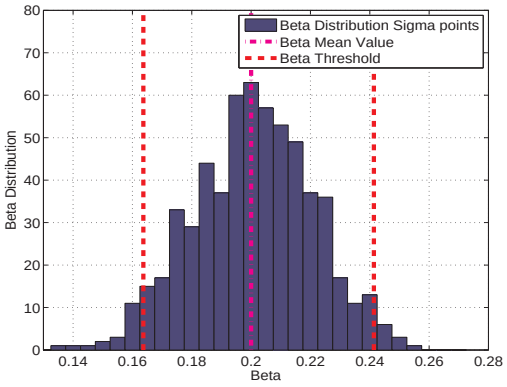

(a) *β distribution.*

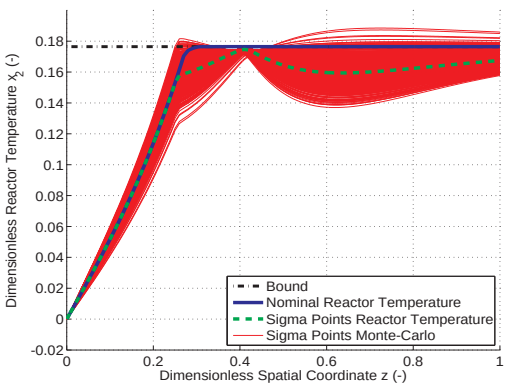

(b) *Temperature profiles for each Monte-Carlo realisation.*

Figure 5.8: *Jacketed tubular reactor: Monte-Carlo realisations for the sigma points robust OCP.*

Table 5.2: *Jacketed tubular reactor: exceeding temperature profiles with β as uncertain parameter.*

OCP	# Violations	# Realisations	% Violations
Nominal	589	600	98.17%
Linearisation	5	600	0.83%
Sigma points	42	600	7.00%

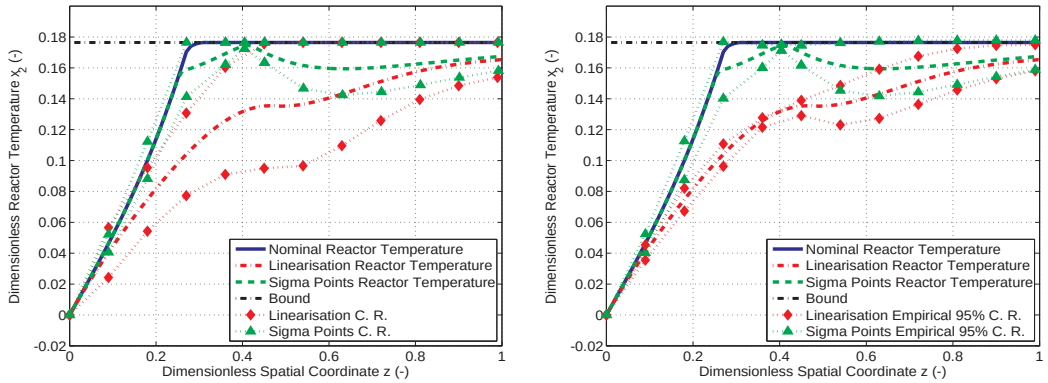

(a) *Predicted* 95% *confidence regions.* **(b)** *Empirical* 95% *confidence regions.*

Figure 5.9: *Jacketed tubular reactor: temperature profiles and their predicted and empirical* 95% *confidence regions with* β *as uncertain parameter.*

5.3 only in 93% of the simulations. This means that the sigma points approach, in this case does not meet the required confidence level of 95%.

A comparison of the losses induced by the robustification approaches on the obective function is also interesting to investigate and it will be done at the end of Section 5.2.3, in Table 5.4.

5.2.3 Jacketed tubular reactor with uncertainties on α and β

In this section, similar results to those of Section 5.2.2 are reported and discussed. However, now the robust OCP is solved in order to account for more than one single uncertain parameter. Together with the already considered β, also the parameter α is now assumed to be uncertain. Again, they are both assumed to be normally distributed, with mean values $\alpha = 0.0581$ and $\beta = 0.2$ and variance-covariance matrix

$$\mathbf{V} = \begin{pmatrix} 0.00581^2 & 0 \\ 0 & 0.02^2 \end{pmatrix} \tag{5.4}$$

from which it can be seen that a standard deviation of 10% on each parameter is considered. Additionally, matrix $\mathbf{V}$ is diagonal, meaning that no correlation is assumed between the two parameters.

Once again, the results are obtained by adhering to the general guidelines reported in Section 3.4. As in the previous case, 100 discretisation points are used in order to solve the optimal control problems.

The optimal controls for the three OCPs are depicted in Figure 5.10b. In order to facilitate the comparison between the two cases, the profiles for both the robustification with respect to one and two uncertain parameters are shown in Figure 5.10. From this Figure, it can be seen that, by introducing a degree of uncertainty on a second

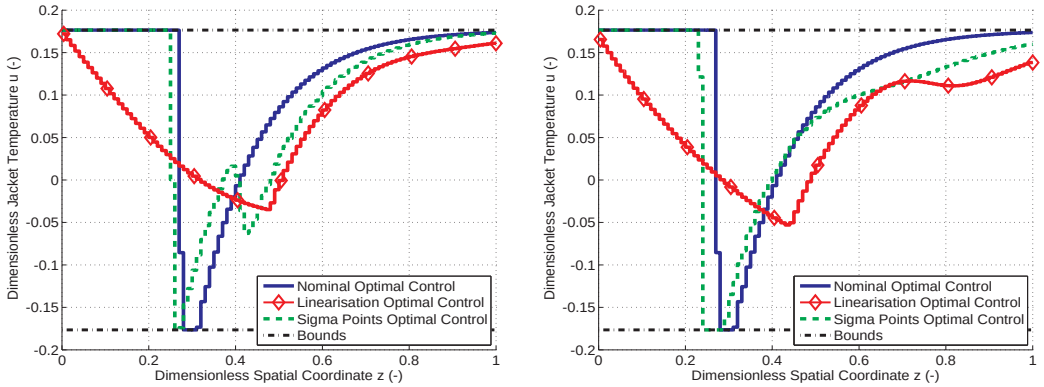

(a) *One uncertain parameter, β.* **(b)** *Two uncertain parameters, α and β.*

Figure 5.10: *Jacketed tubular reactor: comparison of the optimal control profiles.*

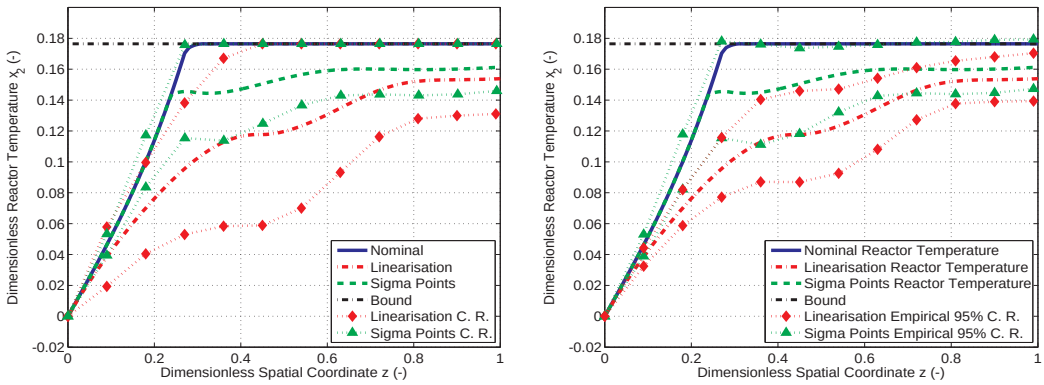

(a) *Predicted 95% confidence regions.* **(b)** *Empirical 95% confidence regions.*

Figure 5.11: *Jacketed tubular reactor: temperature profiles and their predicted and empirical 95% confidence regions with α and β as uncertain parameters.*

parameter, the robust optimal control profiles undergo some important changes. In particular, concerning the linearisation approach, a maximum and a minimum are encountered at $z = 0.7$ and $z = 0.8$ of Figure 5.10b. For the sigma points approach, instead, the maximum and minimum that were formerly present around $z = 0.4$ disappear, leading to a monotonically increasing profile, from $z = 0.3$ to $z = 1$.

The optimal temperature profiles, together with their expected and predicted confidence regions are depicted in Figure 5.11. From Figure 5.11b it can be seen that, as it was in Figure 5.9, the linearisation approach, when predicting the confidence region is clearly overestimating it. The sigma points approach, instead, predicts the confidence region more accurately, except for the points $z = 0.3$ and $z \geq 0.7$, where violations are present.

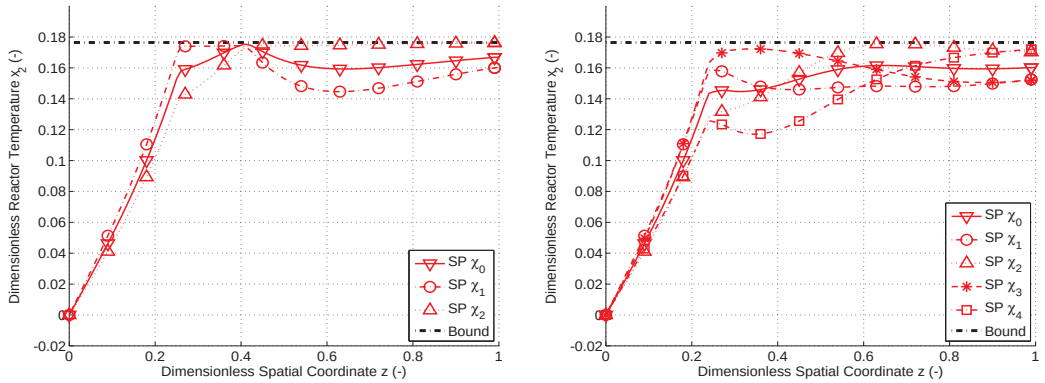

(a) *β as uncertain parameter.* **(b)** *α and β as uncertain parameters.*

Figure 5.12: *Jacketed tubular reactor: comparison of the sigma points profiles.*

Table 5.3: *Jacketed tubular reactor: exceeding temperature profiles with α and β as uncertain parameters.*

OCP	# Violations	# Realisations	% Violations
Nominal	580	600	96.67%
Linearisation	1	600	0.17%
Sigma points	69	600	11.50%

Moreover, it can be seen that, for the two uncertain parameters case, no pinch is present. There is, in fact no point where the empirical 95% confidence region is close to 0. This is true for both the predicted and empirical 95% confidence regions and it can be better understood from Figure 5.12b, where the five sigma points are depicted. In order to facilitate the comparison, the sigma points calculated in Section 5.2.2 are also reported in Figure 5.12a. From Figure 5.12b, it is evident that two of the sigma points are not crossing nor touching the others around the point $z = 0.4$. In particular, these sigma points are SP χ_4 and SP χ_5, those representing the temperature profiles of the terms $\mathbf{Y}_\mathrm{i}$ of Equation 2.32 when the uncertainty on the second parameter α is taken into account.

It can then be concluded that, for both the approximations, the introduction of a second uncertain parameter leads to a significant increase in the size of both predicted and empirical confidence regions. Nevertheless, this increase is more evident in the sigma points approximation results, due to the disappearance of the pinch at $z = 0.4$.

From Figure 5.11b, it can also be seen that the 95% empirical confidence region of the linearised OCP is completely between the two given bounds, while the same confidence region of the sigma points robust OCP is exceeding around the point $z = 0.3$ and for $z \geq 0.7$. This means that the additional Constraints 5.2 are satisfied in at least 95% of the realisations for the linearisation approach, while, as for the

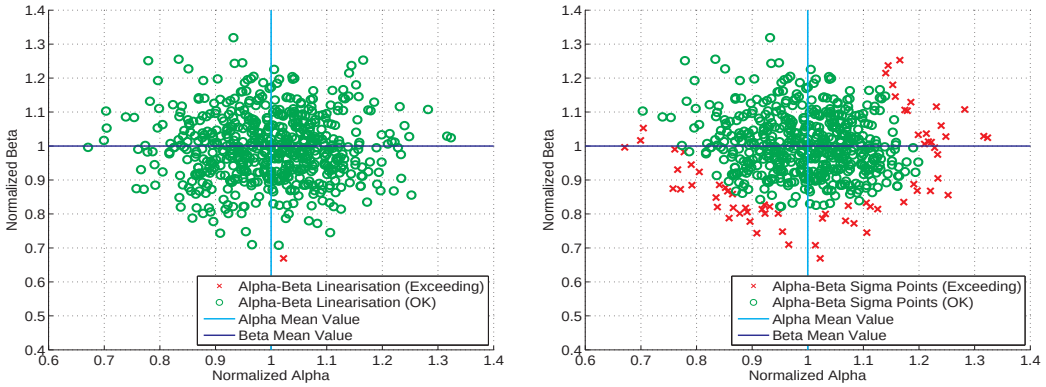

(a) *Linear approximation.* **(b)** *Sigma points approximation.*

Figure 5.13: *Jacketed tubular reactor: α and β distribution, comparison between the two robustification approaches.*

Table 5.4: *Jacketed tubular reactor: objective function values for the solution of the optimal control problems.*

	Objective function $\left[\frac{\text{mol}}{\text{L}}\right]$
Nominal	$6.16 \cdot 10^{-3}$
Linearisation, β	$3.97 \cdot 10^{-2}$
Linearisation, α and β	$6.16 \cdot 10^{-2}$
Sigma points, β	$1.26 \cdot 10^{-2}$
Sigma points, α and β	$2.38 \cdot 10^{-2}$

case treated in Section 5.2.2, the sigma points approach fails to satisfy the additional Constraints 5.3 for the required confidence level. The exact number of exceeding realisations for each OCP are enlisted in Table 5.3.

In Figure 5.13, the sample of normally distributed parameters used for all the Monte-Carlo realisations of this Section is shown. The values have ben normalised, by dividing each sample $[\alpha_\text{i}, \beta_\text{i}]$ by the mean values of α and β, respectively. Depicted in red and green, there can be seen the couples $[\alpha_\text{i}, \beta_\text{i}]$ which, for each robustified OCPs, lead or lead not to violation.

As anticipated in Section 5.2.2, the values of the objective function are reported in Table 5.4. It is important to highlight that, as predicted in Sections 2.6.1 and 2.6.2, by applying the robustification approaches to the nominal system the objective function increases. This has a clear physical meaning if someone keeps in mind that the objective J represents the concentration of the reactant A at the end of the reactor. In fact, as it can be seen from Figures 5.4 and 5.11 the robust temperature profiles are not approaching the upper bound as in the nominal case, leading to less favoured reaction kinetics. The same explanation is valid to understand why the sigma points

Table 5.5: *Jacketed tubular reactor: number of states, variables and constraints involved and the time required for the solution of the optimal control problems.*

	# States	# Variables	# Constraints	Time required [s]
Nominal	3	1301	2903	1.46
Linearisation, β	9	3701	8706	12.94
Linearisation, α and β	9	3701	8706	29.87
Sigma Points, β	9	3701	8503	7.84
Sigma Points, α and β	15	6101	14108	9.76

approximation has a lower objective function than the linear approximation. As expected, the values of the objective function are worsening when two uncertain parameters are present in the system.

Moreover, what is also investigated is the time required to solve the OCPs presented in this section. In Table 5.5, the sizes of the problems and the time required for their solutions is provided. As expected, the nominal case is the faster, requiring one order of magnitude less than the two robustification approaches. However, it is much more interesting to look at the time necessary for the robustified solutions. It is evident that the linear approximations are more time demanding than the related sigma points ones, in spite of their smaller or equal sizes. This observation is rather counter-intuitive. As a matter of fact, the sigma points approaches should have been expected to necessitate higher computational time, due to the bigger sizes of the problems.

Nevertheless, this expectation is not respected and this can be regarded as a consequence of the construction of the two robustified problems. In fact, in the linear approximation the additional states are calculated from Taylor expansions of the original states, leading, in this case, to 9 states strongly interconnected. In the sigma points approach, instead, the additional states are calculated by creating $2n_\mathrm{p}$ system dynamics which are, in essence, a copy of the original one. These $2n_\mathrm{p}$ additional systems are then solved together with the original one, leading to 9, or even 15, states which are not directly influencing each other and that only experience the same control action.

This last consideration becomes rather important, especially when higher scale problems and more complicated systems dynamics are considered. In fact, it was already pointed out that the sigma points approach is not able to achieve the pre-defined confidence level for this case study. This is a direct consequence of the fact that the assumption of normally distributed states, made in Section 5.2.2 is not satisfied. However, it must be remembered that the achievement of the required confidence level is case-sensitive, thus this result can not be extrapolated to more general cases.

However, this method could still be exploited to achieve the required confidence

Table 5.6: *Jacketed tubular reactor: exceeding temperature profiles and objective function for different values of q and with α and β as uncertain parameters, after Telen et al. (July 2014).*

	# Violations	# Realisations	% Violations	Objective function $\left[\frac{\text{mol}}{\text{L}}\right]$
$q = 1.96$	69	600	11.50 %	$2.38 \cdot 10^{-2}$
$q = 2.17$	44	600	7.33 %	$2.69 \cdot 10^{-2}$
$q = 2.81$	7	600	1.17 %	$3.72 \cdot 10^{-2}$
$q = 2.43$	23	600	3.83 %	$3.06 \cdot 10^{-2}$

level (Telen et al., July 2014). By changing the value of the factor q in Equation 5.3, and thus changing the optimal control profile, the requested 95% confidence level could be reached. However, the new control profile obtained by changing the value of q must be verified again through the procedure explained in Section 3.4. Depending whether the 95% confidence level is satisfied or not, q can be adapted once more, until only 5% of the Monte-Carlo realisations violates the system boundaries.

This iterative loop was accomplished on the two uncertain parameter case and the values of q with their related number of violations are provided in Table 5.6. When performing these iterations, q is first changed to the value 2.17. Unfortunately, the percentage of violations is still higher than the required one, so q is increased again and set to 2.81. In this case, the percentage of violations is much lower than the desired one. This over-conservative result is of course not an issue in terms of safety, but, as it can be seen from Table 5.6 the objective function is increased. This means that it is still possible to tune the factor q in order to reach the desired confidence level while also allowing a lower loss in terms of the objective function. The factor q is then set to 2.43 and it can be seen that violations now occur only in 3.83% of the cases (Telen et al., July 2014).

It is also worth remarking that the value of the objective function is still lower than the one obtained with the linear approximation, shown in Table 5.4. Unfortunately, these iterations required some time to be performed. In particular, performing 600 Monte-Carlo realisations takes around 15 minutes, while the time required for each robust optimal control problem is comparable to that reported in Table 5.5. At this stage, this iterative loop might seem useless, since the linear approximation already gave satisfactory results for the first value of q. However, when solving robust optimal control for real industrial case problems it is not straight-forward to obtain appropriate solutions with the linear approximation, thus this iterative loop can help in reaching good results and saving computational time and effort during the optimisation procedure.

All the values of q were chosen according to the assumption that the parameters uncertainties follow a two-sided normal distribution, following the explanation already given in Section 5.2.2. In particular, if the assumption of normally distributed states had been satisfied, the chosen q values would have resulted in confidence regions of

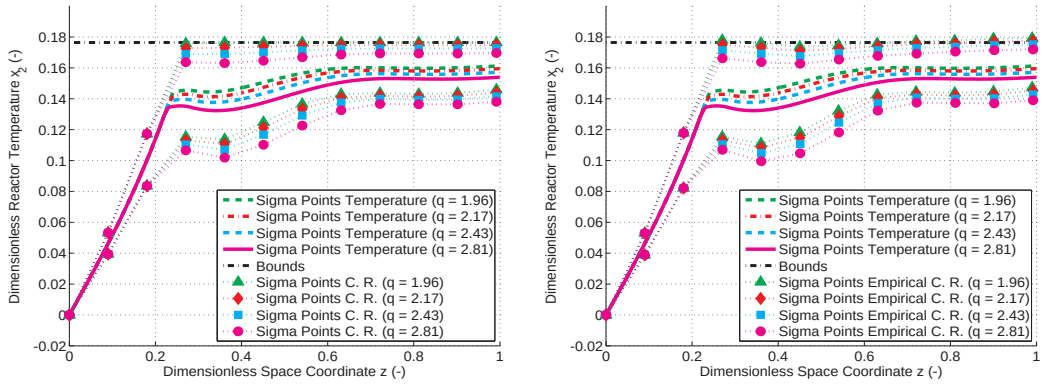

(a) *Predicted 95% confidence regions.* **(b)** *Empirical 95% confidence regions.*

Figure 5.14: *Jacketed tubular reactor: temperature profiles and their predicted and empirical 95% confidence regions for different values of the factor q and α and β as uncertain parameters.*

97%, 99.5% and 98.5%, respectively. Figure 5.14 shows the temperature profiles and their predicted and empirical confidence regions for all investigated values of q.

5.3 Williams-Otto reactor results

In this Section, the results for the robust OC of the Williams-Otto reactor (Williams and Otto, 1960) (Forbes, 1994) (Hannemann and Marquardt, 2010) will be presented. The aim of this Section is to compare and assess the two robustification approaches on a different case study than the one already presented. Thus, no comparison with ACADO Toolkit will be performed.

The system dynamics were already given in Section 3.3.3, together with the formulation of the OCP. The parameters assumed to be uncertain are the collision factors k_1, k_2 and k_3 and the heat exchange-related factor l_1. They are again assumed to be normally distributed with mean values $k_1 = 1.6599 \cdot 10^6$, $k_2 = 7.2117 \cdot 10^8$, $k_3 = 1.44234 \cdot 10^9$ and $l_1 = 2.434546857 \cdot 10^{-4}$ and variance-covariance matrix

$$\mathbf{V} = \begin{pmatrix} \left(1.6599 \cdot 10^5\right)^2 & 0 & 0 & 0 \\ 0 & \left(7.2117 \cdot 10^7\right)^2 & 0 & 0 \\ 0 & 0 & \left(1.4423 \cdot 10^8\right)^2 & 0 \\ 0 & 0 & 0 & \left(2.435 \cdot 10^{-5}\right)^2 \end{pmatrix} \tag{5.5}$$

from which it is possible to see that, on each parameter, a standard deviation of 10% is assumed. Again, as in Section 5.2.3, the variance covariance matrix $\mathbf{V}$ is diagonal, meaning that no correlation between the parameters is considered. The physical meanings of all these parameters were already explained in Section 3.3.3.

As in Section 5.2.2, additional constraints must be added, due to the uncertainties present on the system. The most critical state for the WO reactor is, again, the reactor temperature T. In order to meet the boundaries given in Equation 3.9d while also accounting for the uncertain parameters, two additional constraints must be imposed, according to the formulations already given in Equations 2.34 and 2.37. This will lead to the additional constraints for the linear approximation

$$T(t) + q\sqrt{\mathrm{P}_{\mathrm{TT}}(t)} \leq 90°C \tag{5.6a}$$

$$T(t) - q\sqrt{\mathrm{P}_{\mathrm{TT}}(t)} \geq 60°C \tag{5.6b}$$

and for the sigma points approximation

$$\bar{y}_{\mathrm{TT}}(t) + q\sqrt{\mathrm{P}_{\mathrm{TT}}(t)} \leq 90°C \tag{5.7a}$$

$$\bar{y}_{\mathrm{TT}}(t) - q\sqrt{\mathrm{P}_{\mathrm{TT}}(t)} \geq 60°C \tag{5.7b}$$

These additional constraints must be added to the OCP of Equation 3.9. Again, a value of 1.96 is assigned to the factor q, due to the fact that a 95% confidence level for a two-sided normal distrbution is required.

The results for the Williams-Otto reactor are given in two sections. In Section 5.3.1, only two uncertain parameters, k_1 and l_1 are considered, while the results of the four-parameters case will be given in Section 5.3.2. All the OCPs in the following Sections were solved with a discretisation of 50 intervals.

5.3.1 Williams-Otto reactor with uncertainties on k_1 and l_1

In this section the results obtained with linear and sigma points approximations for the WO reactor with two uncertain parameters will be given. These parameters are k_1 and l_1. Their variance-covariance matrix is adapted from the one given in Section 5.3:

$$\mathbf{V} = \begin{pmatrix} \left(1.6599 \cdot 10^{5}\right)^2 & 0 \\ 0 & \left(2.435 \cdot 10^{-5}\right)^2 \end{pmatrix} \tag{5.8}$$

Figure 5.15 shows the optimal control actions for the solution of the OCP described in Section 3.3.3 for the nominal and the two robustification cases. It can be clearly seen that the only control action which is influenced by the robustifications is $T_{\mathrm{W}}(t)$, the dimensionless cooling water temperature. Moreover, it is interesting to note that the $T_{\mathrm{W}}(t)$ profile obtained with the linearisation approach is overlapping the nominal control action at almost every time interval. This observation can already lead to the conclusion that, for these two cases, the reactor temperature profiles will not differ substantially.

This is proven in Figure 5.16, where the reactor temperature profiles are showed together with the confidence regions predicted by the two robustification approaches. As it was expected, the temperature profile obtained with the linear approximation is

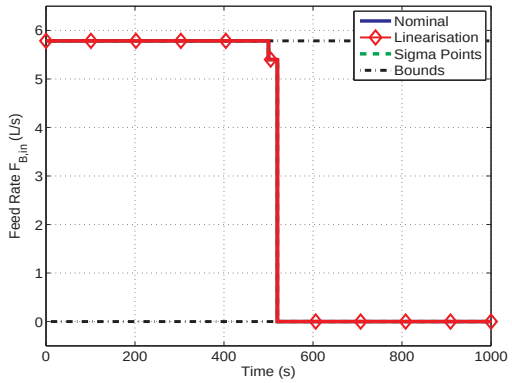

(a) *Inlet feed rate* $F_{\mathrm{B,in}}(t)$.

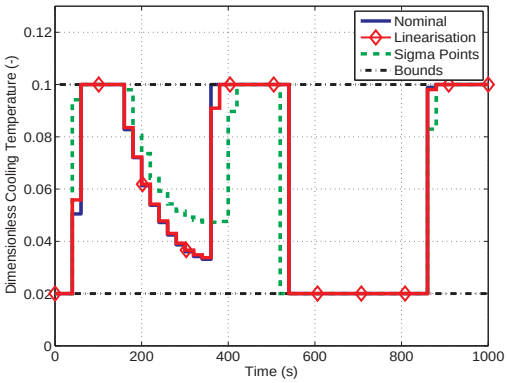

(b) *Dimensionless cooling water temperature* $T_{\mathrm{W}}(t)$.

Figure 5.15: *Williams-Otto reactor: control actions with* k_1 *and* l_1 *as uncertain parameters.*

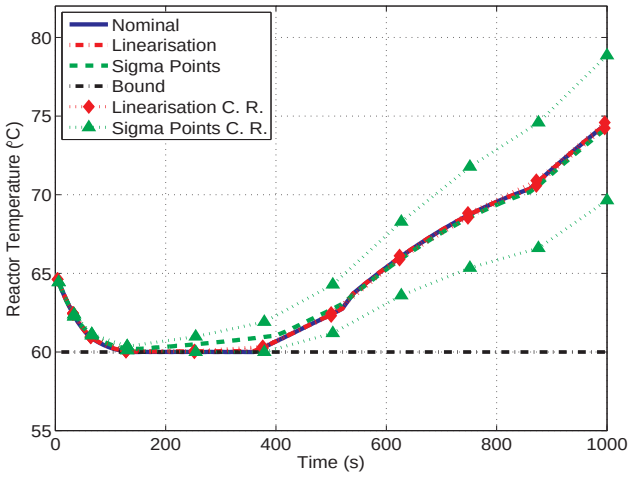

Figure 5.16: *Williams-Otto reactor: temperature profiles and their related* 95% *confidence regions with* k_1 *and* l_1 *as uncertain parameters.*

almost identical to the nominal one. What is more interesting to notice, however, is that the 95% confidence region predicted by the linear approximation is also essentially lying on the same curve, leading to a collapsing uncertainty region. The sigma points approximation, instead predicts a larger 95% confidence region, with a temperature profile which differs from the nominal one especially at $200[\mathrm{s}] \leq t \leq 500[\mathrm{s}]$.

The most evident consequence of these temperature profiles are shown in Table 5.7, where the number of boundary violations is reported for each solved OCP. It is possible to see that the amount of violations for the linear approximation is close to that of the nominal case, with only a 5% difference. Thus, it can be concluded that the linear approximation, for the Williams-Otto reactor is completely ineffective. In

Table 5.7: *Williams-Otto reactor: exceeding temperature profiles with k_1 and l_1 as uncertain parameters.*

OCP	# Violations	# Realisations	% Violations
Nominal	284	600	47.33%
Linearisation	256	600	42.67%
Sigma points	8	600	1.33%

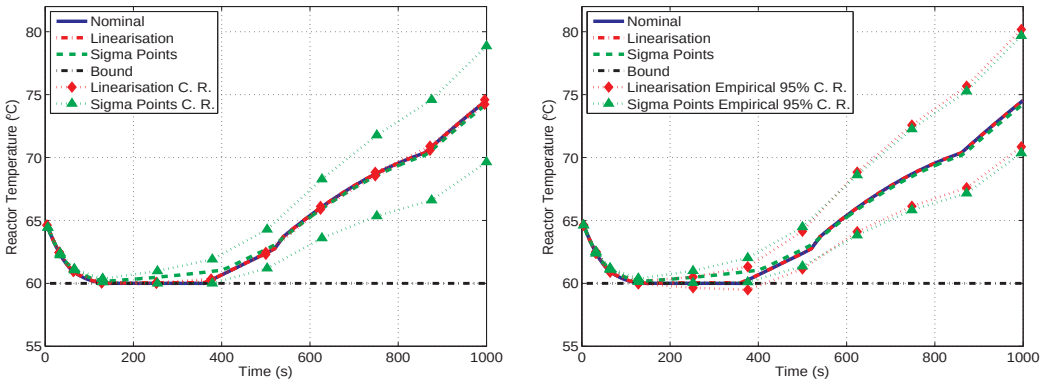

(a) *Predicted 95% confidence region.* **(b)** *Empirical 95% confidence region.*

Figure 5.17: *Williams-Otto reactor: temperature profiles and their predicted and empirical 95% confidence regions with k_1 and l_1 as uncertain parameters.*

fact, while the 95% confidence region predicted with the linear approximation is rather small, from Figure 5.17b it can be seen that the empirical one has approximately the same size of the one calculated with the sigma points approximation. This leads to violations in the range $200[\text{s}] \leq t \leq 400[\text{s}]$. The sigma points approximation, instead, respects the required number of violations. It results in fact in 8 exceedings out of 600 Monte-Carlo realisations, meaning only 1.33%, a value significantly lower than the required 5%.

Readers should not be surprised by such a difference with the jacketed tubular reactor example. There, in fact, the linearisation approach led to very good results because non-linearity entered the model Equations 3.5 only in the Arrhenius form. In the system dynamics of the WO reactor, instead, the non-linearity is more pronounced, thus the linear approximation is less suitable for treating such a problem than the sigma points.

The sample of normally distributed k_1 and l_1 leading to the results presented in this Section is depicted in Figure 5.18, where in red and green there can be seen the couples $[k_{1,\text{i}}, l_{1,\text{i}}]$ leading or not to violation. The values represented are the samples $[k_{1,\text{i}}, l_{1,\text{i}}]$ scaled by the mean values of k_1 and l_1, respectively. It is relevant to see that the parameter which plays the biggest role in the violations is k_1. As a matter

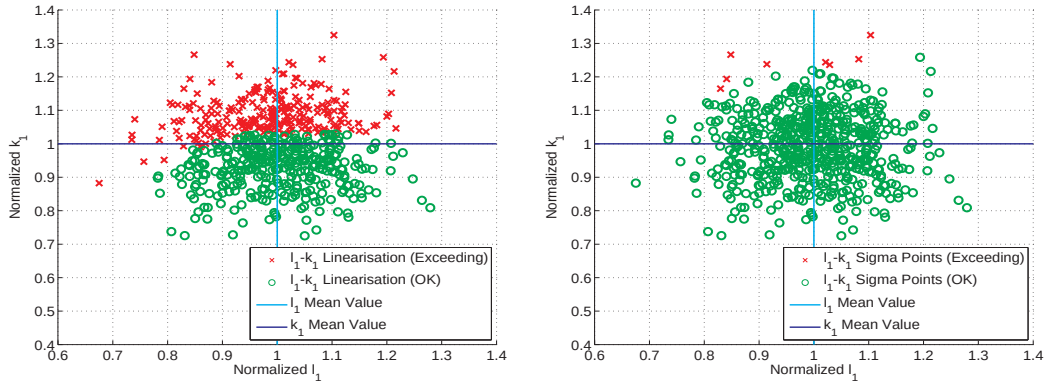

(a) *Linear approximation.* **(b)** *Sigma points approximation.*

Figure 5.18: *Williams-Otto reactor: k_1 and l_1 distribution, comparison between the two robustification approaches.*

of fact, for both robustification approaches high values of k_1 lead to violations, while the influence of l_1 is rather small.

A discussion concerning the loss in terms of objective function, size of the problems and time needed to solve the OCPs will be given in Section 5.3.2, in Tables 5.9 and 5.10.

5.3.2 Williams-Otto reactor with uncertainties on k_1, k_2, k_3 and l_1

In this Section, four uncertain parameters, k_1, k_2, k_3 and l_1 will be considered during the optimisation of the WO reactor. Their mean values and variance-covariance matrix were provided in Section 5.3. However, in Section 5.3.1, it was already demonstrated that the linearisation approach is ineffective for this case study. For this reason, when considering the four uncertain parameters case, only results obtained through the sigma points approximation will be shown.

In Figure 5.19, the optimal control profiles for the sigma points approach are presented. In order to compare with the previous case, both the four-parameters and the two-parameters profiles are depicted.

The empirical and predicted 95% confidence regions are given in Figure 5.20. It is clear that the introduction of two additional uncertain parameters leads to only a modest increase in the confidence region, when compared to the one shown in Section 5.3.1. This holds for both the predicted and empirical confidence regions.

Moreover, in Figure 5.20b it is evident that the empirical 95% confidence region is kept within the boundaries of the states, for each time interval. Thus, again, less than 30 violations have occurred. The exact values of violations for each of the solved OCPs are given in Table 5.8. Even with four uncertain parameters, the sigma points

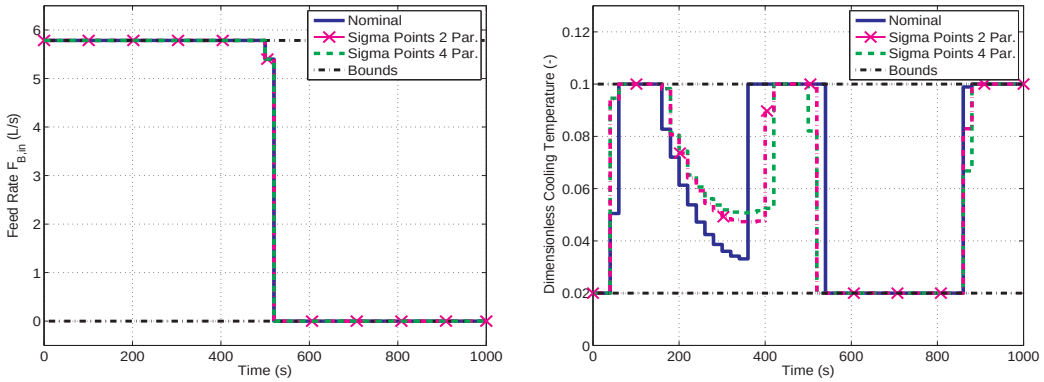

(a) *Inlet feed rate* $F_{\mathrm{B,in}}(t)$. **(b)** *Dimensionless cooling water temperature* $T_{\mathrm{W}}(t)$.

Figure 5.19: *Williams-Otto reactor: control actions with* k_1, k_2, k_3 *and* l_1 *as uncertain parameters.*

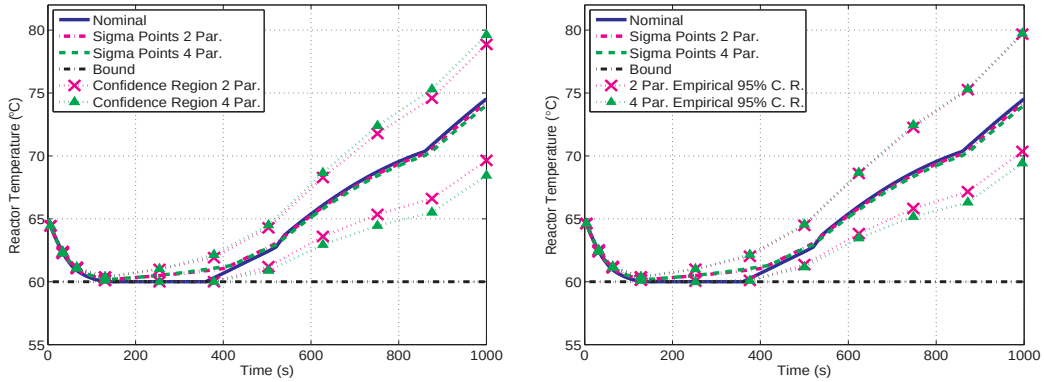

(a) *Predicted* 95% *confidence region.* **(b)** *Empirical* 95% *confidence region.*

Figure 5.20: *Williams-Otto reactor: temperature profiles and their predicted and empirical* 95% *confidence regions with* k_1, k_2, k_3 *and* l_1 *as uncertain parameters.*

Table 5.8: *Williams-Otto reactor: exceeding temperature profiles with* k_1, k_2, k_3 *and* l_1 *as uncertain parameters.*

OCP	# Violations	# Realisations	% Violations
Nominal	296	600	49.33%
Linearisation	260	600	43.33%
Sigma points	12	600	2.00%

approach is able to meet the required confidence level.

The representation of the parameters sample used for the four-parameters case is not as straight-forward as it was in the previous Sections, since a normal Cartesian plane is no more sufficient. Nevertheless, it could be interesting to see which parameters values are leading to boundary violations. In order to provide a better understanding, the Euclidean distance from the vector of mean values $\mathbf{p}_{\text{mean}} = [k_{1,\text{mean}}\ k_{2,\text{mean}}\ k_{3,\text{mean}}\ l_{1,\text{mean}}]$ is used. For each sample vector $\mathbf{p}_{\text{i}} = [k_{1,\text{i}}\ k_{2,\text{i}}\ k_{3,\text{i}}\ l_{1,\text{i}}]$ the distance is calculated according to Equation 5.9.

$$d_{\text{i}} = \sqrt{(k_{1,\text{mean}} - k_{1,\text{i}})^2 + (k_{2,\text{mean}} - k_{2,\text{i}})^2 + (k_{3,\text{mean}} - k_{3,\text{i}})^2 + (l_{1,\text{mean}} - l_{1,\text{i}})^2} \tag{5.9}$$

For all parameters k_1, k_2, k_3 and l_1 a plot is created, where the single coordinates $k_{1,\text{i}}$, $k_{2,\text{i}}$, $k_{3,\text{i}}$ and $l_{1,\text{i}}$ are plotted on the x-axis and their related distance d_{i} from the vector of mean values $\mathbf{p}_{\text{mean}}$ on the y-axis. These plots can be seen in Figure 5.21.

The coloured crosses and the green circles respectively represent the vectors $\mathbf{p}_{\text{i}}$ which are leading or not to violations. The crosses are of different colours, in order to make it easier to identify the sample $[k_{1,\text{i}}\ k_{2,\text{i}}\ k_{3,\text{i}}\ l_{1,\text{i}}]$. For example, the magenta and red crosses with distance d_{i} approximately $2.5 \cdot 10^8$ in Figure 5.21a can be found at the same distance in all the other figures, allowing to match the values of the four parameters. However, what is most important to highlight is that violations occur irrespectively of the values of k_2 and k_3. In fact, in Figures 5.21b and 5.21c, the crosses are found throughout all the depicted ranges of k_2 and k_3. On the other hand, from Figures 5.21a and 5.21d it is evident that violations occur only for $k_{1,\text{i}} \geq k_{1,\text{mean}}$ and $l_{1,\text{i}} \leq l_{1,\text{mean}}$. It can thus be concluded that the most critical parameters are k_1 and l_1.

The losses in terms of performance of the objective function, for all the OCPs solved in this Section and in Section 5.3.1, are reported in Table 5.9. Bigger losses are present for the sigma points approximation. This was expected due to the similarity of the nominal and linearised control actions. Nevertheless, since the sigma points is over-satisfying, the iterative loop that was introduced in Section 5.2.3 can be applied once more, to slightly relax Constraints 5.7. By doing this, the number

Table 5.9: *Williams-Otto reactor: objective function values for the solution of the optimal control problems.*

	Objective function $\left[\frac{\text{mol}}{\text{m}^3}\right]$
Nominal	−4768.24
Linearisation, k_1 and l_1	−4768.04
Linearisation, k_1, k_2, k_3, and l_1	−4768.04
Sigma points, k_1 and l_1	−4765.32
Sigma points, k_1, k_2, k_3, and l_1	−4747.96

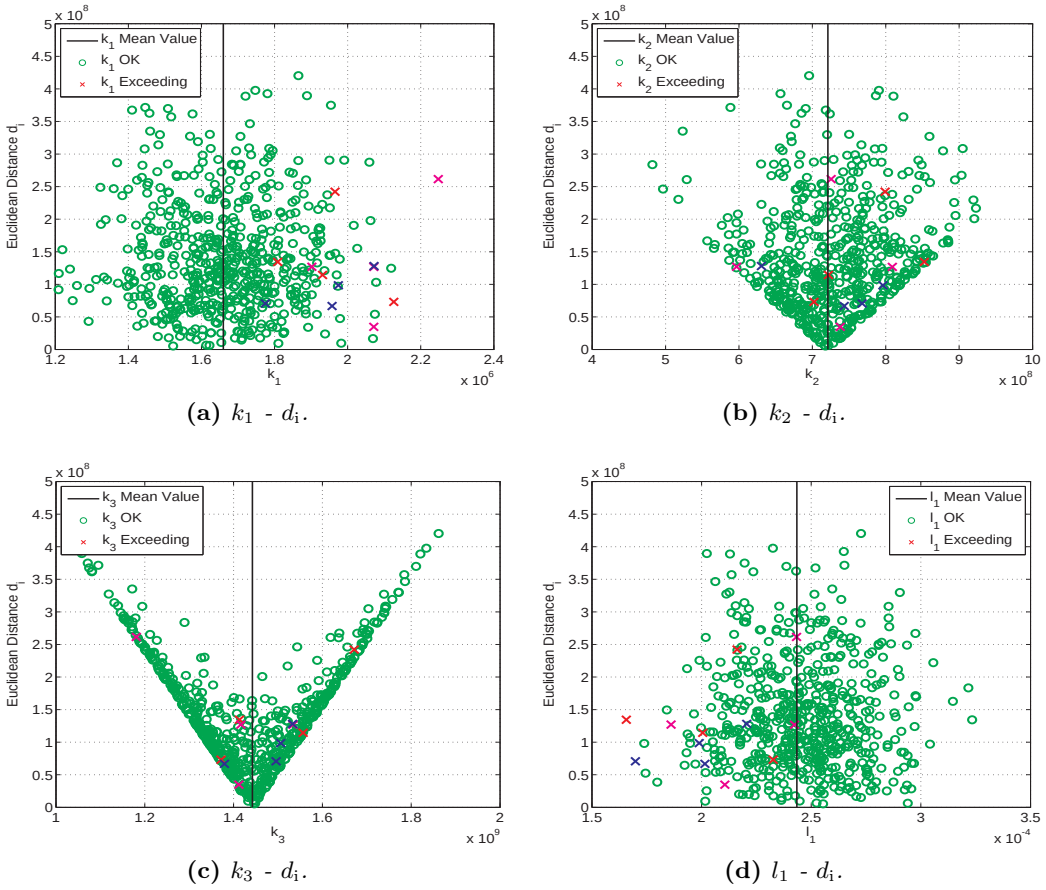

(a) k_1 - d_i. **(b)** k_2 - d_i.

(c) k_3 - d_i. **(d)** l_1 - d_i.

Figure 5.21: *Williams-Otto reactor:* $[k_1\ k_2\ k_3\ l_1]$ *samples for the Monte-Carlo realisations, sigma points approach.*

Table 5.10: *Williams-Otto reactor: number of states, variables and constraints involved and the time required for the solution of the optimal control problems.*

	# States	# Variables	# Constraints	Time [s]
Nominal	8	1700	3800	2.43
Linearisation, k_1 and l_1	44	8900	20200	299.77
Linearisation, k_1, k_2, k_3, and l_1	44	8900	20200	371.30
Sigma points, k_1 and l_1	40	8100	18400	12.04
Sigma points, k_1, k_2, k_3, and l_1	72	14500	32800	35.52

of violations can be increased up to the required 5% and the loss in the objective function moderately reduced.

Lastly, Table 5.10 gives an overview of the sizes of the problems solved in this Section and Section 5.3.1 and of the time required to reach the optimal solutions. Again, the sigma points approximations proves to be less time-demanding than the related linear ones. Additionally, a comparison could be made with the time required for the solution of the jacketed tubular reactor of Section 5.2. Considering in both cases the biggest problem, the number of variables and constraints is more than doubled for the WO, which presents $14,500$ variables and $32,800$ constraints to be handled. Readers should not be misleaded by the time required to reach the optimal solution. Although the time is certainly affordable, this is a rather complicated problem, involving 72 differential equations, which can not be solved such easily by all the solution methodologies presented in Section 2.3.

Nevertheless, it is important to highlight that this difference in computing time has increased with respect to the jacketed tubular reactor example. As a matter of fact, for the WO reactor, the time required by the linear approximation is, respectively, one and two orders of magnitude higher than those required by the sigma points approximation and the nominal case.

5.4 Conclusion

In this Chapter, robust optimal control was investigated. The jacketed tubular reactor example was solved both with ACADO Toolkit and Pomodoro, with the aim of assessing the algorithms implemented in the latter. It was seen that the results are close enough to be comparable and, after the one of Chapter 4, this is an additional indication of the reliability of Pomodoro.

All the successive Sections of this Chapter were then devoted to the computationally efficient solution of robust OCPs. This was done for two case studies, a jacketed tubular reactor (Logist et al., 2011) (Houska et al., 2012) and the Williams-Otto reactor (Williams and Otto, 1960) (Forbes, 1994) (Hannemann and Marquardt, 2010).

The linearisation led to better results in the first example but, when dealing with higher degrees of non-linearity, as in the WO case study, it has proven to be completely ineffective. It was also shown that the sigma points approximation brings to solutions faster than the linear approach, even if, aiming at the highest degree of generalisation, four uncertain parameters were considered, as in Section 5.3.2.

However, the required confidence level is not always satisfied. In order to deal with this feature, an iterative loop was introduced in Section 5.2.3, with the aim of reaching the desired confidence level.

Based on this, the sigma points approach should be the natural choice also for practical industrial problems, when highly non-linear systems are involved. This

will be done in the following Chapter, when the optimisation of a chemical vapour deposition reactor will be accomplished.

Chapter 6

Robust multi-objective optimal control of a CVD reactor

6.1 Introduction

In this Chapter, the optimisation of a real industrial process is investigated with the techniques presented in the previous Chapters. The process considered is the chemical vapour deposition for the production of polysilicon rods. Polysilicon consists of high purity silicon crystals, according to del Coso et al. (2011) up to 99.9999999% purity, and is mainly produced for the micro-electronics and photo-voltaic (PV) markets (del Coso et al., 2011). In particular, until 1997, the polysilicon demand for the production of solar cells was entirely covered by micro-electronics waste or excess of industrial capacity (del Coso et al., 2007) (Braga et al., 2008). However, in the early 2000's a rapid change in the market has taken place, mainly due to the fast growth of the PV industry. While in 2000 PV demanded just 10% of the overall polysilicon production, in 2005 it's share was comparable to that of the micro-electronics industry, ranging around $15,000 \left[\frac{\text{ton}}{\text{year}}\right]$ (Rogol, 2006 as cited in del Coso et al. (2007)). In 2009, the total amount of polysilicon produced was $100,000 \left[\frac{\text{ton}}{\text{year}}\right]$, with the PV industry consuming approximately $80,000 \left[\frac{\text{ton}}{\text{year}}\right]$ (Rogol, 2010 as cited in del Coso et al. (2011)).

Moreover, it is important to highlight that, in spite of the global crisis, the photo-voltaic industry is expected to be expanding also in the next future (Masson et al., 2013). The amount of PV capacity installed worldwide in 2013 has been 24% higher than that of 2012 (Market report 2013. EPIA - European Photovoltaic Industry Association, 2014) and by 2017 it is expected to be between 55% and 170% higher than that of 2012, depending whether a business-as-usual or policy-driven scenario will develop (Masson et al., 2013). However, care should be taken when handling these data, since polysilicon is not the only technology applied in the PV industry (Masson et al., 2013). Nevertheless, together with mono-crystalline silicon, it accounts for a market share ranging between 80% and 90% and the manufacturing

is shifting more and more towards polycrystalline silicon technology (solarbuzz, 2014). For all these reasons, polysilicon production through CVD is a relevant industrial process to be investigated in this thesis.

The reactor where the deposition takes place is often called Siemes reactor, due to its first application (Viganò et al., 2010). This reactor operates in semi-batch mode. At start, depending on the reactor configuration, 36, 48 or 60 seed bars of pure silicon with radius $r_0 = 0.5$[cm] and length $L = 2$[m] are placed inside the reactor (del Coso et al., 2011). The deposition reaction takes then place over these seed bars, which are connected two-by-two with a U-turn at their top and are usually placed in concentric circles in the bell-shaped reactor (Viganò et al., 2010) (del Coso et al., 2011). For this reason, they are usually referred to as U-rods. The bars are kept inside the reactor until their radius has increased to a certain extent, then the reactor is stopped and the bars are replaced with new seeds. Silanes are continuously fed to the reactor chamber and, due to the high temperatures, silicon reduces and deposits on the seed bars, according to the reaction Scheme 6.1. The hydrogen produced is continuously removed.

In practice, due to the low vapour pressure of silanes, the Siemens reactor is operated at low pressure (Viganò et al., 2010). In this thesis, $P = 1$[atm] is chosen. The reactor temperature is always kept at values $T \geq 750$[K] (Viganò et al., 2010). High temperatures are needed due to the endothermicity of the reaction. For this reason, energy must be provided to the system. This is done through the *Joule effect*, meaning that electric current is sent through the seed bars of silicon, increasing their temperatures (Viganò et al., 2010). In this thesis, the current intensity sent through the bars is the control variable of the system. However, this heating system has one important drawback. The continuous flow of electric current through the silicon bars leads to high energy consumptions for a CVD reactor, in the range $45 - 50 \left[\frac{\text{kWh}}{\text{kg}}\right]$ (Ramos et al., 2013). This accounts for around 65% of the overall energy consumption of a polysilicon production plant (Keck, 2012 as cited in Ramos et al. (2013)) making the feedstock material impacting for 28% on the energy payback time of a PV module (Alsema and de Wild-scholten, 2007 as cited in Ramos et al. (2013)). The necessity to minimise energy consumption is thus evident.

The aim of this Chapter is to optimise the CVD reactor with respect to the maximisation of the production and the minimisation of the energy consumption. These are clearly conflicting objectives since, as said, high temperature is needed because of the endothermicity of the reaction. Additionally, high temperature enhances the kinetics of the reaction, leading to faster radius growth.

The system dynamics describing the reactor will be introduced and explained in Section 6.2, together with the reaction scheme. Afterwards, Section 6.3 will present all the results obtained for the optimisation of the CVD reactor. These will be subdivided in several subsections.

Firstly, in Sections 6.3.1 and 6.3.2, the start-up of the reactor will be accomplished

and the OCPs for the solution of the single objectives reported, together with the multi-objective optimal control problem.

Secondly, in Section 6.3.3, the OCPs for the anchor points will be solved by accounting for one and two uncertain parameters. This will be done by exploiting the sigma points approximation.

Thirdly, in Section 6.3.4, the concept of robustification will be applied to the multi-objective optimal control problem of Section 6.3.2.

Finally, Section 6.4 will conclude the Chapter, summarising and highlighting the most important results.

6.2 The problem

In this thesis, a lab-scale reactor with a single seed bar is investigated. A schematic representation of the reactor is given in Figure 6.1. The dimensions of the system are also different from those of the industrial process, since the length of the bar is just $L = 30$[cm]. The radius of the seed bar is not given directly but calculated from the initial external surface area, which is $A_0 = 120\ [\text{cm}^2]$. Moreover, the reactor is not cilindrical, but it has the shape of a parallelepipedon. More information on the geometrical and operating parameters of the reactor are given in Appendix A.

The reactions taking place in the CVD reactor are shown in Equation 6.1. The presented scheme was firstly introduced by Weerts et al. (1998) and then adapted

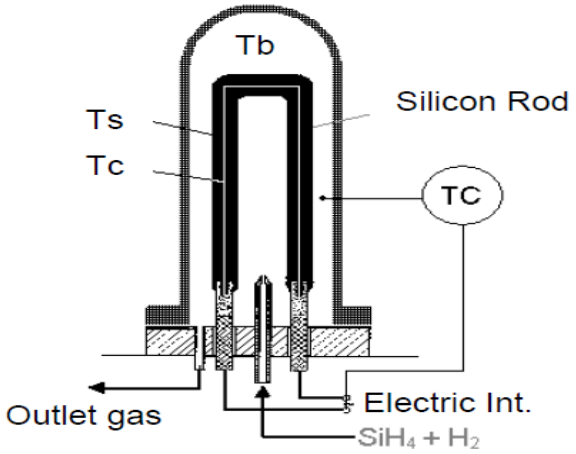

Figure 6.1: *Chemical vapour deposition reactor: schematic representation. Gentle courtesy of Viganò et al. (2010).*

and lumped by Masi et al. (2000).

$$SiH_4 \rightarrow SiH_2 + H_2 \tag{6.1a}$$

$$SiH_2 \xrightarrow{\text{surface}} Si_{(s)} + H_2 \tag{6.1b}$$

$$SiH_4 \xrightarrow{\text{surface}} Si_{(s)} + 2H_2 \tag{6.1c}$$

The product of interest is the surface silicon $Si_{(s)}$. This can be obtained either from direct deposition of the silane feed, according to Reaction 6.1c or from the deposition of the intermediate product, sylilene, conforming to Reaction 6.1b. The deposition reactions of silane and sylilene take place after their adsorption on the surface of the rod, which can be seen as a catalyst (Viganò et al., 2010). The silane is fed to the reactor together with hydrogen as a carrier fluid (Viganò et al., 2010).

The system dynamics is composed of 10 differential states and one manipulated variable, which is the current intensity $I(t)\left[\frac{\mathrm{A}}{\mathrm{m}^2}\right]$. It has been proposed by Viganò et al. (2010) and adapted subsequently in Claessens (2013), Vallerio et al. (2014) and Vallerio et al. (July 2014), to which interested readers are referred to for additional information on the model development.

The terms $C_{\mathrm{i}}^{\mathrm{V}}\left[\frac{\mathrm{mol}}{\mathrm{cm}^3}\right]$ and $C_{\mathrm{i}}^{\mathrm{S}}\left[\frac{\mathrm{mol}}{\mathrm{cm}^3}\right]$, with $\mathrm{i} = SiH_4,\ SiH_2,\ H_2,\ Si$ represent the concentrations of all the species in the vapour phase inside the reactor and on the surface of the bar. $\dot{F}_{\mathrm{IN}}\left[\frac{\mathrm{mol}}{\mathrm{s}}\right]$ and $\dot{F}_{\mathrm{OUT}}\left[\frac{\mathrm{mol}}{\mathrm{s}}\right]$ stand for the molar flow rate of the inlet and outlet stream, respectively. The mass and heat transfer coefficients are represented by the terms $h_{\mathrm{m,i}}\left[\frac{\mathrm{cm}}{\mathrm{s}}\right]$ and $h_{\mathrm{T}}\left[\frac{\mathrm{W}}{\mathrm{m}^2\ \mathrm{K}}\right]$. The latter is calculated as $h_{\mathrm{T}} = \frac{\mathrm{Nu}_{\mathrm{T}} k_{\mathrm{T}}}{H}$. $A\left[\mathrm{cm}^2\right]$ and $V\left[\mathrm{cm}^3\right]$ are emboding the surface of the rods and the vapour-phase reactor volume. $R\,[\mathrm{cm}]$ and $V_{\mathrm{R}}\left[\mathrm{cm}^3\right]$ are instead the bar radius and volume. The factors $k_1\left[\frac{1}{\mathrm{s}}\right]$, $k_2\left[\frac{\mathrm{cm}}{\mathrm{s}}\right]$, $k_3\left[\frac{\mathrm{cm}}{\mathrm{s}}\right]$, represent the kinetic constants for the three reactions already introduced in Equation 6.1. $\mathrm{NC} = 3$ is the number of vapour-phase components, $\mathrm{NRS} = 2$ and $\mathrm{NRV} = 1$ those of surface and vapour-phase reactions. The molar reaction enthalpies are embodied in $\Delta\tilde{H}_{\mathrm{R,j}}\left[\frac{\mathrm{kJ}}{\mathrm{mol}}\right]$. $\tilde{H}_{\mathrm{f,i}}\left[\frac{\mathrm{kJ}}{\mathrm{mol}}\right]$ and $C_{\mathrm{p,i}}\left[\frac{\mathrm{J}}{\mathrm{mol\ K}}\right]$ are the formation enthalpies and specific heats for all components i, while $\rho_{\mathrm{Si}}\left[\frac{\mathrm{mol}}{\mathrm{cm}^3}\right]$ is the silicon molar density.

The thermal and electrical conductivities of the silicon rod are respectively represented by $\lambda_{\mathrm{T}}\left[\frac{\mathrm{W}}{\mathrm{m\ K}}\right]$ and $\lambda_{\mathrm{e}}\left[\frac{\mathrm{S}}{\mathrm{m}}\right]$. $\sigma\left[\frac{\mathrm{W}}{\mathrm{m}^2\ \mathrm{K}^4}\right]$ is the Stefan-Boltzmann constant, while the factor F accounts for the absorptivity of the bulk. This dimensionless factor is defined as the fraction of radiation absorbed by the vapour bulk with respect to the original amount of radiation emitted by the rod (Claessens, 2013) (Vallerio et al., July 2014). Consequently, $(1 - F)$ is the fraction of radiation absorbed by the wall. ε is instead the reflectivity factor of the wall, identifying how much of the radiation heat which is absorbed by the wall itself is sent back on the surface road. Lastly, T, T_{W}, T_{S} and T_{C} stand for the temperatures of the vapour-phase, that of the reactor wall and those of the rod surface and core. They are all measured in [K].

Most of the values of the constants introduced in these paragraphs are provided

in Appendix A, together with the dimensions of the reactor and with the feed stream concentration.

$$\frac{dC^{V}_{SiH4}}{dt} = \frac{\dot{F}_{IN}}{V}C^{IN}_{SiH4} - \frac{\dot{F}_{OUT}}{V}C^{V}_{SiH4} - h_{m,SiH4}\frac{A}{V}\left(C^{V}_{SiH4} - C^{S}_{SiH4}\right) - k_1 C^{V}_{SiH4} \tag{6.2a}$$

$$\frac{dC^{S}_{SiH4}}{dt} = h_{m,SiH4}\frac{A}{V}\left(C^{V}_{SiH4} - C^{S}_{SiH4}\right) - k_3 C^{S}_{SiH4}\frac{A}{V}, \tag{6.2b}$$

$$\frac{dC^{V}_{SiH2}}{dt} = \frac{\dot{F}_{IN}}{V}C^{IN}_{SiH2} - \frac{\dot{F}_{OUT}}{V}C^{V}_{SiH2} - h_{m,SiH2}\frac{A}{V}\left(C^{V}_{SiH2} - C^{S}_{SiH2}\right) + k_1 C^{V}_{SiH4} \tag{6.2c}$$

$$\frac{dC^{S}_{SiH2}}{dt} = h_{m,SiH2}\frac{A}{V}\left(C^{V}_{SiH2} - C^{S}_{SiH2}\right) - k_2 C^{S}_{SiH2}\frac{A}{V} \tag{6.2d}$$

$$\frac{dC^{V}_{H2}}{dt} = \frac{\dot{F}_{IN}}{V}C^{IN}_{H2} - \frac{\dot{F}_{OUT}}{V}C^{V}_{H2} - h_{m,H2}\frac{A}{V}\left(C^{V}_{H2} - C^{S}_{H2}\right) + k_1 C^{V}_{SiH4} \tag{6.2e}$$

$$\frac{dC^{S}_{H2}}{dt} = h_{m,H2}\frac{A}{V}\left(C^{V}_{H2} - C^{S}_{H2}\right) + k_2 C^{S}_{SiH2}\frac{A}{V} + 2k_3 C^{S}_{SiH4}\frac{A}{V} \tag{6.2f}$$

$$\frac{dC^{S}_{Si}}{dt} = k_2 C^{S}_{SiH2}\frac{A}{V} + k_3 C^{S}_{SiH4}\frac{A}{V} \tag{6.2g}$$

$$\begin{aligned}\sum_{i=1}^{NC} C_i V \tilde{C}p_i \frac{dT}{dt} &= \dot{F}_{IN}\sum_{i=1}^{NC} C^{IN}_i \left(\tilde{H}_{f,i}(T_{rif}) + \int_{T_{rif}}^{T_{IN}} \tilde{C}p_i dt\right) \\ &- \dot{F}_{OUT}\sum_{i=1}^{NC} C^{V}_i \left(\tilde{H}_{f,i}(T_{rif}) + \int_{T_{rif}}^{T} \tilde{C}p_i dt\right) + \sum_{j=1}^{NRV} r_i V\left(-\Delta\tilde{H}_{R,j}(T)\right) \\ &+ h_T A\left(T_S - T\right) + h_T A_R\left(T_W - T\right) + \varepsilon\left(F\right)\sigma A\left(T_S^4 - T_W^4\right)\end{aligned} \tag{6.2h}$$

$$\begin{aligned}\left(\rho_{Si} V_R Cp_{Si}\right)\frac{dT_S}{dt} &= -h_T A\left(T_S - T\right) - \varepsilon\left(1 - F\right)\sigma A\left(T_S^4 - T_W^4\right) \\ &+ \frac{\lambda_T}{R}A\left(T_C - T_S\right) + \sum_{k=1}^{NRS} r_i A\left(-\Delta\tilde{H}_{R,k}(T_S)\right)\end{aligned} \tag{6.2i}$$

$$T_C = T_S + \left(\frac{I^2}{\lambda_e}\right)\frac{R^2}{4\lambda_T} \tag{6.2j}$$

As anticipated, two objective functions will be considered in this work. The first one is the maximisation of the production, which is expressed as the maximisation of the external surface area $A(t_f)$. This objective, however, can directly be associated to the maximisation of $C^{S}_{Si}(t_f)$. The higher the silicon surface concentration, in fact, the bigger will be the final external surface area of the bar. This objective will be posed in the Mayer form, according to the definition given in Section 2.2.

The second one is the minimisation of the energy consumption. This is of course an objective in the Lagrange form, since it is important to minimise the sum of the energy consumed at all time. However, as explained in Section 2.2, by introducing an additional state equation in the system this objective function is re-written in the Mayer formulation.

The energy E is calculated by integrating over time the instantaneous power P required by the electric current. For the formulation of the second objective function, a three-phase alternate current is assumed to be used. Such a system is composed of three sinusoidal voltages, with same magnitude, but out of phase of a value $\frac{2\pi}{3}$ (Schavemaker and van der Sluis, 2008). The power consumed by such a system can be expressed as (Weedy and Cory, 2004)

$$P = \sqrt{3}\Delta V \left(2I\pi R^2\right) pf \tag{6.3}$$

where P[W] is the power and ΔV[V] is the voltage of the current which will be assumed to be $\Delta V = 220$[V], as the standard load in Belgium (VREMCO, 2014). $2I\pi R^2$[A] is the current intensity. The power factor pf, instead, is accounting for the phase angle between the three voltages. It is usually expressed as a cosine (Weedy and Cory, 2004) (Schavemaker and van der Sluis, 2008), thus, aiming at the most conservative case, in this thesis it will be assumed $pf = 1$.

The final MOOCP is given in Equation 6.4

$$\underset{\mathbf{x}(t),u(t),\mathbf{p},t_\mathrm{f}}{\text{minimise}} \quad \left\{J_1 = -C^\mathrm{S}_\mathrm{Si}(t_\mathrm{f}),\ J_2 = E(t_\mathrm{f})\right\} \tag{6.4a}$$

$$\text{subject to} \quad \frac{d\mathbf{x}}{dt} = \mathbf{f}(\mathbf{x}(t), u(t), \mathbf{p}, t) \tag{6.4b}$$

$$\frac{dE}{dt} = \int_{t=0}^{t=t_\mathrm{f}} P\ dt \tag{6.4c}$$

$$\mathbf{x}(0) = \mathbf{x}_0 \tag{6.4d}$$

$$C^\mathrm{S}_\mathrm{i} \geq 0 \qquad \forall \mathrm{i} = \mathrm{SiH_4},\ \mathrm{SiH_2},\ \mathrm{H_2},\ \mathrm{Si} \tag{6.4e}$$

$$C^\mathrm{V}_\mathrm{i} \geq 0 \qquad \forall \mathrm{i} = \mathrm{SiH_4},\ \mathrm{SiH_2},\ \mathrm{H_2} \tag{6.4f}$$

$$[373.15,\ 1065.15,\ 1065.15] \leq [T(t),\ T_\mathrm{S}(t),\ T_\mathrm{C}(t)] \leq [2000,\ 1687,\ 1687] \tag{6.4g}$$

$$[0] \leq u(t) \leq [150] \tag{6.4h}$$

which is created according to the formulation given in Section 2.4. The two objective functions have already been explained. The only remark is that the production maximisation is transformed in a minimisation problem, by adding a minus sign in front of it. The dynamic system enters the OCP in Constraints 6.4b and 6.4c. It is known that a concentration can not be negative. Thus, in Equations 6.4e and 6.4f, the concentrations C^S_i and C^V_i, are asked to always be higher than 0.

The most important bounds, however are those referred to T_S and T_C, in Equation 6.4g. In fact, the former must always be kept at $T_\mathrm{S} \geq 1065.15$[K] to allow the deposition to occur. The latter, instead, must always be $T_\mathrm{C} \leq 1687$[K] which is the melting temperature of polysilicon. The initial conditions $\mathbf{x}(0)$ are not given explicitly in this Section, since before operating the reactor, the necessary start-up operation must be accomplished.

6.3 Chemical vapour deposition results

In this Section, the results for the multi-objective and robust optimal control problem of the CVD reactor are reported. Firstly, in Section 6.3.1 the start-up operation is accomplished. Afterwards, in Sections 6.3.2 and 6.3.3 the results of the multi-objective optimisation and the robust OCPs are reported. Lastly in Section 6.3.4, the robustification concept is applied to the multi-objective optimal control problem and the effects on the Pareto set are observed.

All the simulations except the one presented in Section 6.3.1 have been accomplished for a batch time of 3 days and a discretisation of 432 equally spaced points, meaning one point every 10 minutes. The time-span, instead has been chosen as comparable to that of an industrial-scale batch, which is typically $80 - 100$ hours (Ramos et al., 2013). Concerning the MOOCPs, all the Pareto sets which will be shown are composed of 21 Pareto optimals. Furthermore, according to Equation 6.4a, the production objective is expressed in a negative form, to allow its maximisation. As a consequence, all Pareto sets presented in this Chapter will depict a negative external surface.

Additionally, as it is possible to see in the initial Conditions 6.5, the gaseous bulk is composed for a fraction of 99.9% of hydrogen gas. Thus, the bulk absorptivity coefficient of Equations 6.2h and 6.2i is assumed to be $F = 0$ (Claessens, 2013).

6.3.1 Start-up

At first, the reactor is assumed to be shut down. Thus in order to bring it at the correct temperature, start-up must be executed. This is done by solving an OCP with the aim of minimising the time required to reach a surface temperature of 1070[K]. To the purpose of this thesis, this optimisation does not lead to fundamental results, but it is a necessary step to find the correct initial conditions to fill in Equation 6.4d, which can then be rewritten as:

$$\begin{aligned}&\left(\mathrm{C}^{\mathrm{V}}_{\mathrm{SiH4}},\ \mathrm{C}^{\mathrm{S}}_{\mathrm{SiH4}},\ \mathrm{C}^{\mathrm{V}}_{\mathrm{SiH2}},\ \mathrm{C}^{\mathrm{S}}_{\mathrm{SiH2}},\ \mathrm{C}^{\mathrm{V}}_{\mathrm{H2}},\ \mathrm{C}^{\mathrm{S}}_{\mathrm{H2}},\ \mathrm{C}^{\mathrm{S}}_{\mathrm{Si}},\ \mathrm{T},\ \mathrm{T_S},\ \mathrm{E}\right)(0) = \\ &\quad [3.176 \cdot 10^{-2},\ 5.686 \cdot 10^{-4},\ 5.370 \cdot 10^{-3},\ 4.759 \cdot 10^{-8},\ 30.76,\ 2.023, \\ &\quad 5.081 \cdot 10^{-4},\ 435,\ 1070,\ 13.17]\end{aligned} \tag{6.5}$$

The units were already given in the model description in Section 6.2.

In Equation 6.5, no initial condition on T_{C} is given. As a matter of fact, from the system dynamics in Equations 6.2, it is possible to see that the core temperature T_{C} is influencing only the dynamic equation of the surface temperature T_{S}. Thus, in order to decrease the number of states and to make the problem less computationally intensive its formulation is directly replaced in Equation 6.2i eliminating the differential state Equation 6.2j from the system. T_{C}, when needed, will then be calculated outside the optimisation problem.

With the initial conditions assessed, it is possible to present the results of the optimisations accomplished in this Chapter.

6.3.2 Multi-objective optimal control problem

In this section, the results for the multi-objective optimisation of the chemical vapour deposition reactor are provided. As a first step, the two anchor points are solved individually.

The control profiles can be seen in Figure 6.2. Important to notice is that the current intensity necessary for the maximisation of the radius is decreasing with time. This is a direct consequence of the increasing size of the bar. In fact, careful readers, could have already anticipated that, for this objective function, the temperature profile would have been very close to its upper bound, to enhance reaction kinetics and thermodynamics. However, as the radius grows, the current intensity has to decrease or the bar core would melt.

This feature can be better understood by looking at Figure 6.3a, where it is clear how the T_C is always kept at its upper bound, while T_S is slightly decreasing, due to the bar growth. Figure 6.3b, instead, shows the profiles of T_C and T_S when the objective J_2 is minimised. It is evident that the surface temperature is kept at its lower bound, in order to avoid excessive heating. Moreover, a behaviour opposite to that of Figure 6.3a is observed. Here, in fact, T_C is increasing, to keep T_S constant.

Additionally, it is interesting to look at the behaviour of the two objective functions. From Figure 6.4a, it is possible to see that, after three days of operation, the external surface of the bar is either 136.89 $[\text{cm}^2]$ or 136.20 $[\text{cm}^2]$ depending on the objective function considered. On the other hand, the related energy consumptions are 1395[kJ]

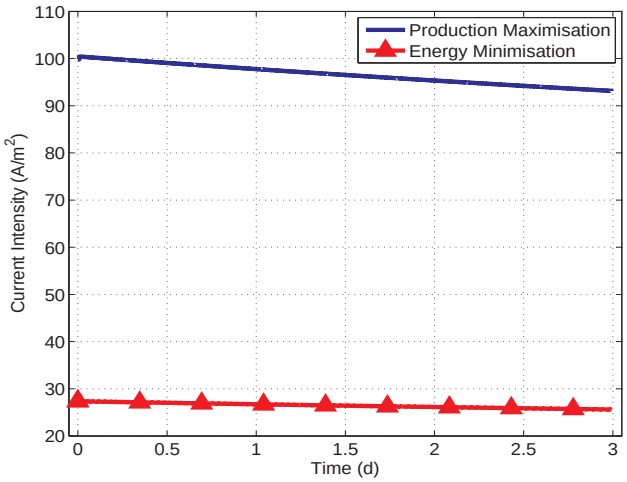

Figure 6.2: *Chemical vapour deposition reactor: optimal control profiles for the two anchor points.*

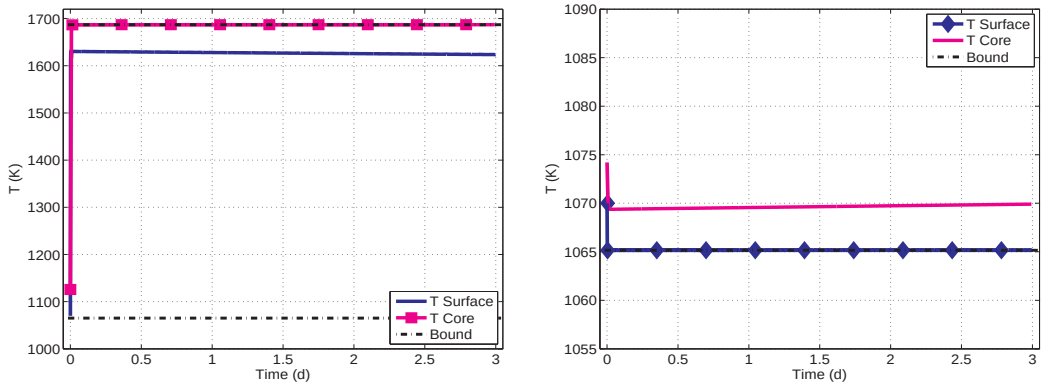

(a) *Production maximisation, J_1.* **(b)** *Energy minimisation, J_2.*

Figure 6.3: *Chemical vapour deposition reactor: core and surface temperatures for the two anchor points.*

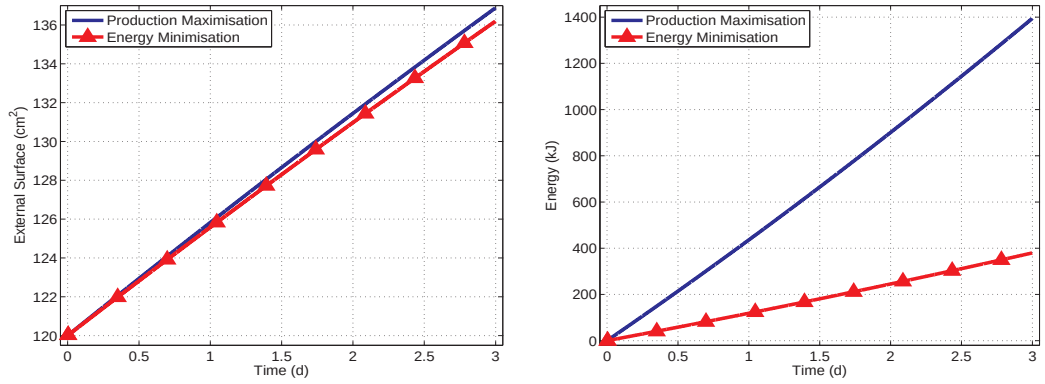

(a) *External surface area, A.* **(b)** *Energy consumption, E.*

Figure 6.4: *Chemical vapour deposition reactor: external surface area of the bar and energy consumption for the two anchor points.*

and 380 [kJ]. This implies that, a decrease in the production of only 0.5% can lead to energy saving in the order of 70%. This can be a really valuable information for the plant-manager or the decision-maker in general. Nevertheless, in some particular circumstances, pushing the production to its maximum might still be worthwhile. This can be done, for instance, at night, when energy prices are generally lower, or when the world-wide polysilicon demand is raising, leading to higher prices at which the product can be sold.

Up to this point, only the extreme points have been discussed. However, there can be the case when the decision-maker is interested in none of the two, preferring some intermediate points. Thus a multi-objective optimal control problem needs to be solved, exploiting the techniques presented in Section 2.5.

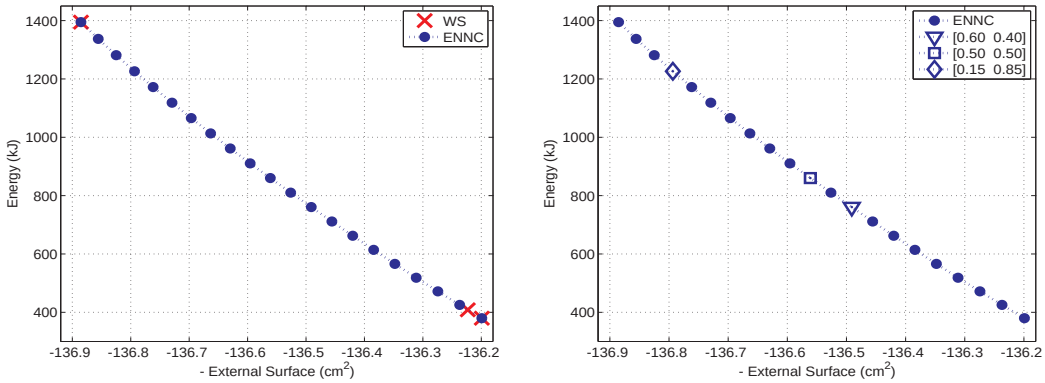

(a) *Pareto set calculated with WS and ENNC methods.*

(b) *Pareto set calculated with the ENNC method and intermediate points highlighted.*

Figure 6.5: *Chemical vapour deposition reactor: Pareto sets calculated with the WS and ENNC methods.*

In particular, in Figure 6.5a, the Pareto sets obtained with the WS and ENNC methods are presented. It is possible to see how, due to the highly non-linear behaviour of the system dynamics, the WS method is not even able to depict a Pareto set. Although 21 points were required, only 3 of them were detected. All others are perfectly overlying to the energy anchor point, in the rigth bottom corner. Instead, as it was expected from the previous experience of Chapter 4, the ENNC method returns 21 equally spread Pareto optimals.

In Figure 6.5b, the same Pareto set is reported. However three Pareto optimals are stressed, with the aim of showing the behaviour of some intermediate points which the decision-maker might be interested in. The decision-maker can benefit from them and can use them to pick the solution which is considered to be the best, according to her or his preferences. Several algorithm and methodologies are available to help the decision-maker expressing his or her preferences and to help him or her making a sound choice, but they are not treated in this master thesis. Interested readers can find several examples in Miettinen (1999) and references therein.

In this work, instead, three intermediate points are selected and depicted with illustrative purposes. Their related control profiles are reported in Figure 6.6. The weighing system should be read as follows: the weights are varying in the range [0 1] and [1 0]. The former is focusing only on the production objective function, while the latter only on the energy one. Thus, the weight [0.50 0.50] implies equal importance for both objectives. Concerning the point [0.60 0.40], limited more importance is given to the energy objective function, while the point [0.15 0.85] gives significant more importance to the production objective function.

The depicted controls will give raise to different states profiles and objective functions values. In particular, the profiles of T_S and T_C are reported in Figure 6.7.

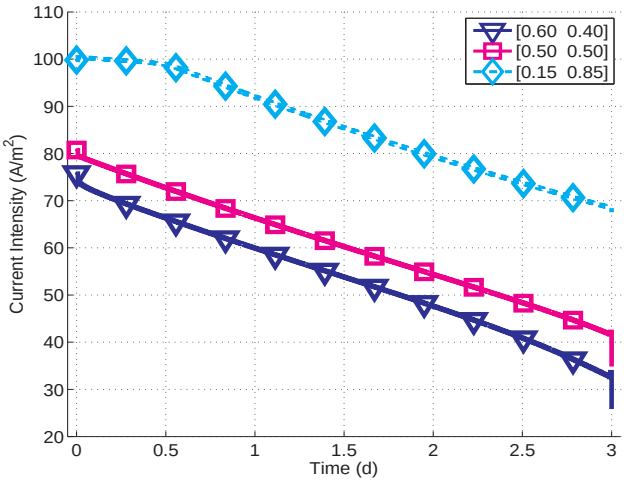

Figure 6.6: *Chemical vapour deposition reactor: optimal control profiles for three intermediate points of the Pareto set.*

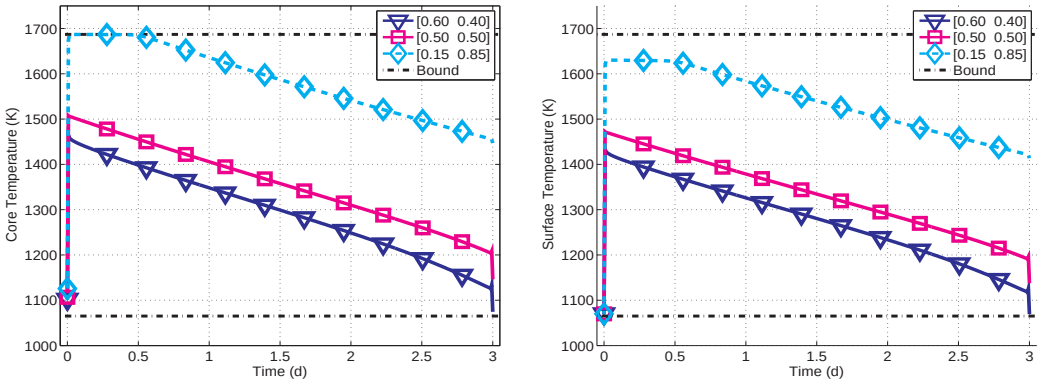

(a) T_C. **(b)** T_S.

Figure 6.7: *Chemical vapour deposition reactor: temperature profiles for three intermediate points.*

Figure 6.8, instead, shows the objective functions obtained for the three intermediate points. The external surface area has been zoomed in, to make the difference visible. However, these values are also reported in Table 6.3, when a comparison with the robust MOOCP is made.

So far, the results presented in this Section, assumed complete knowledge of the system dynamics and, in particular, of all the parameters involved. In the next Sections, the robust OCP and robust MOOCP of the CVD reactor will be addressed.

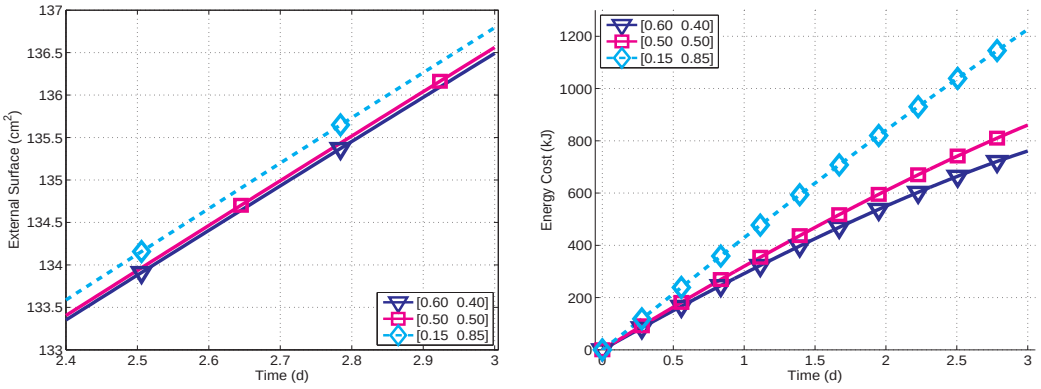

(a) *External surface area, A.* **(b)** *Energy consumption, E.*

Figure 6.8: *Chemical vapour deposition reactor: external surface area of the bar and energy consumption for three intermediate points.*

6.3.3 Robust optimal control problem

In this Section, uncertainties on two parameters will be considered when solving the anchor points of the MOOCP presented in Equation 6.4. In Chapter 5, it was already demonstrated that, for highly non-linear system dynamics, the sigma points approximation works better than the linear one, when handling parameter uncertainties. Thus, due to the high complexity of the model presented in this Chapter, the sigma points will be the approach exploited.

The uncertain parameters considered are ε, the emissivity constant of the reactor wall, and λ_e, the electrical conductivity of the silicon rod. As it has been done in Chapter 5, both parameters are assumed to be normally distributed. In particular, their mean values are $\varepsilon = 0.7$ and $\lambda_e = 2.52 \cdot 10^{-4} \left[\frac{S}{m}\right]$. Two variance-covariance matrices will be considered, respectively with standard deviation of 10% and 20% on both parameters.

$$\mathbf{V}_1 = \begin{pmatrix} 0.07^2 & 0 \\ 0 & \left(2.52 \cdot 10^{-5}\right)^2 \end{pmatrix} \tag{6.6}$$

and

$$\mathbf{V}_2 = \begin{pmatrix} 0.14^2 & 0 \\ 0 & \left(5.04 \cdot 10^{-5}\right)^2 \end{pmatrix} \tag{6.7}$$

One last remark needs to be done before presenting the results. In Chapter 5, results for the robust OCPs were always presented in accordance to the number of uncertain parameters. However, in all the examples treated in that Chapter, only one objective function was considered. On the other hand, in this Section, two different objective functions are examined. Thus, according to the author, it is more meaningful to structure the following Sections depending on the objective function

considered, rather than on the number of uncertain parameters involved. For this reason, Sections 6.3.3.1 and 6.3.3.2 respectively present the results of the robust OC for the production maximisation and for the energy minimisation problem. In both Sections, results for both one and two uncertain parameters cases are provided together.

6.3.3.1 Robust optimal control of the production maximisation problem

In this Section, the effects of one and two uncertain parameters on the production maximisation problem is considered. As it was done in Section 5.2.2, additional constraints must be introduced to the system, in order to account for the uncertain parameters.

$$\bar{y}_{\mathrm{T_C}}(t) + q\sqrt{\mathrm{P}_{\mathrm{T_C},\mathrm{T_C}}(t)} \leq 1687[\mathrm{K}] \tag{6.8a}$$

$$\bar{y}_{\mathrm{T_C}}(t) - q\sqrt{\mathrm{P}_{\mathrm{T_C},\mathrm{T_C}}(t)} \geq 1065.15[\mathrm{K}] \tag{6.8b}$$

The assumption of normally distributed profiles which was taken in the previous Chapter is accepted also for this problem. $q = 1.96$ is then chosen, implying a 95% confidence region, as in Chapter 5. This implies that local melting of the silicon rod is accepted for no more than 5% of the batches.

Additionally, the formulation of the objective function is rewritten, according to Equation 2.35, as

$$J_1 = -\left(\bar{y}_{\mathrm{C^S_{Si}}}(t_\mathrm{f}) - \tau\sqrt{\mathrm{P}_{\mathrm{C^S_{Si}},\mathrm{C^S_{Si}}}(t_\mathrm{f})}\right) \tag{6.9}$$

Again, a confidence region of 95% is taken. However, $\tau = 1.645$ since, for the objective function manipulation, only a one-sided normal distribution must be considered. In fact the variance-covariance matrix can only influence the objective function in one direction, increasing it.

The control actions for one and two uncertain parameters are shown in Figure 6.9. The blue and straight line is the control already described in Section 6.3.2 and it is used as bench-mark. As expected, the current intensity is decreased, in order to account for the additional Constraints 6.8. Moreover, accounting for two uncertain parameters leads to more extensive decreases in the control actions.

From Figure 6.10 it is possible to understand what is causing this decrease in the current intensity. The predicted 95% confidence regions of the core temperature, for all cases, are hitting the upper bound for almost all the batch duration. Thus the control action can not push the core temperature profile to its upper bound. The greater predicted 95% confidence regions of Figure 6.10b force the core temperature profiles to be lower than those of Figure 6.10a. This holds when the standard deviations taken on the parameters are either 10% or 20%.

The loss in terms of production can be seen from Table 6.1, together with the decrease in energy consumption. From Table 6.1, it is clear that the introduction of

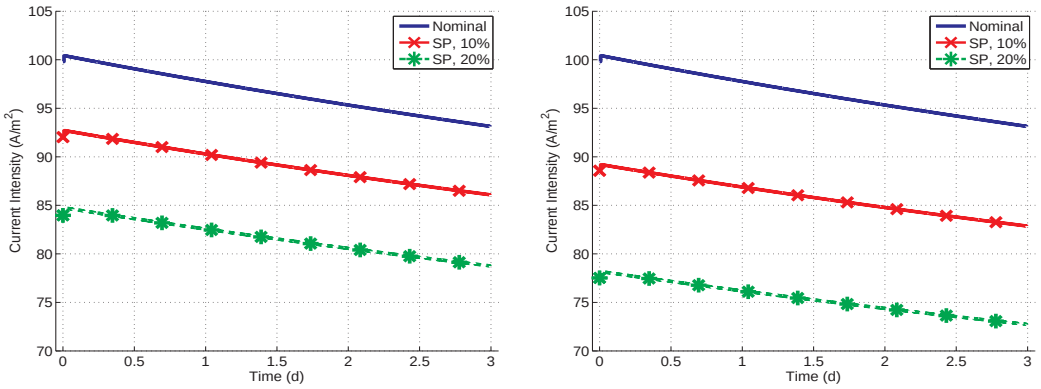

(a) *One uncertain parameter, ε.* **(b)** *Two uncertain parameters, ε and λ_e.*

Figure 6.9: *Chemical vapour deposition reactor: control profiles for the production maximisation problem with different uncertain parameters.*

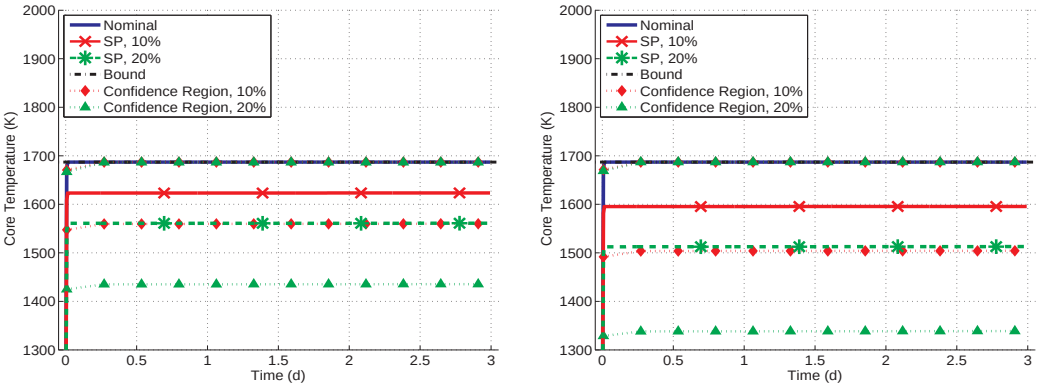

(a) *One uncertain parameter, ε.* **(b)** *Two uncertain parameters, ε and λ_e.*

Figure 6.10: *Chemical vapour deposition reactor: T_C profiles and their predicted 95% confidence regions for the production maximisation problem with different uncertain parameters.*

Table 6.1: *Chemical vapour deposition reactor: external surface area and energy consumption for the production maximisation problem.*

	$A\,(t_f)\,[\mathrm{cm}^2]$	$E\,(t_f)\,[\mathrm{kJ}]$
Nominal	136.89	1395
1 uncertainty, 10%	136.77	1288
1 uncertainty, 20%	136.66	1178
2 uncertainties, 10%	136.72	1240
2 uncertainties, 20%	136.56	1087

one or two uncertainties leads, in the worst case, at a loss of around 0.25% in terms of production. This is a negligible value. The main issue when dealing with these uncertainties, is in fact the core temperature profile, which has to be decreased up to 200[K] in order to avoid melting of the rod.

6.3.3.2 Robust optimal control of the energy minimisation problem

In this Section, the influence of one or two uncertain parameters on the second anchor point, namely the energy minimisation problem, will be considered. The two uncertain parameters considered were already described in Section 6.3.3. Both results for one and two uncertain parameters will be given in this Section, as in the previous one.

Additional constraints are again introduced, to account for the parameters uncertainties.

$$\bar{y}_{\mathrm{T_S}}(t) + q\sqrt{\mathrm{P}_{\mathrm{T_S},\mathrm{T_S}}(t)} \leq 1687[\mathrm{K}] \tag{6.10a}$$

$$\bar{y}_{\mathrm{T_S}}(t) - q\sqrt{\mathrm{P}_{\mathrm{T_S},\mathrm{T_S}}(t)} \geq 1065.15[\mathrm{K}] \tag{6.10b}$$

In this case, the most critical state is the surface temperature T_{S}, as it could be seen from Figure 6.3b.

The objective function is also manipulated, to take into account for the uncertainty over the estimated value $\bar{y}_{\mathrm{T_S}}(t)$. Following the formulation given in Equation 2.35, it can be rewritten as

$$J_2 = \left(\bar{y}_{\mathrm{E}}(t_{\mathrm{f}}) + \tau\sqrt{P_{\mathrm{E,E}}(t_{\mathrm{f}})}\right) \tag{6.11}$$

Again, the states are assumed to be normally distributed. Thus $q = 1.96$ and $\tau = 1.645$, requiring a confidence region of 95% as in the previous Section. Such a value for the confidence region means that only 5% of the batches are allowed and accepted to stop the production due to their possibly too low surface temperature T_{S}.

The control profiles are depicted in Figure 6.11. In order to account for the uncertainties, the current intensity is kept higher than in the nominal case, irrespectively of the number and the standard deviation of the uncertain parameters. As in Section 6.3.3.1, this is a consequence of the introduction of the predicted 95% confidence region in the OCP. From Figure 6.12, it is clear that the predicted 95% confidence regions are hitting the lower boundary of the surface temperature, forcing the estimated profile $\bar{y}_{\mathrm{T_S}}$ to be higher than in the nominal case. Again, it is clear that the two-parameters cases of Figure 6.12b predict greater confidence regions than the one-parameter cases of Figure 6.12a.

However, it is interesting to look at Table 6.2 to understand the increase of the energy objective function and the related changes in the production.

Differently from the previous Section, the objective function increases, in the worst case, of about 36%. Despite this relatively great increase, the production change is negligible, such that notable changes are recorded only at the 6^{th} significant digit.

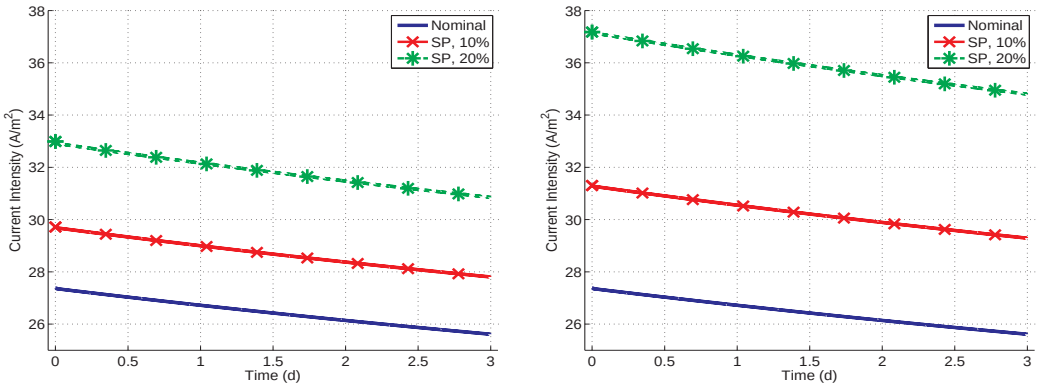

(a) *One uncertain parameter, ε.* **(b)** *Two uncertain parameters, ε and λ_e.*

Figure 6.11: *Chemical vapour deposition reactor: control profiles for the energy minimisation problem with different uncertain parameters.*

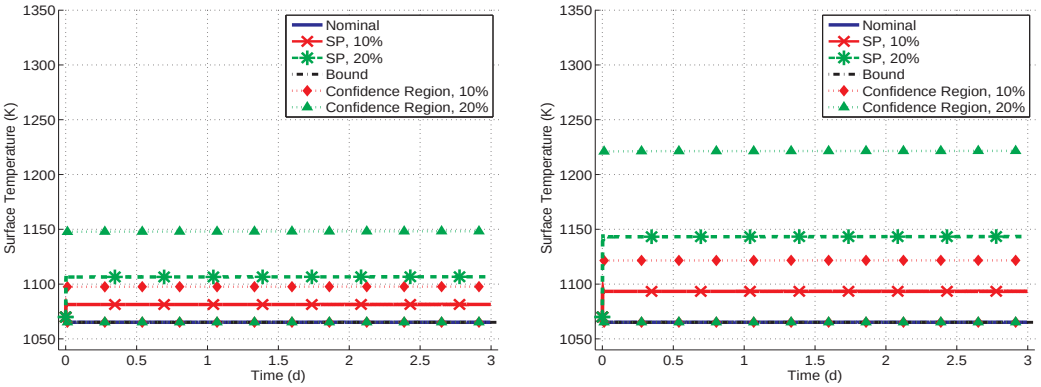

(a) *One uncertain parameter, ε.* **(b)** *Two uncertain parameters, ε and λ_e.*

Figure 6.12: *Chemical vapour deposition reactor: T_C profiles and their predicted 95% confidence regions for the energy minimisation problem with different uncertain parameters.*

Table 6.2: *Chemical vapour deposition reactor: external surface area and energy consumption for the energy minimisation problem.*

	$A\,(t_f)\,[\mathrm{cm}^2]$	$E\,(t_f)\,[\mathrm{kJ}]$
Nominal	136.1991	380
1 uncertainty, 10%	136.2034	412
1 uncertainty, 20%	136.2108	458
2 uncertainties, 10%	136.2066	434
2 uncertainties, 20%	136.2218	517

Additionally, it is interesting to notice that considering one uncertain parameter with 20% standard deviation leads to worse results, in terms of the objective function $E(t_f)$, than considering two uncertain parameters with 10% standard deviation each. The same could have been said by looking at Table 6.1, where the objective to be considered is $A(t_f)$. Thus from an economic point of view, it can be stated that it is more meaningful to work with two uncertain parameters with a given standard deviation than to have perfect knowledge on one of them but a two-fold standard deviation on the other.

In the next Section, the sigma points approach is applied to the multi-objective optimal control problem, considering the objective functions described both in this Section and in the previous one.

6.3.4 Robust multi-objective optimal control problem

In this Section, the concept of robustification is applied to a multi-objective optimal control problem. Some examples are already present in the literature. Logist et al. (2011), for instance, applied the robustification approach presented in Section 2.6.1 to the MOOCPs of the fed-batch bio-reactor and the jacketed tubular reactor respectively discussed in Chapters 4 and 5. However, as in the previous Sections, the sigma points approximation method is applied for the CVD reactor.

With respect to the MOOCP presented in Section 6.3.2, two specific changes to the Problem formulation 6.4 are made. Firstly, both constraints presented in Equations 6.8 and 6.10 need to be considered. Secondly, the objective functions are adapted, according to Equations 6.9 and 6.11.

Figure 6.13 presents the Pareto sets obtained with one or two uncertain parameters. The standard deviations used are again 10% and 20%. The effects of the uncertainties

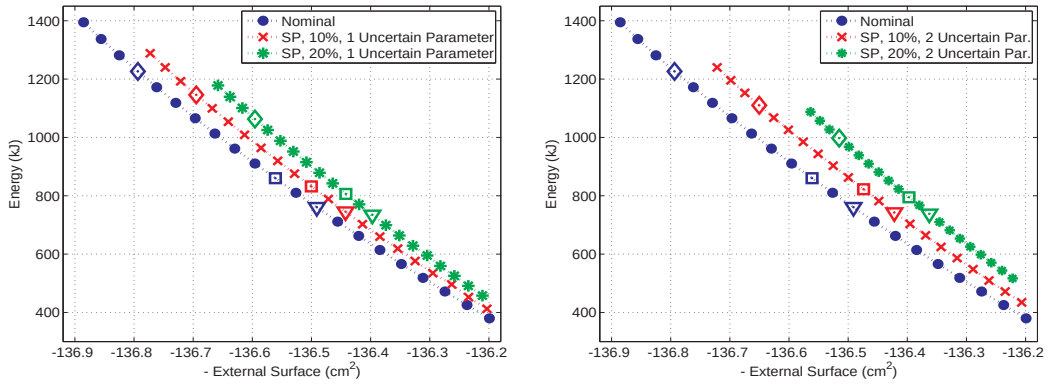

(a) *One uncertain parameter.* **(b)** *Two uncertain parameters.*

Figure 6.13: *Chemical vapour deposition reactor: Pareto sets calculated with one or two uncertain parameters.*

on the Pareto set are evident. In fact, the nominal Pareto front is shifted towards the right, which means that a fraction of the original feasible set, as it was defined in Definition 1, has now become un-feasible region. Moreover, it is also possible to see that the higher the uncertainty, the more the Pareto sets are shrinking towards the middle, drifting away from the original anchor points.

Three intermediate points are highlighted as it was in Figure 6.5b. These points are obtained with the same weights as in Section 6.3.2. In particular, the weights are [0.15 0.85], [0.50 0.50] and [0.60 0.40] for the diamond, the square and the downward-pointing triangle respectively. They are depicted in all of the Pareto sets represented, to make clearly visible the shift to which the nominal Pareto set undergoes. Their control profiles are depicted in Figure 6.14. Both the profiles for the one and two-parameters cases are reported, in Figures 6.14a and 6.14b, respectively. In Figure 6.14, only the 20% cases are depicted. The nominal profiles are not reported here, but interested readers can find them in Figure 6.6.

Figure 6.15 depicts the temperature profiles of the core and surface of the rod for one and two uncertain parameters with 20% standard deviation. The predicted 95% confidence regions are not represented, not to overcrowd the Figures. However, the T_{C} profile for the Pareto optimal [0.15 0.85] has been clearly influenced. In fact, in Figures 6.15a and 6.15b, it flattens before reaching the upper temperature bound. On the other hand, when the nominal MOOCP is solved, the same T_{C} profile meets its upper bound, as seen in Figure 6.7a.

A similar consideration can be made looking at Figure 6.15c, where the T_{S} profiles of the Pareto optimals [0.50 0.50] and [0.60 0.40] are flattening at a value higher than the lower bound.

Although with different final values, the external surface area and the energy consumption profiles for the robust MOOCP are not different from those depicted in Figure 6.8. Thus, only the final values of the objective functions for the intermediate points are reported in Table 6.3. These have been calculated according to Equations 6.9 and 6.11. Readers interested in the actual profiles are referred to Appendix B.1, Figures B.1 and B.2. For the nominal case, the values reported are calculated according to Equation 6.4a.

In Figures 6.13a and 6.13b, where the Pareto sets are presented, the number of uncertain parameters was kept constant, while their standard deviation was varied. An additional comparison could be made considering the Pareto sets obtained for different number of uncertain parameters whose standard deviations are fixed. This is done choosing a 20% standard deviation for all uncertain parameters. Nevertheless, results are found not to be different from those already presented. Thus they are not shown in this Chapter, but interested readers can find them in Appendix B.1, Figures B.3, B.4, B.5 and B.6.

A last consideration should be made analysing the sizes of the problems solved.

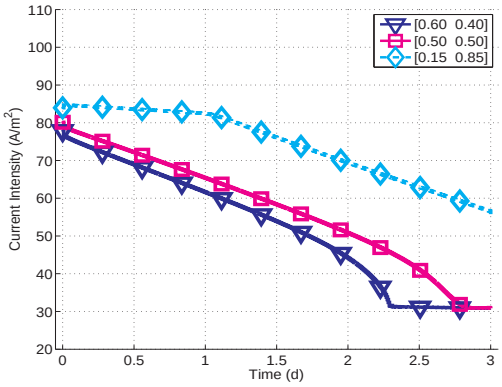

(a) *One uncertain parameter,* 20%.

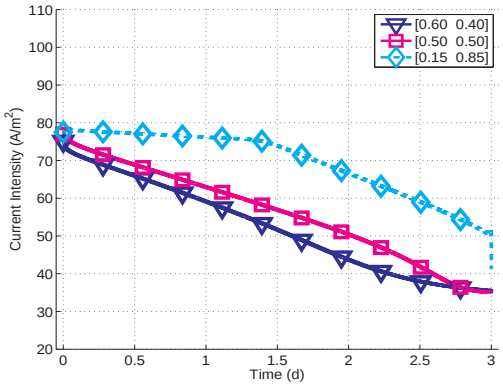

(b) *Two uncertain parameters,* 20%.

Figure 6.14: *Chemical vapour deposition reactor: optimal control profiles for three intermediate points of the robustified Pareto sets.*

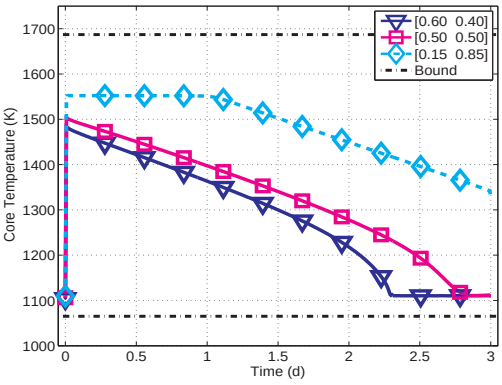

(a) T_{C}, *one uncertain parameter,* 20%.

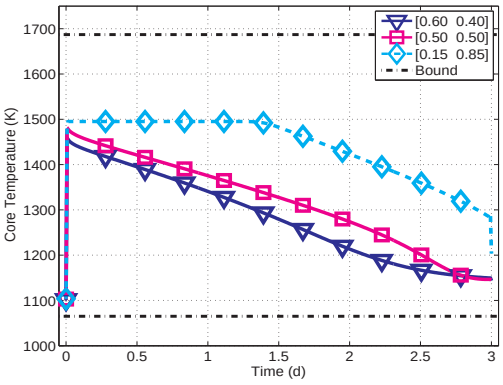

(b) T_{C}, *two uncertain parameters,* 20%.

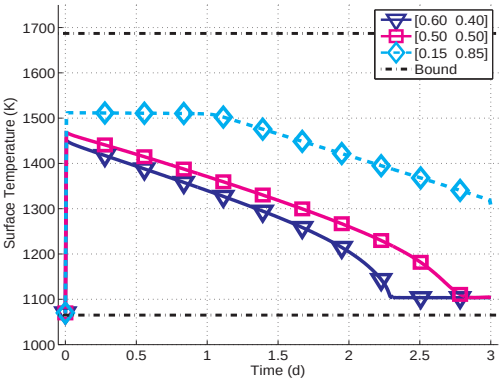

(c) T_{S}, *one uncertain parameter,* 20%.

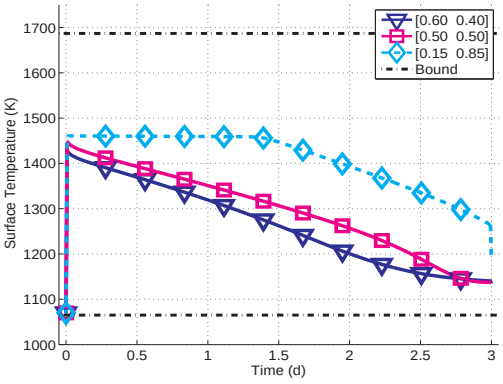

(d) T_{S},, *two uncertain parameters,* 20%.

Figure 6.15: *Chemical vapour deposition reactor: temperature profiles for three intermediate points of the robustified Pareto sets.*

Table 6.3: *Chemical vapour deposition reactor: external surface area and energy consumption for three intermediate points.*

	Weight	$A(t_f)\,[\mathrm{cm}^2]$	$E(t_f)\,[\mathrm{kJ}]$
Nominal	[0.60 0.40]	136.49	761
Robust, 1 uncertainty, 10%	[0.60 0.40]	136.44	746
Robust, 1 uncertainties, 20%	[0.60 0.40]	136.40	734
Robust, 2 uncertainty, 10%	[0.60 0.40]	136.42	742
Robust, 2 uncertainties, 20%	[0.60 0.40]	136.36	738
Nominal	[0.50 0.50]	136.56	860
Robust, 1 uncertainty, 10%	[0.50 0.50]	136.50	832
Robust, 1 uncertainties, 20%	[0.50 0.50]	136.44	806
Robust, 2 uncertainty, 10%	[0.50 0.50]	136.47	822
Robust, 2 uncertainties, 20%	[0.50 0.50]	136.40	795
Nominal	[0.15 0.85]	136.79	1226
Robust, 1 uncertainty, 10%	[0.15 0.85]	136.69	1146
Robust, 1 uncertainties, 20%	[0.15 0.85]	136.60	1063
Robust, 2 uncertainty, 10%	[0.15 0.85]	136.65	1110
Robust, 2 uncertainties, 20%	[0.15 0.85]	136.52	997

Table 6.4: *Chemical vapour deposition reactor: number of states, variables and constraints involved and time required for the solution of the OCPs and MOOCPs.*

	# States	# Variables	# Constraints	Time [s]
Nominal OCP	10	17712	40608	20
Nominal MOOCP	10	17712	40608	304
Robust OCP, 1 uncertainty	30	52272	123552	260
Robust OCP, 2 uncertainties	50	86832	203040	927
Robust MOOCP, 1 uncertainty	30	52272	123552	1163
Robust MOOCP, 2 uncertainties	50	86832	203040	3985

The number of states, variables and constraints involved are reported in Table 6.4, together with the time required for the solution of each problem. All the OCPs presented in Table 6.4 are referring to the energy minimisation problems. However, when considering the production maximisation, the amount of states, variables and constraints are the same and the computational times closely comparable to those reported.

The system dynamics are highly non-linear and the problems sizes greater than those presented in Chapter 5, in Tables 5.5 and 5.10. Again, these are non-trivial problems that can not be easily handled by all solution methodologies of Section 2.3. Nevertheless, although longer than in Chapter 5, the time necessary to reach the optimal solution is still affordable, requiring around 15 minutes for the largest

OCP problem. The most complicated MOOCP, instead required around one hour, meaning just three minutes for each Pareto optimal.

6.4 Conclusion

In this Chapter, a bi-objective optimisation of a chemical vapour deposition reactor was accomplished. The considered objectives were the production maximisation and the energy consumption. These are conflicting objectives and it was seen that focusing only on one of the two can not be satisfactory for a decision-maker. Thus, intermediate points, taken from the Pareto sets, were also described, to make the readers aware of the power of multi-objective optimisation. Decision-makers are then able to make a sound decision, since also the intermediate objective functions values can be investigated.

Additionally, the same study was performed when uncertain parameters were present in the system dynamics. It was seen that the feasible set is influenced by the presence of uncertain parameters and that the Pareto set shifts towards higher values of the objective functions. Moreover, a drift of the anchor points towards less performing results was noticed, when uncertainties were introduced.

Lastly, the computational times required to solve the OCPs and MOOCPs for the CVD were compared in Section 6.3.4. It was seen that, despite the highly non-linearity of the system dynamics and the considerable sizes of the problems, reasonable computational times were necessary for this industrial case. In particular, this holds also for the robust multi-objective optimisation problem, enforcing the conclusion given already in Chapter 5, where the sigma points was presented as a good candidate for real industrial robust optimal control problems.

Chapter 7

Conclusion

After the start of OCP theory, several solution methodologies have been developed, in order to deal with non-linear system dynamics. Some of them have been presented in this work, although only one has been exploited. As a matter of fact, direct orthogonal collocation, as implemented in Pomodoro, proved its ability in handling and solving optimal control problems also when highly non-linear system dynamics and considerable problem sizes were involved. The importance of a good insight of the process was stressed, since model equations highly influence the solution of any optimal control problem.

However, next to the classical view of OC, two variations are gaining importance in the (bio-)chemical industrial world, namely robust OC and multi-objective optimal control. Both of them were investigated in this thesis work, on some small-scale examples as well as on a real industrial case problem.

The relevance of robust OC comes from the possible presence of uncertainties in the model equations of the considered process. In particular, it is required the compliance of the states boundaries even if uncertainties are present. Thus, a safety margin is usually introduced, although this implies a worse value for the objective function.

In this work, two methods were investigated, to assess their reliability when dealing with uncertain parameters. These were the linear approximation as proposed by Srinivasan et al. (2003) and the sigma points approach (Julier and Uhlmann, 1996) (Recker et al., 2012). The optimisation of a jacketed tubular reactor and of the Williams-Otto reactor were accomplished exploiting both methods. It was found that, while the first works good for barely linear system dynamics, it fails in dealing with highly non-linear systems. The sigma points approximation, instead, not only was able to deal with complex dynamic systems, but also required less computational time, although still longer than in the nominal case. This makes it a good candidate also for dealing with industrial-scale problems.

The industrial importance of multi-objective optimal control is instead a direct consequence of its capability to deal with more than a single objective. It allows in fact

to focus on more than just one aspect of the unit operation or the plant considered. In this thesis, multi-objective optimal control was applied to a chemical vapour deposition reactor, where the maximisation of the production and the minimisation of the energy consumption were treated simultaneously. Several mathematically equivalent solutions were obtained, gathered in the so-called Pareto set. However, the control actions and the results attained are different for each of these points. As a consequence the decision-maker is called to pick the solution which has to be implemented in practice. Nevertheless, the possibility to analise all or some of the Pareto optimals can be really helpful in this choice.

Although just a combination of the two variations, also robust MOOCP was applied to the CVD reactor. The most relevant results are that the Pareto set is forced to shift towards less performing objective functions values and that the feasible set is reduced in size. This is due to the safety margin introduced by the robustification. This term introduces an additional trade-off between performance and safe operation. The safety margin itself can then be seen as an additional objective function. As before, even in this case the decision-maker is called to choose the control profile to be implemented.

As anticipated, optimal control in all its variations can be seen as a useful tool towards sustainable development. Although usually the economical aspect is still the most relevant, it might in fact be a good answer to social and environmental pressure to which industries are nowadays exposed. This was demonstrated in the multi-objective optimisation of the CVD reactor, where it was proven that reducing the production of a factor 0.5% could lead to an overall energy saving of about 70%.

Finally, some suggestions for further research are made. In particular, the robust optimal solution of the CVD reactor could be assessed through a Monte-Carlo simulation, in order to evaluate whether the required confidence level is satisfied or not by the sigma points approximation.

Moreover, the system dynamics of the chemical vapour deposition reactor should be adapted to the size of the silicon rods in a real Siemens reactor. In this thesis, in fact, a lab-scale reactor was investigated. In addition, the same model should be adapted to account for more than a single bar. As a matter of fact, industrial Siemens reactors are composed of 36 or more bars, each controlled in an independent way. The radiation heat exchanged between the bars should then be included in the system dynamics, in order to allow a fine control for each of the silicon rods.

Appendices

Appendix A

CVD reactor

A.1 Model parameters

Table A.1: *CVD reactor: geometrical and operating parameters.*

Constant	Value	Units
V	480	cm^3
A_0	120	cm^2
H	40	cm
v	10	cm/s
x_{H2}^{IN}	99.8	%
x_{SiH4}^{IN}	0.1	%
x_{SiH2}^{IN}	0.1	%
T_{IN}	373.15	K
P	1	atm
$Nu_M = Nu_T$	3.66	-
$\tilde{H}_{f,H2}$	0	kJ/mol
$\tilde{H}_{f,SiH4}$	33.91	kJ/mol
$\tilde{H}_{f,SiH2}$	270.42	kJ/mol
$\tilde{H}_{f,Si}$	0	kJ/mol
ρ_{Si}	0.19	mol/cm^3
D_{H2}	$1.28 \times (T[K]/300)^{1.68}$	cm^2/s
D_{SiH4}	$0.58 \times (T[K]/300)^{1.8}$	cm^2/s
D_{SiH2}	$0.59 \times (T[K]/300)^{1.8}$	cm^2/s
$\tilde{C}_{p,H2}$	$27.21 + 66.98 \cdot 10^{-4} \times T[K]$	J/mol·K
$\tilde{C}_{p,SiH4}$	$20,51 + 75,35 \cdot 10^{-3} \times T[K]$	J/mol·K
$\tilde{C}_{p,SiH2}$	$25.12 + 41.86 \cdot 10^{-4} \times T[K]$	J/mol·K
$\tilde{C}_{p,Si}$	22.60	J/mol·K
k_1	$2.7 \times 10^{14} \times \exp(-57000/R/T[K])$	1/s
k_2	1.9×10^4	cm/s
k_3	5.4	cm/s
k_T	$5.44 \times 10^{-2} + 14.44 \times 10^{-2} \times T[K]/300$ $-12.14 \times 10^{-3} \times (T[K]/300)^2$	W/m·K
λ_T	30	W/m·K
λ_e	$2.52 \cdot 10^{-4}$	S/m
ε	0.7	–

Appendix B

CVD reactor

B.1 Additional figures

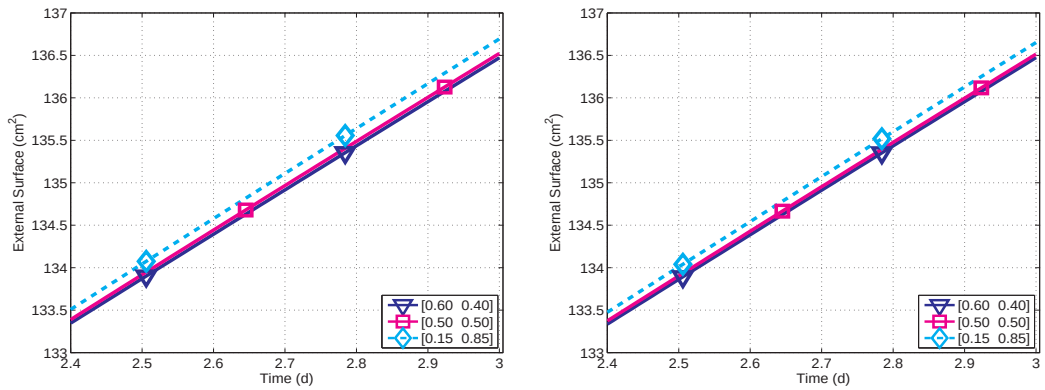

(a) *One uncertain parameter, 20%.* **(b)** *Two uncertain parameters, 20%.*

Figure B.1: *Chemical vapour deposition reactor: external surface area of the bar for three intermediate points of the robust Pareto sets.*

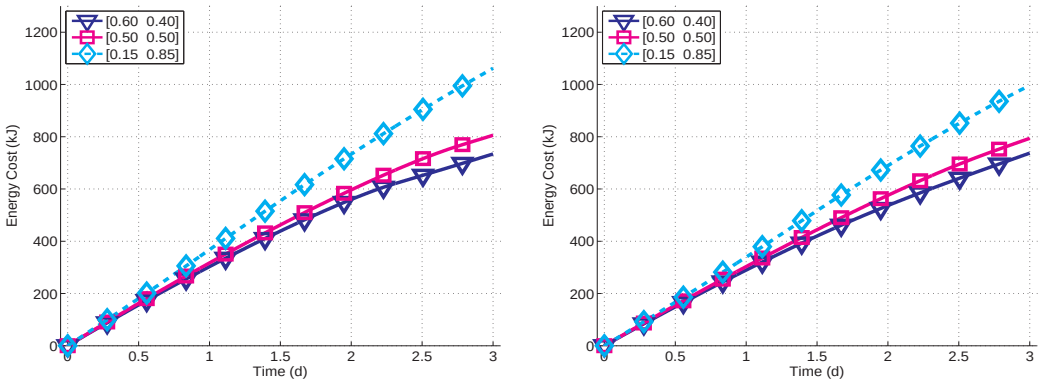

(a) *One uncertain parameter,* 20%. **(b)** *Two uncertain parameters,* 20%.

Figure B.2: *Chemical vapour deposition reactor: energy consumption for three intermediate points of the robust Pareto sets.*

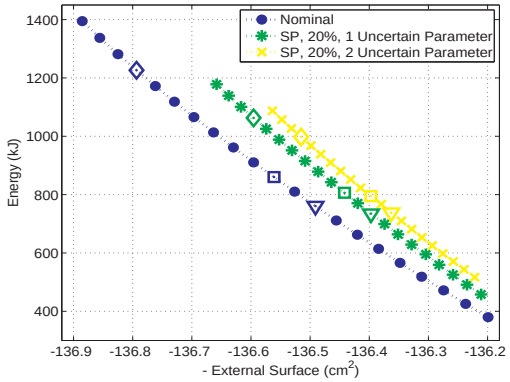

Figure B.3: *Chemical vapour deposition reactor: Pareto sets calculated with one and two uncertain parameters with same standard deviations.*

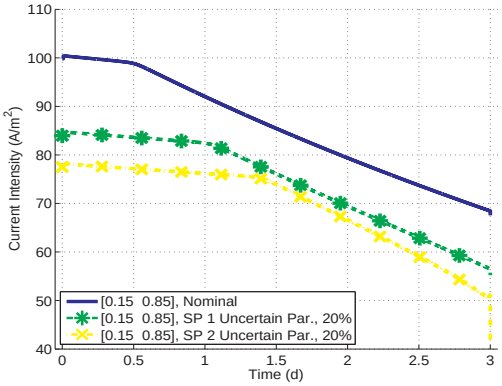

Figure B.4: *Chemical vapour deposition reactor: optimal control profiles for the corresponding intermediate point of the nominal and robust Pareto sets, calculated with one and two uncertain parameters with same standard deviations.*

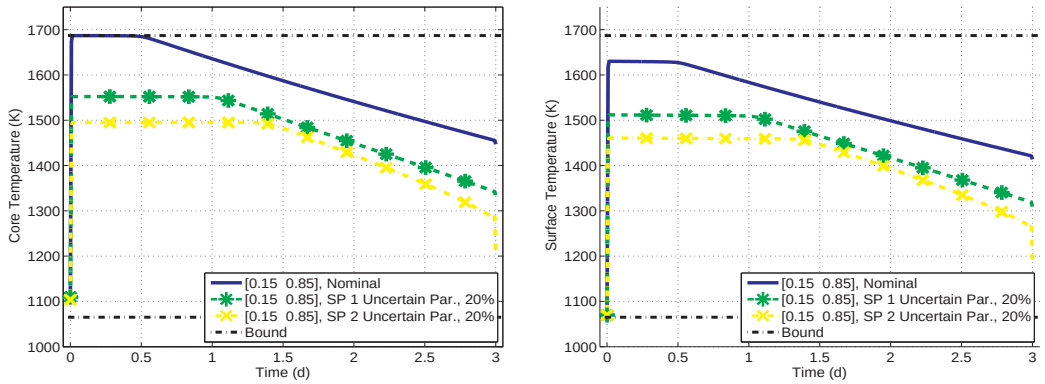

(a) T_C. **(b)** T_S.

Figure B.5: *Chemical vapour deposition reactor: temperature profiles for the corresponding intermediate point of the nominal and robust Pareto sets, calculated with one and two uncertain parameters with same standard deviations.*

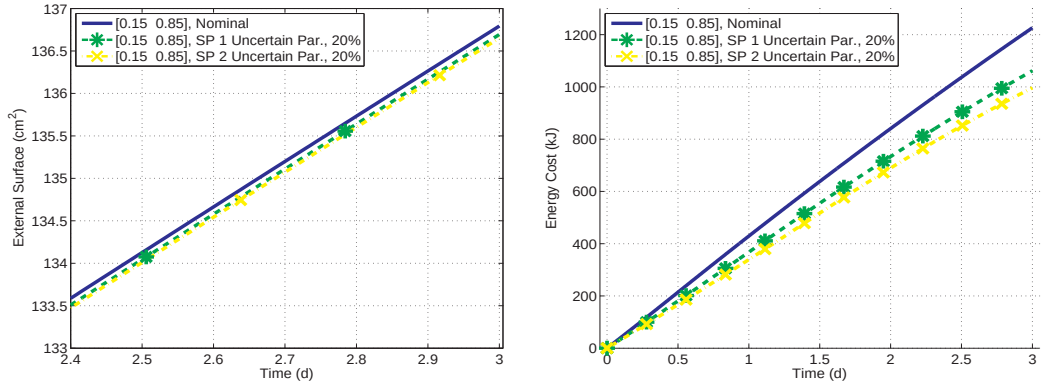

(a) *External surface area, A.* **(b)** *Energy consumption, E.*

Figure B.6: *Chemical vapour deposition reactor: external surface area and energy consumption for the corresponding intermediate point of the nominal and robust Pareto sets, calculated with one and two uncertain parameters with same standard deviations.*

Appendix C

CVD reactor programming code

C.1 Robust MOOCP with 2 uncertain parameters

```
""" Created on Sat May 3 15:56:27 2014 author: Lorenzo """

import time
import numpy as NP
from pomodoro.problem.moproblem import MOproblem
from pomodoro.solver.multiobjective import Multiobjective
from pomodoro.discs.expression import Expression
from pomodoro.graphgenerator.paretobrowser import ParetoBrowser
from casadi import *

t = time.time()
prob=MOproblem(21,'ENNC')



    # geometrical parameters
L = 30.0e-2
H = 4.0e-2
B = 4.0e-2
A = L*H
V = L*H*B
v = 10.0e-2
W = H*B*v
Ar = (B*H)*2.0 + (L*H)*4.0
A0_b = 120.0e-4
r0_b = A0_b /(2.0*L*pi)
V0_b = (r0_b**2.0)*pi*L



    # T and P
```

```
Tp = 1100.0
Trif = 298.15
Tin = 373.15
Tw = 973.15
P = 1.0
Pt = 3.1e6


    # gas constant
R_cal = 1.98
R_atm = 82.0575e-6


    # Inlet mole fractions
x0_H2 = 0.998
x0_Si4 = 0.001
x0_Si2 = 0.001


    # Inlet concentrations
C_H2 = x0_H2 * P/(R_atm*Tin)
C_Si4 = x0_Si4 * P/(R_atm*Tin)
C_Si2 = x0_Si2 * P/(R_atm*Tin)


    # Molecular weights
PM_H2 = 2.0
PM_Si4 = 32.0
PM_Si2 = 30.0
PM_Sis = 28.0


    # densities of the silicon
roMol_Sis = 0.19e6
roMas_Sis = roMol_Sis *PM_Sis
MolIN = P*W/(R_atm *Tin)
i0 = 0.005
Nu = 3.66


    # Specific heat # ACP_i + BCp_i * x[7]
ACp_H2 = 6.5
BCp_H2 = 0.0016
ACp_Si4 = 4.9
BCp_Si4 = 0.018
```

```
ACp_Si2 = 6.0
BCp_Si2 = 0.001
ACp_Sis = 5.4
BCp_Sis = 0.0


    # formation enthalpy
DHf_H2 = 0.0
DHf_Si4 = 8100.0
DHf_Si2 = 64590.0
DHf_Sis = 0.0


    # formation entropy
DSf_H2 = 31.2
DSf_Si4 = 48.8
DSf_Si2 = 49.5
DSf_Sis = 4.5


    # radiation constants
irr_J = 5.67e-8 # boltzmann constant in W/(m*K)
irr = irr_J / 4.186 # boltzmann constant in cal/(m*K)
emiss = 0.7 # emissivity constant
# sigma points calculation
n=2.0
k=3.0-n
pEmiss = 0.0049 # 10%
sigmaEmiss = sqrt((n+k)*pEmiss)


    # kinetic constants
k_sup1 = 1.9e2 # = k_2
k_sup2 = 5.4e-2 # = k_3


    # conduction constants
kT_Sis_J = 30.0 # thermal conductivity in W/(m*K)
kT_Sis = 30.0 / 4.186 # thermal conductivity in cal/(m*K)
kE_Sis = 2.52e-4 # electrical conductivity in 1/(ohm*m)
# sigma points calculation
pElec = (kE_Sis*0.10)**2.0
sigmaElec = sqrt((n+k)*pElec)
```

```
    # time constants
t_start = 0.0
t_end = 60.0 * 60.0*24.0*3.0

t1 = prob.setTimeRange(t_start,t_end)

xlower = [
0.0,0.0,0.0,0.0,0.0,0.0,0.0,373.15,1065.15,0.0,
0.0,0.0,0.0,0.0,0.0,0.0,0.0,373.15,1065.15,0.0,
0.0,0.0,0.0,0.0,0.0,0.0,0.0,373.15,1065.15,0.0,
0.0,0.0,0.0,0.0,0.0,0.0,0.0,373.15,1065.15,0.0,
0.0,0.0,0.0,0.0,0.0,0.0,0.0,373.15,1065.15,0.0]

xupper =[
1e7,1e7,1e7,1e7,1e7,1e7,1e7,2000.0,1687.0,1e7,
1e7,1e7,1e7,1e7,1e7,1e7,1e7,2000.0,1687.0,1e7,
1e7,1e7,1e7,1e7,1e7,1e7,1e7,2000.0,1687.0,1e7,
1e7,1e7,1e7,1e7,1e7,1e7,1e7,2000.0,1687.0,1e7,
1e7,1e7,1e7,1e7,1e7,1e7,1e7,2000.0,1687.0,1e7]

x = prob.addStates(50,xlower,xupper,method=['LagrangeColl',432])
x.load("2par/states_sigma2par_energy_10%_Volt2_1.645.txt")

u = prob.addControls(1,[0.0],[150.0], method=['PiecewiseConstant',432])
u.load("2par/control_sigma2par_energy_10%_Volt2_1.645.txt")


    """ Solving Nominal Problem"""
rhs = Expression(SXMatrix.zeros(50))

D_H2 = 1.276e-4 *((x[7]/300.0)**1.68)# diffusion coefficient
D_Si4 = 0.58e-4 *((x[7]/300.0)**1.8)# diffusion coefficient
D_Si2 = 0.59e-4 *((x[7]/300.0)**1.8) # diffusion coefficient

kc_H2 = Nu*D_H2/H
kc_Si4 = Nu*D_Si4/H
kc_Si2 = Nu*D_Si2/H

kt = 1.3e-2 + 3.45e-2 * x[7] / 300.0 - 2.9e-3*((x[7]/300.0)**2.0)
hlim = Nu * kt / H
hlim_J = hlim * 4.186
k_gas = 2.7e14*exp(-57000.0/(R_cal*x[7])) # = k_1
rhs[0] = MolIN * x0_Si4 / V - W * x[0] / V - kc_Si4 * (2.0 * L * pi * (((V0_b +
x[6] * V / roMol_Sis)/(L * pi))**0.5)) * (x[0] - x[1]) / V - k_gas * x[0]
```

rhs[1] = kc_Si4 * (2.0 * L * pi * (((V0_b + x[6] * V / roMol_Sis)/(L * pi))**0.5))* (x[0] - x[1]) / V - k_sup2 * (2.0 * L * pi * (((V0_b + x[6] * V / roMol_Sis)/(L * pi))**0.5)) * x[1] / V

rhs[2] = MolIN * x0_Si2 / V - W * x[2] / V - kc_Si2 * (2.0 * L * pi * (((V0_b + x[6] * V / roMol_Sis)/(L * pi))**0.5)) * (x[2] - x[3]) / V + k_gas * x[0]

rhs[3] = kc_Si2 * (2.0 * L * pi * (((V0_b + x[6] * V / roMol_Sis)/(L * pi))**0.5)) * (x[2] - x[3]) / V - k_sup1 * (2.0 * L * pi * (((V0_b + x[6] * V / roMol_Sis)/(L * pi))**0.5)) * x[3] / V

rhs[4] = MolIN * x0_H2 / V - W * x[4] / V - kc_H2* (2.0 * L * pi * (((V0_b + x[6] * V / roMol_Sis)/(L * pi))**0.5)) * (x[4] - x[5]) / V + k_gas * x[0]

rhs[5] = kc_H2* (2.0 * L * pi * (((V0_b + x[6] * V / roMol_Sis)/(L * pi))**0.5)) * (x[4] - x[5]) / V + k_sup1 * (2.0 * L * pi * (((V0_b + x[6] * V / roMol_Sis)/(L * pi))**0.5)) * x[3] / V + 2.0 * k_sup2 * (2.0 * L * pi * (((V0_b + x[6] * V / roMol_Sis)/(L * pi))**0.5)) * x[1] / V

rhs[6] = k_sup1 * (2.0 * L * pi * (((V0_b + x[6] * V / roMol_Sis)/(L * pi))**0.5)) * x[3] / V + k_sup2 * (2.0 * L * pi * (((V0_b + x[6] * V / roMol_Sis)/(L * pi))**0.5)) * x[1] / V

rhs[7] = (MolIN *(x0_Si4 * (DHf_Si4 + ACp_Si4 * (Tin - Trif)+ BCp_Si4 /2.0* ((Tin**2.0) - (Trif**2.0)))+ x0_Si2 * (DHf_Si2 + ACp_Si2 * (Tin - Trif)+ BCp_Si2 /2.0* ((Tin**2.0) - (Trif**2.0)))+ x0_H2 * (DHf_H2 + ACp_H2* (Tin - Trif) + BCp_H2 /2.0* ((Tin**2.0) - (Trif**2.0))))- W * (x[0] * (DHf_Si4+ ACp_Si4 * (x[7] - Trif)+ BCp_Si4 /2.0* ((x[7]**2.0) - (Trif**2.0)))+ x[2] * (DHf_Si2 + ACp_Si2 * (x[7] - Trif)+ BCp_Si2 /2.0* ((x[7]**2.0) - (Trif**2.0))) + x[4] * (DHf_H2+ ACp_H2* (x[7] - Trif) + BCp_H2/2.0* ((x[7]**2.0) - (Trif**2.0))))+ k_gas *x[0] * V *(-(DHf_Si4+ ACp_Si4 * (x[7] - Trif) + BCp_Si4 /2.0* ((x[7]**2.0) - (Trif**2.0)))+ (DHf_Si2 + ACp_Si2 * (x[7] - Trif) + BCp_Si2 /2.0* ((x[7]**2.0) - (Trif**2.0)))+ (DHf_H2+ ACp_H2* (x[7] - Trif) + BCp_H2/2.0* ((x[7]**2.0) - (Trif**2.0))))+ hlim * (2.0 * L * pi * (((V0_b + x[6] * V / roMol_Sis)/(L * pi))**0.5)) * (x[8] -x[7]) + hlim * Ar * (Tw - x[7]))/(x[0] * V * (ACp_Si4 + 2.0*BCp_Si4 * x[7]) + x[2] * V * (ACp_Si2 + 2.0*BCp_Si2 * x[7])+ x[4] * V * (ACp_H2 + 2.0*BCp_H2 * x[7]))

rhs[8] = (- hlim * (2.0 * L * pi * (((V0_b + x[6] * V / roMol_Sis)/(L * pi))**0.5)) * (x[8] - x[7])- emiss * irr * (2.0 * L * pi * (((V0_b + x[6] * V / roMol_Sis)/(L * pi))**0.5)) * ((x[8]**4.0) - Tw**4.0)+ kT_Sis * (2.0 * L * pi * (((V0_b + x[6] * V / roMol_Sis)/(L * pi))**0.5)) * ((x[8] + ((u[0]**2.0) * ((((V0_b + x[6] * V / roMol_Sis)/(L * pi))**0.5)**2.0) /(kE_Sis * 4.0 * kT_Sis))) - x[8]) / (((V0_b + x[6] * V / roMol_Sis)/(L * pi))**0.5)+ k_sup1 *x[3] * (2.0 * L * pi * (((V0_b + x[6] * V / roMol_Sis)/(L * pi))**0.5)) * (- (DHf_Si2 + ACp_Si2 * (x[8] - Trif)+ BCp_Si2 /2.0* ((x[8]**2.0) - (Trif**2.0)))+ (DHf_Sis + ACp_Sis * (x[8] - Trif) +

```
BCp_Sis /2.0* ((x[8]**2.0) - (Trif**2.0)))+ (DHf_H2 + ACp_H2* (x[8] - Trif)+
BCp_H2/2.0* ((x[8]**2.0) - (Trif**2.0))))+ k_sup2 *x[1] * (2.0 * L * pi * (((V0_b
+ x[6] * V / roMol_Sis)/(L * pi))**0.5)) * ( -(DHf_Si4 + ACp_Si4 * (x[8] - Trif)+
BCp_Si4 /2.0* ((x[8]**2.0) - (Trif**2.0)))+ (DHf_Sis + ACp_Sis * (x[8] - Trif) +
BCp_Sis /2.0* ((x[8]**2.0) - (Trif**2.0))) + 2.0*(DHf_H2+ ACp_H2* (x[8] - Trif)+
BCp_H2/2.0* ((x[8]**2.0) - (Trif**2.0)))))/(roMol_Sis * pi * L * ((((V0_b + x[6] *
V / roMol_Sis)/(L * pi))**0.5)**2.0))

rhs[9] = sqrt(3.0)*u[0]*((pi*(((V0_b + x[6] * V / roMol_Sis)/(L * pi))**0.5)**2.0))


    """ Solving Problem with +sigma on the parameter emiss"""
emiss1 = emiss+sigmaEmiss

D_H2_1 = 1.276e-4 *((x[17]/300.0)**1.68)
D_Si4_1 = 0.58e-4 *((x[17]/300.0)**1.8)
D_Si2_1 = 0.59e-4 *((x[17]/300.0)**1.8)

kc_H2_1 = Nu*D_H2_1/H
kc_Si4_1 = Nu*D_Si4_1/H
kc_Si2_1 = Nu*D_Si2_1/H

kt_1 = 1.3e-2 + 3.45e-2 * x[17] / 300.0 - 2.9e-3*((x[17]/300.0)**2.0)
hlim_1 = Nu * kt_1 / H
hlim_J_1 = hlim_1 * 4.186
k_gas_1 = 2.7e14*exp(-57000.0/(R_cal*x[17]))

rhs[10] = MolIN * x0_Si4 / V - W * x[10] / V - kc_Si4_1 * (2.0 * L * pi *
(((V0_b + x[16] * V / roMol_Sis)/(L * pi))**0.5)) * (x[10] - x[11]) / V - k_gas_1 *
x[10]

rhs[11] = kc_Si4_1 * (2.0 * L * pi * (((V0_b + x[16] * V / roMol_Sis)/(L *
pi))**0.5))* (x[10] - x[11]) / V - k_sup2 * (2.0 * L * pi * (((V0_b + x[16] * V /
roMol_Sis)/(L * pi))**0.5)) * x[11] / V

rhs[12] = MolIN * x0_Si2 / V - W * x[12] / V - kc_Si2_1 * (2.0 * L * pi *
(((V0_b + x[16] * V / roMol_Sis)/(L * pi))**0.5)) * (x[12] - x[13]) / V + k_gas_1
* x[10]

rhs[13] = kc_Si2_1 * (2.0 * L * pi * (((V0_b + x[16] * V / roMol_Sis)/(L *
pi))**0.5)) * (x[12] - x[13]) / V - k_sup1 * (2.0 * L * pi * (((V0_b + x[16] * V /
roMol_Sis)/(L * pi))**0.5)) * x[13] / V

rhs[14] = MolIN * x0_H2 / V - W * x[14] / V - kc_H2_1 * (2.0 * L * pi *
(((V0_b + x[16] * V / roMol_Sis)/(L * pi))**0.5)) * (x[14] - x[15]) / V + k_gas_1
```

* x[10]

rhs[15] = kc_H2_1 * (2.0 * L * pi * (((V0_b + x[16] * V / roMol_Sis)/(L * pi))**0.5)) * (x[14] - x[15]) / V + k_sup1* (2.0 * L * pi * (((V0_b + x[16] * V / roMol_Sis)/(L * pi))**0.5)) * x[13] / V + 2.0 * k_sup2 * (2.0 * L * pi * (((V0_b + x[16] * V / roMol_Sis)/(L * pi))**0.5)) * x[11] / V

rhs[16] = k_sup1 * (2.0 * L * pi * (((V0_b + x[16] * V / roMol_Sis)/(L * pi))**0.5)) * x[13] / V + k_sup2 * (2.0 * L * pi * (((V0_b + x[16] * V / roMol_Sis)/(L * pi))**0.5)) * x[11] / V

rhs[17] = (MolIN * (x0_Si4 * (DHf_Si4 + ACp_Si4 * (Tin - Trif)+ BCp_Si4 /2.0 * ((Tin**2.0) - (Trif**2.0))) + x0_Si2 * (DHf_Si2 + ACp_Si2 * (Tin - Trif)+ BCp_Si2 /2.0 * ((Tin**2.0) - (Trif**2.0))) + x0_H2 * (DHf_H2 + ACp_H2 * (Tin - Trif) + BCp_H2 /2.0 * ((Tin**2.0) - (Trif**2.0))))- W * (x[11] * (DHf_Si4 + ACp_Si4 * (x[17] - Trif)+ BCp_Si4 /2.0 * ((x[18]**2.0) - (Trif**2.0)))+ x[12] * (DHf_Si2 + ACp_Si2 * (x[17] - Trif)+ BCp_Si2 /2 * ((x[17]**2.0) - (Trif**2.0))) + x[14] * (DHf_H2 + ACp_H2 * (x[17] - Trif) + BCp_H2 /2.0 * ((x[17]**2.0) - (Trif**2.0))))+ k_gas_1 *x[10] * V *(- (DHf_Si4 + ACp_Si4 * (x[17] - Trif) + BCp_Si4 /2.0 * ((x[17]**2.0) - (Trif**2.0)))+ (DHf_Si2 + ACp_Si2 * (x[17] - Trif) + BCp_Si2 /2.0 * ((x[17]**2.0) - (Trif**2.0)))+ (DHf_H2 + ACp_H2 * (x[17] - Trif) + BCp_H2 /2.0 * ((x[17]**2.0) - (Trif**2.0))))+ hlim_1 * (2.0 * L * pi * (((V0_b + x[16] * V / roMol_Sis)/(L * pi))**0.5)) * (x[18] -x[17]) + hlim_1 * Ar * (Tw - x[17]))/(x[10] * V * (ACp_Si4 + 2.0*BCp_Si4 * x[17]) + x[12] * V * (ACp_Si2 + 2.0*BCp_Si2 * x[17])+ x[14] * V * (ACp_H2 + 2.0*BCp_H2 * x[17]))

rhs[18] = (- hlim_1 * (2.0 * L * pi * (((V0_b + x[16] * V / roMol_Sis)/(L * pi))**0.5)) * (x[18] - x[17])- emiss1* irr * (2.0 * L * pi * (((V0_b + x[16] * V / roMol_Sis)/(L * pi))**0.5)) * ((x[18]**4.0) - Tw**4.0)+ kT_Sis * (2.0 * L * pi * (((V0_b + x[16] * V / roMol_Sis)/(L * pi))**0.5)) * ((x[18] + ((u[0]**2.0) * ((((V0_b + x[16] * V / roMol_Sis)/(L * pi))**0.5)**2.0) /(kE_Sis * 4.0 * kT_Sis))) - x[18]) / (((V0_b + x[16] * V / roMol_Sis)/(L * pi))**0.5)+ k_sup1 *x[13] * (2.0 * L * pi * (((V0_b + x[16] * V / roMol_Sis)/(L * pi))**0.5)) * (- (DHf_Si2 + ACp_Si2 * (x[18] - Trif)+ BCp_Si2 /2.0 * ((x[18]**2.0) - (Trif**2.0)))+ (DHf_Sis + ACp_Sis * (x[18] - Trif) + BCp_Sis /2.0 * ((x[18]**2.0) - (Trif**2.0))) + (DHf_H2 + ACp_H2 * (x[18] - Trif)+ BCp_H2 /2.0 * ((x[18]**2.0) - (Trif**2.0))))+ k_sup2 *x[11] * (2.0 * L * pi * (((V0_b + x[16] * V / roMol_Sis)/(L * pi))**0.5)) * (-(DHf_Si4 + ACp_Si4 * (x[18] - Trif)+ BCp_Si4 /2.0 * ((x[18]**2.0) - (Trif**2.0)))+ (DHf_Sis + ACp_Sis * (x[18] - Trif) + BCp_Sis /2 * ((x[18]**2.0) - (Trif**2.0))) + 2.0*(DHf_H2 + ACp_H2 * (x[18] - Trif)+ BCp_H2 /2.0 * ((x[18]**2.0) - (Trif**2.0)))))/(roMol_Sis * pi * L * ((((V0_b + x[16] * V / roMol_Sis)/(L * pi))**0.5)**2.0))

rhs[19] = sqrt(3.0)*u[0]*((pi*(((V0_b + x[16] * V / roMol_Sis)/(L * pi))**0.5)**2.0))

```
    """ Solving Problem with -sigma on the parameter emiss"""
emiss2 = emiss-sigmaEmiss

D_H2_2 = 1.276e-4 *((x[27]/300.0)**1.68)
D_Si4_2 = 0.58e-4 *((x[27]/300.0)**1.8)
D_Si2_2 = 0.59e-4 *((x[27]/300.0)**1.8)

kc_H2_2 = Nu*D_H2_2/H
kc_Si4_2 = Nu*D_Si4_2/H
kc_Si2_2 = Nu*D_Si2_2/H

kt_2 = 1.3e-2 + 3.45e-2 * x[27] / 300.0 - 2.9e-3*((x[27]/300.0)**2.0)
hlim_2 = Nu * kt_2 / H
hlim_J_2 = hlim_2 * 4.186
k_gas_2 = 2.7e14*exp(-57000.0/(R_cal*x[27]))

rhs[20] = MolIN * x0_Si4 / V - W * x[20] / V - kc_Si4_2 * (2.0 * L * pi *
(((V0_b + x[26] * V / roMol_Sis)/(L * pi))**0.5)) * (x[20] - x[21]) / V - k_gas_2 *
x[20]

rhs[21] = kc_Si4_2 * (2.0 * L * pi * (((V0_b + x[26] * V / roMol_Sis)/(L *
pi))**0.5))* (x[20] - x[21]) / V - k_sup2 * (2.0 * L * pi * (((V0_b + x[26] * V /
roMol_Sis)/(L * pi))**0.5)) * x[21] / V

rhs[22] = MolIN * x0_Si2 / V - W * x[22] / V - kc_Si2_2 * (2.0 * L * pi *
(((V0_b + x[26] * V / roMol_Sis)/(L * pi))**0.5)) * (x[22] - x[23]) / V + k_gas_2
* x[20]

rhs[23] = kc_Si2_2 * (2.0 * L * pi * (((V0_b + x[26] * V / roMol_Sis)/(L *
pi))**0.5)) * (x[22] - x[23]) / V - k_sup1 * (2.0 * L * pi * (((V0_b + x[26] * V /
roMol_Sis)/(L * pi))**0.5)) * x[23] / V

rhs[24] = MolIN * x0_H2 / V - W * x[24] / V - kc_H2_2 * (2.0 * L * pi *
(((V0_b + x[26] * V / roMol_Sis)/(L * pi))**0.5)) * (x[24] - x[25]) / V + k_gas_2
* x[20]

rhs[25] = kc_H2_2 * (2.0 * L * pi * (((V0_b + x[26] * V / roMol_Sis)/(L *
pi))**0.5)) * (x[24] - x[25]) / V + k_sup1 * (2.0 * L * pi * (((V0_b + x[26] * V /
roMol_Sis)/(L * pi))**0.5)) * x[23] / V + 2.0 * k_sup2 * (2.0 * L * pi * (((V0_b +
x[26] * V / roMol_Sis)/(L * pi))**0.5)) * x[21] / V

rhs[26] = k_sup1 * (2.0 * L * pi * (((V0_b + x[26] * V / roMol_Sis)/(L * pi))**0.5))
* x[23] / V + k_sup2 * (2.0 * L * pi * (((V0_b + x[26] * V / roMol_Sis)/(L *
pi))**0.5)) * x[21] / V
```

```
rhs[27] = (MolIN * (x0_Si4 * (DHf_Si4 + ACp_Si4 * (Tin - Trif)+ BCp_Si4
/2.0 * ((Tin**2.0) - (Trif**2.0))) + x0_Si2 * (DHf_Si2 + ACp_Si2 * (Tin - Trif)+
BCp_Si2 /2.0 * ((Tin**2.0) - (Trif**2.0))) + x0_H2 * (DHf_H2 + ACp_H2 * (Tin
- Trif) + BCp_H2 /2.0 * ((Tin**2.0) - (Trif**2.0))))- W * (x[20] * (DHf_Si4 +
ACp_Si4 * (x[27] - Trif)+ BCp_Si4 /2.0 * ((x[27]**2.0) - (Trif**2.0)))+ x[22] *
(DHf_Si2 + ACp_Si2 * (x[27] - Trif)+ BCp_Si2 /2.0 * ((x[27]**2.0) - (Trif**2.0)))
+ x[24] * (DHf_H2 + ACp_H2 * (x[27] - Trif) + BCp_H2 /2 * ((x[27]**2.0) -
(Trif**2.0))))+ k_gas_2 *x[20] * V * (- (DHf_Si4 + ACp_Si4 * (x[27] - Trif) +
BCp_Si4 /2.0 * ((x[27]**2.0) - (Trif**2.0)))+ (DHf_Si2 + ACp_Si2 * (x[27] - Trif)
+ BCp_Si2 /2.0 * ((x[27]**2.0) - (Trif**2.0)))+ (DHf_H2 + ACp_H2 * (x[27] -
Trif) + BCp_H2 /2.0 * ((x[27]**2.0) - (Trif**2.0))))+ hlim_2 * (2.0 * L * pi *
(((V0_b + x[26] * V / roMol_Sis)/(L * pi))**0.5)) * (x[28] -x[27]) + hlim_2 *
Ar * (Tw - x[27]))/( x[20] * V * (ACp_Si4 + 2.0*BCp_Si4 * x[27]) + x[22] * V
* (ACp_Si2 + 2.0*BCp_Si2 * x[27])+ x[24] * V * (ACp_H2 + 2.0*BCp_H2 * x[27]))

rhs[28] = (- hlim_2 * (2.0 * L * pi * (((V0_b + x[26] * V / roMol_Sis)/(L *
pi))**0.5)) * (x[28] - x[27])- emiss2 * irr * (2.0 * L * pi * (((V0_b + x[26] * V /
roMol_Sis)/(L * pi))**0.5)) * ((x[28]**4.0) - Tw**4.0)+ kT_Sis * (2.0 * L * pi *
(((V0_b + x[26] * V / roMol_Sis)/(L * pi))**0.5)) * ((x[28] + ((u[0]**2.0) * ((((V0_b
+ x[26] * V / roMol_Sis)/(L * pi))**0.5)**2.0) /(kE_Sis * 4.0 * kT_Sis))) - x[28]) /
(((V0_b + x[26] * V / roMol_Sis)/(L * pi))**0.5)+ k_sup1 *x[23] * (2.0 * L * pi *
(((V0_b + x[26] * V / roMol_Sis)/(L * pi))**0.5)) * ( - (DHf_Si2 + ACp_Si2 *
(x[28] - Trif)+ BCp_Si2 /2.0 * ((x[28]**2.0) - (Trif**2.0)))+ (DHf_Sis + ACp_Sis *
(x[28] - Trif) + BCp_Sis /2.0 * ((x[28]**2.0) - (Trif**2.0))) + (DHf_H2 + ACp_H2 *
(x[28] - Trif)+ BCp_H2 /2.0 * ((x[28]**2.0) - (Trif**2.0))))+ k_sup2 *x[21] * (2.0 * L
* pi * (((V0_b + x[26] * V / roMol_Sis)/(L * pi))**0.5)) * ( -(DHf_Si4 + ACp_Si4
* (x[28] - Trif)+ BCp_Si4 /2.0 * ((x[28]**2.0) - (Trif**2.0)))+ (DHf_Sis + ACp_Sis
* (x[28] - Trif) + BCp_Sis /2.0 * ((x[28]**2.0) - (Trif**2.0))) + 2.0*(DHf_H2 +
ACp_H2 * (x[28] - Trif)+ BCp_H2 /2.0 * ((x[28]**2.0) - (Trif**2.0)))))/(roMol_Sis
* pi * L * ((((V0_b + x[26] * V / roMol_Sis)/(L * pi))**0.5)**2.0))

rhs[29] = sqrt(3.0)*u[0]*((pi*(((V0_b + x[26] * V / roMol_Sis)/(L * pi))**0.5)**2.0))


    """ Solving Problem with +sigma on the parameter KE_Sis1"""
kE_Sis1 = kE_Sis + sigmaElec

D_H2 = 1.276e-4 *((x[37]/300.0)**1.68)
D_Si4 = 0.58e-4 *((x[37]/300.0)**1.8)
D_Si2 = 0.59e-4 *((x[37]/300.0)**1.8)

kc_H2 = Nu*D_H2/H
kc_Si4 = Nu*D_Si4/H
kc_Si2 = Nu*D_Si2/H
```

```
kt = 1.3e-2 + 3.45e-2 * x[37] / 300.0 - 2.9e-3*((x[37]/300.0)**2.0)
hlim = Nu * kt / H
hlim_J = hlim * 4.186
k_gas = 2.7e14*exp(-57000.0/(R_cal*x[37]))

rhs[30] = MolIN * x0_Si4 / V - W * x[30] / V - kc_Si4 * (2.0 * L * pi * (((V0_b +
x[36] * V / roMol_Sis)/(L * pi))**0.5)) * (x[30] - x[31]) / V - k_gas * x[30]

rhs[31] = kc_Si4 * (2.0 * L * pi * (((V0_b + x[36] * V / roMol_Sis)/(L * pi))**0.5))*
(x[30] - x[31]) / V - k_sup2 * (2.0 * L * pi * (((V0_b + x[36] * V / roMol_Sis)/(L *
pi))**0.5)) * x[31] / V

rhs[32] = MolIN * x0_Si2 / V - W * x[32] / V - kc_Si2 * (2.0 * L * pi * (((V0_b +
x[36] * V / roMol_Sis)/(L * pi))**0.5)) * (x[32] - x[33]) / V + k_gas * x[30]

rhs[33] = kc_Si2 * (2.0 * L * pi * (((V0_b + x[36] * V / roMol_Sis)/(L * pi))**0.5))
* (x[32] - x[33]) / V - k_sup1 * (2.0 * L * pi * (((V0_b + x[36] * V / roMol_Sis)/(L
* pi))**0.5)) * x[33] / V

rhs[34] = MolIN * x0_H2 / V - W * x[34] / V - kc_H2 * (2.0 * L * pi * (((V0_b +
x[36] * V / roMol_Sis)/(L * pi))**0.5)) * (x[34] - x[35]) / V + k_gas * x[30]

rhs[35] = kc_H2 * (2.0 * L * pi * (((V0_b + x[36] * V / roMol_Sis)/(L * pi))**0.5))
* (x[34] - x[35]) / V + k_sup1 * (2.0 * L * pi * (((V0_b + x[36] * V / roMol_Sis)/(L
* pi))**0.5)) * x[33] / V + 2.0 * k_sup2 * (2.0 * L * pi * (((V0_b + x[36] * V /
roMol_Sis)/(L * pi))**0.5)) * x[31] / V

rhs[36] = k_sup1 * (2.0 * L * pi * (((V0_b + x[36] * V / roMol_Sis)/(L * pi))**0.5))
* x[33] / V + k_sup2 * (2.0 * L * pi * (((V0_b + x[36] * V / roMol_Sis)/(L *
pi))**0.5)) * x[31] / V

rhs[37] = (MolIN * (x0_Si4 * (DHf_Si4 + ACp_Si4 * (Tin - Trif)+ BCp_Si4
/2.0 * ((Tin**2.0) - (Trif**2.0))) + x0_Si2 * (DHf_Si2 + ACp_Si2 * (Tin - Trif)+
BCp_Si2 /2.0 * ((Tin**2.0) - (Trif**2.0))) + x0_H2 * (DHf_H2 + ACp_H2 *
(Tin - Trif) + BCp_H2 /2 * ((Tin**2.0) - (Trif**2.0))))- W * (x[30] * (DHf_Si4
+ ACp_Si4 * (x[37] - Trif)+ BCp_Si4 /2.0 * ((x[37]**2.0) - (Trif**2.0)))+ x[32] *
(DHf_Si2 + ACp_Si2 * (x[37] - Trif)+ BCp_Si2 /2.0 * ((x[37]**2.0) - (Trif**2.0)))
+ x[34] * (DHf_H2 + ACp_H2 * (x[37] - Trif) + BCp_H2 /2.0 * ((x[37]**2.0)
- (Trif**2.0))))+ k_gas *x[30] * V * (- (DHf_Si4 + ACp_Si4 * (x[37] - Trif) +
BCp_Si4 /2.0 * ((x[37]**2.0) - (Trif**2.0)))+ (DHf_Si2 + ACp_Si2 * (x[37] -
Trif) + BCp_Si2 /2.0 * ((x[37]**2.0) - (Trif**2.0)))+ (DHf_H2 + ACp_H2 *
(x[37] - Trif) + BCp_H2 /2.0 * ((x[37]**2.0) - (Trif**2.0))))+ hlim * (2.0 * L *
pi * (((V0_b + x[36] * V / roMol_Sis)/(L * pi))**0.5)) * (x[38] -x[37]) + hlim *
Ar * (Tw - x[37]))/( x[30] * V * (ACp_Si4 + 2.0*BCp_Si4 * x[37]) + x[32] * V
* (ACp_Si2 + 2.0*BCp_Si2 * x[37])+ x[34] * V * (ACp_H2 + 2.0*BCp_H2 * x[37]))
```

```
rhs[38] = (- hlim * (2.0 * L * pi * (((V0_b + x[36] * V / roMol_Sis)/(L * pi))**0.5))
* (x[38] - x[37])- emiss * irr * (2.0 * L * pi * (((V0_b + x[36] * V / roMol_Sis)/(L *
pi))**0.5)) * ((x[38]**4.0) - Tw**4.0)+ kT_Sis * (2.0 * L * pi * (((V0_b + x[36] *
V / roMol_Sis)/(L * pi))**0.5)) * ((x[38] + ((u[0]**2.0) * ((((V0_b + x[36] * V /
roMol_Sis)/(L * pi))**0.5)**2.0) /(kE_Sis1 * 4.0 * kT_Sis))) - x[38]) / (((V0_b +
x[36] * V / roMol_Sis)/(L * pi))**0.5)+ k_sup1 *x[33] * (2.0 * L * pi * (((V0_b +
x[36] * V / roMol_Sis)/(L * pi))**0.5)) * ( - (DHf_Si2 + ACp_Si2 * (x[38] - Trif)+
BCp_Si2 /2.0 * ((x[38]**2.0) - (Trif**2.0)))+ (DHf_Sis + ACp_Sis * (x[38] - Trif)
+ BCp_Sis /2.0 * ((x[38]**2.0) - (Trif**2.0))) + (DHf_H2 + ACp_H2 * (x[38] -
Trif)+ BCp_H2 /2.0 * ((x[38]**2.0) - (Trif**2.0))))+ k_sup2 *x[31] * (2.0 * L * pi
* (((V0_b + x[36] * V / roMol_Sis)/(L * pi))**0.5)) * ( -(DHf_Si4 + ACp_Si4 *
(x[38] - Trif)+ BCp_Si4 /2.0 * ((x[38]**2.0) - (Trif**2.0)))+ (DHf_Sis + ACp_Sis
* (x[38] - Trif) + BCp_Sis /2.0 * ((x[38]**2.0) - (Trif**2.0))) + 2.0*(DHf_H2 +
ACp_H2 * (x[38] - Trif)+ BCp_H2 /2.0 * ((x[38]**2.0) - (Trif**2.0)))))/(roMol_Sis
* pi * L * ((((V0_b + x[36] * V / roMol_Sis)/(L * pi))**0.5)**2.0))

rhs[39] = sqrt(3.0)*u[0]*((pi*(((V0_b + x[36] * V / roMol_Sis)/(L * pi))**0.5)**2.0))


    """ Solving Problem with -sigma on the parameter kE_Sis1"""
kE_Sis2 = kE_Sis - sigmaElec

D_H2 = 1.276e-4 *((x[47]/300.0)**1.68)
D_Si4 = 0.58e-4 *((x[47]/300.0)**1.8)
D_Si2 = 0.59e-4 *((x[47]/300.0)**1.8)

kc_H2 = Nu*D_H2/H
kc_Si4 = Nu*D_Si4/H
kc_Si2 = Nu*D_Si2/H

kt = 1.3e-2 + 3.45e-2 * x[47] / 300.0 - 2.9e-3*((x[47]/300.0)**2.0)
hlim = Nu * kt / H
hlim_J = hlim * 4.186
k_gas = 2.7e14*exp(-57000.0/(R_cal*x[47]))

rhs[40] = MolIN * x0_Si4 / V - W * x[40] / V - kc_Si4 * (2.0 * L * pi * (((V0_b +
x[46] * V / roMol_Sis)/(L * pi))**0.5)) * (x[40] - x[41]) / V - k_gas * x[40]

rhs[41] = kc_Si4 * (2.0 * L * pi * (((V0_b + x[46] * V / roMol_Sis)/(L * pi))**0.5))*
(x[40] - x[41]) / V - k_sup2 * (2.0 * L * pi * (((V0_b + x[46] * V / roMol_Sis)/(L *
pi))**0.5)) * x[41] / V

rhs[42] = MolIN * x0_Si2 / V - W * x[42] / V - kc_Si2 * (2.0 * L * pi * (((V0_b +
x[46] * V / roMol_Sis)/(L * pi))**0.5)) * (x[42] - x[43]) / V + k_gas * x[40]
```

```
rhs[43] = kc_Si2 * (2.0 * L * pi * (((V0_b + x[46] * V / roMol_Sis)/(L * pi))**0.5))
* (x[42] - x[43]) / V - k_sup1 * (2.0 * L * pi * (((V0_b + x[46] * V / roMol_Sis)/(L
* pi))**0.5)) * x[43] / V

rhs[44] = MolIN * x0_H2 / V - W * x[44] / V - kc_H2 * (2.0 * L * pi * (((V0_b +
x[46] * V / roMol_Sis)/(L * pi))**0.5)) * (x[44] - x[45]) / V + k_gas * x[40]

rhs[45] = kc_H2 * (2.0 * L * pi * (((V0_b + x[46] * V / roMol_Sis)/(L * pi))**0.5))
* (x[44] - x[45]) / V + k_sup1 * (2.0 * L * pi * (((V0_b + x[46] * V / roMol_Sis)/(L
* pi))**0.5)) * x[43] / V + 2.0 * k_sup2 * (2.0 * L * pi * (((V0_b + x[46] * V /
roMol_Sis)/(L * pi))**0.5)) * x[41] / V

rhs[46] = k_sup1 * (2.0 * L * pi * (((V0_b + x[46] * V / roMol_Sis)/(L * pi))**0.5))
* x[43] / V + k_sup2 * (2.0 * L * pi * (((V0_b + x[46] * V / roMol_Sis)/(L *
pi))**0.5)) * x[41] / V

rhs[47] = (MolIN * (x0_Si4 * (DHf_Si4 + ACp_Si4 * (Tin - Trif)+ BCp_Si4
/2.0 * ((Tin**2.0) - (Trif**2.0))) + x0_Si2 * (DHf_Si2 + ACp_Si2 * (Tin - Trif)+
BCp_Si2 /2.0 * ((Tin**2.0) - (Trif**2.0))) + x0_H2 * (DHf_H2 + ACp_H2 *
(Tin - Trif) + BCp_H2 /2 * ((Tin**2.0) - (Trif**2.0))))- W * (x[40] * (DHf_Si4
+ ACp_Si4 * (x[47] - Trif)+ BCp_Si4 /2.0 * ((x[47]**2.0) - (Trif**2.0)))+ x[42] *
(DHf_Si2 + ACp_Si2 * (x[47] - Trif)+ BCp_Si2 /2.0 * ((x[47]**2.0) - (Trif**2.0)))
+ x[44] * (DHf_H2 + ACp_H2 * (x[47] - Trif) + BCp_H2 /2.0 * ((x[47]**2.0)
- (Trif**2.0))))+ k_gas *x[40] * V * (- (DHf_Si4 + ACp_Si4 * (x[47] - Trif) +
BCp_Si4 /2.0 * ((x[47]**2.0) - (Trif**2.0)))+ (DHf_Si2 + ACp_Si2 * (x[47] -
Trif) + BCp_Si2 /2.0 * ((x[47]**2.0) - (Trif**2.0)))+ (DHf_H2 + ACp_H2 *
(x[47] - Trif) + BCp_H2 /2.0 * ((x[47]**2.0) - (Trif**2.0))))+ hlim * (2.0 * L *
pi * (((V0_b + x[46] * V / roMol_Sis)/(L * pi))**0.5)) * (x[48] -x[47]) + hlim *
Ar * (Tw - x[47]))/( x[40] * V * (ACp_Si4 + 2.0*BCp_Si4 * x[47]) + x[42] * V
* (ACp_Si2 + 2.0*BCp_Si2 * x[47])+ x[44] * V * (ACp_H2 + 2.0*BCp_H2 * x[47]))

rhs[48] = (- hlim * (2.0 * L * pi * (((V0_b + x[46] * V / roMol_Sis)/(L * pi))**0.5))
* (x[48] - x[47])- emiss * irr * (2.0 * L * pi * (((V0_b + x[46] * V / roMol_Sis)/(L *
pi))**0.5)) * ((x[48]**4.0) - Tw**4.0)+ kT_Sis * (2.0 * L * pi * (((V0_b + x[46] *
V / roMol_Sis)/(L * pi))**0.5)) * ((x[48] + ((u[0]**2.0) * ((((V0_b + x[46] * V /
roMol_Sis)/(L * pi))**0.5)**2.0) /(kE_Sis2 * 4.0 * kT_Sis))) - x[48]) / (((V0_b +
x[46] * V / roMol_Sis)/(L * pi))**0.5)+ k_sup1 *x[43] * (2.0 * L * pi * (((V0_b +
x[46] * V / roMol_Sis)/(L * pi))**0.5)) * ( - (DHf_Si2 + ACp_Si2 * (x[48] - Trif)+
BCp_Si2 /2.0 * ((x[48]**2.0) - (Trif**2.0)))+ (DHf_Sis + ACp_Sis * (x[48] - Trif)
+ BCp_Sis /2.0 * ((x[48]**2.0) - (Trif**2.0))) + (DHf_H2 + ACp_H2 * (x[48] -
Trif)+ BCp_H2 /2.0 * ((x[48]**2.0) - (Trif**2.0))))+ k_sup2 *x[41] * (2.0 * L * pi
* (((V0_b + x[46] * V / roMol_Sis)/(L * pi))**0.5)) * ( -(DHf_Si4 + ACp_Si4 *
(x[48] - Trif)+ BCp_Si4 /2.0 * ((x[48]**2.0) - (Trif**2.0)))+ (DHf_Sis + ACp_Sis
* (x[48] - Trif) + BCp_Sis /2.0 * ((x[48]**2.0) - (Trif**2.0))) + 2.0*(DHf_H2 +
```

```
ACp_H2 * (x[48] - Trif)+ BCp_H2 /2.0 * ((x[48]**2.0) - (Trif**2.0))))))/(roMol_Sis
* pi * L * ((((V0_b + x[46] * V / roMol_Sis)/(L * pi))**0.5)**2.0))

rhs[49] = sqrt(3.0)*u[0]*((pi*(((V0_b + x[46] * V / roMol_Sis)/(L * pi))**0.5)**2.0))

prob.addOde(x,rhs)

    """ Estimates and Objective Functions"""
y=SXMatrix.zeros(10)
for i in range(10):
    y[i] = 1/(n+k) * (k*x[i]+0.5*(x[i+10]+x[i+20]+x[i+30]+x[i+40]))
y = prob.makeExpression(y)

    """VARIANCE-COVARIANCE MATRIX"""

b=SXMatrix.zeros(10)
for i in range(10):
    b[i]= 1/(n+k) * (k*(x[i] - y[i])**2.0 + 0.5*((x[i+10] - y[i])**2.0 + (x[i+20] -
    y[i])**2.0 + (x[i+30] - y[i])**2.0 + (x[i+40] - y[i])**2.0))
b= prob.makeExpression(b)

conf = 1.96
conf1=1.645
f1 = -(y[6](-1) -conf1*(b[6](-1)+1e-10)**0.5)
f2 = (y[9](-1) + conf1*(b[9](-1)+1e-14)**0.5)
prob.addMultipleObjectives([f2,f1])

    """ BOUNDARY CONDITIONS, use initial conditions calculated from startup.py
file for getting x8=1070.0"""

    prob.addConstraints(x(0),[
5.016209291550912308e-04, 5.698245086236564550e-04, 1.723672586852724800e-02,
3.946413278058101502e-06, 2.291656795666951751e+01, 2.208317211283525339e+01,
6.106553667907978905e-02, 9.563879759246448202e+02, 1.070000000000000000e+03,
1.039253327996013943e-01, # Energy cost

5.016209291550912308e-04, 5.698245086236564550e-04, 1.723672586852724800e-02,
3.946413278058101502e-06, 2.291656795666951751e+01, 2.208317211283525339e+01,
6.106553667907978905e-02, 9.563879759246448202e+02, 1.070000000000000000e+03,
1.039253327996013943e-01, # Energy cost

5.016209291550912308e-04, 5.698245086236564550e-04, 1.723672586852724800e-02,
3.946413278058101502e-06, 2.291656795666951751e+01, 2.208317211283525339e+01,
6.106553667907978905e-02, 9.563879759246448202e+02, 1.070000000000000000e+03,
1.039253327996013943e-01, # Energy cost
```

5.016209291550912308e-04, 5.698245086236564550e-04,1.723672586852724800e-02, 3.946413278058101502e-06, 2.291656795666951751e+01, 2.208317211283525339e+01, 6.106553667907978905e-02, 9.563879759246448202e+02, 1.070000000000000000e+03, 1.039253327996013943e-01, # Energy cost

5.016209291550912308e-04, 5.698245086236564550e-04, 1.723672586852724800e-02, 3.946413278058101502e-06, 2.291656795666951751e+01, 2.208317211283525339e+01, 6.106553667907978905e-02, 9.563879759246448202e+02, 1.070000000000000000e+03, 1.039253327996013943e-01]) # Energy cost

prob.addConstraints(x[8]('coll') + ((u[0]('coll')**2.0) * ((((V0_b + x[6]('coll') * V / roMol_Sis)/(L * pi))**0.5)**2.0) /(kE_Sis * 4.0 * (kT_Sis))),298.15,1687.0)

prob.addConstraints(x[18]('coll') + ((u[0]('coll')**2.0) * ((((V0_b + x[16]('coll') * V / roMol_Sis)/(L * pi))**0.5)**2.0) /(kE_Sis * 4.0 * (kT_Sis))),298.15,1687.0)

prob.addConstraints(x[28]('coll') + ((u[0]('coll')**2.0) * ((((V0_b + x[26]('coll') * V / roMol_Sis)/(L * pi))**0.5)**2.0) /(kE_Sis * 4.0 * (kT_Sis))),298.15,1687.0)

prob.addConstraints(x[38]('coll') + ((u[0]('coll')**2.0) * ((((V0_b + x[36]('coll') * V / roMol_Sis)/(L * pi))**0.5)**2.0) /(kE_Sis * 4.0 * (kT_Sis))),298.15,1687.0)

prob.addConstraints(x[48]('coll') + ((u[0]('coll')**2.0) * ((((V0_b + x[46]('coll') * V / roMol_Sis)/(L * pi))**0.5)**2.0) /(kE_Sis * 4.0 * (kT_Sis))),298.15,1687.0)

"""ADDITIONAL CONSTRAINTS (only with Variance-Covariance Matrix) """

"""Contraints on Tcore"""

prob.addConstraints((y[8]('coll')+conf*((b[8]('coll')+1e-10)**0.5)) + ((u[0]('coll')**2.0) * ((((V0_b + (y[6]('coll')+conf*((b[6]('coll')+1e-10)**0.5)) * V / roMol_Sis)/(L * pi))**0.5)**2.0) /(kE_Sis * 4.0 * (kT_Sis))),298.15,1687.0)

prob.addConstraints((y[8]('coll')-conf*((b[8]('coll')+1e-10)**0.5)) + ((u[0]('coll')**2.0) * ((((V0_b + (y[6]('coll')-conf*((b[6]('coll')+1e-10)**0.5)) * V / roMol_Sis)/(L * pi))**0.5)**2.0) /(kE_Sis * 4.0 * (kT_Sis))),298.15,1687.0)

""" Constraints on Tsurface"""

prob.addConstraints((y[8]('coll')+conf*((b[8]('coll')+1e-10)**0.5)),1065.15,1687.0)

prob.addConstraints((y[8]('coll')-conf*((b[8]('coll')+1e-10)**0.5)),1065.15,1687.0)

"""SOLVER"""

```
solver = Multiobjective(prob,printlevel=0, max_iter= 100000, warm=True,plotting=False)
xs1 = NP.loadtxt('2par/states_sigma2par_energy_10%_Volt2_1.645.txt')
us1 = NP.loadtxt('2par/control_sigma2par_energy_10%_Volt2_1.645.txt')
xs2 = NP.loadtxt('2par/states_sigma2par_radius_10%_Volt2_1.645.txt')
us2 = NP.loadtxt('2par/control_sigma2par_radius_10%_Volt2_1.645.txt')
solver.initializeAnchors([x,u],[[xs1,xs2],[us1,us2]])

print time.time()-t
solver.solve()
print time.time()-t
```

Bibliography

Bibliography

J. Andersson, J. Åkesson, and M. Diehl. CasADi – A Symbolic Package for Automatic Differentiation and Optimal Control. In Shaun Forth, Paul Hovland, Eric Phipps, Jean Utke, and Andrea Walther, editors, *Recent Advances in Algorithmic Differentiation*, volume 87 of *Lecture Notes in Computational Science and Engineering*, pages 297–307. Springer Berlin Heidelberg, 2012.

D.P. Bertsekas. *Dynamic Programming and Optimal Control*, volume 1. Athena Scientific, Belmont, Massachussetts, 2005.

L.T. Biegler. Solution of Dynamic Optimization Problems by Successive Quadratic Programmind and Orthogonal Collocation. *Computers & Chemical Engineering*, 8 (3-4):243–247, 1984.

H.G. Bock and K.J. Plitt. A multiple shooting algorithm for direct solution of optimal control problems. In *Proceedings of the 9th IFAC world congress, Budapest*. Pergamon Press, 1984.

A.F.B. Braga, S.P. Moreira, P.R. Zampieri, J.M.G. Bacchin, and P.R. Mei. New processes for the production of solar-grade polycristalline silicon: A review. *Solar Energy Materials and Solar Cells*, 92(4):418–424, 2008.

D. Claessens. Robust and multi-objective dynamic optimization of chemical reactors. Master of Science Thesis in Chemical Engineering, Chemical and biochemical process engineering. KULeuven, 2013.

I. Das and J.E. Dennis. A Closer Look at Drawbacks of Minimizing Weighted Sums of Objectives for Pareto Set Generation in Multicriteria Optimization Problem. *Structural Optimization*, 14(1):63–69, 1997.

I. Das and J.E. Dennis. Normal-Boundary Intersection: A new Method for Generating the Pareto Surface in NonLinear Multicriteria Optimization Problems. *SIAM Journal on Optimization*, 8(3):631–657, 1998.

G. del Coso, I. Tobías, C. Cañizo, and A. Luque. Temperture homogeneity of polysilicon rods in a Siemens reactor. *Journal of crystal growth*, 299(1):165–170, 2007.

G. del Coso, C. del Cañizo, and A. Luque. Radiative energy loss in a polysilicon CVD reactor. *Solar Energy Materials and Solar Cells*, 95(4):1042–1049, 2011.

M. Diehl. Script for Numerical Optimal Control Course ETH Zurich, Incomplete Draft, (retrieved in May 2014), 2011. URL `http://homes.esat.kuleuven.be/~mdiehl/NUMOPTICON/numopticon.pdf`.

M. Diehl. Numerical Optimal Control Slides, (retrieved in May 2014), 2012. URL `http://homes.esat.kuleuven.be/~mdiehl/AALBORG/OptimalControl.pdf`.

M. Diehl. Script for Numerical Optimization Course B-KUL-H03E3A, (retrieved in May 2014), 2013. URL `http://homes.esat.kuleuven.be/~mdiehl/NUMOPT/numopt.pdf`.

M. Diehl, H.G. Bock, H. Diedam, and P.B. Wieber. Fast direct multiple shooting algorithms for optimal robot control. In *Fast motions in biomechanics and robotics*, volume 340, pages 65–93. Springer, 2006.

J.F. Forbes. Model Structure and Adjustable Parameter Selection for Operation Optimization. Ph.D. Thesis, McMaster University of Hamilton, 1994.

R. Hannemann and W. Marquardt. Continuous and discrete composite adjoints for the Hessian of the Lagrangian in shooting algorithms for dynamic optimization. *SIAM Journal of Scientific Computing*, 31(6):4675–4695, 2010.

B. Houska and M. Diehl. Robust Nonlinear Optimal Control of Dynamic Systems with Affine Uncertanties. In *Decision and Control, 2009 held jointly with the 2009 28th Chinese Control Conference. CDC/CCC 2009. Proceedings of the 48th IEEE Conference on*, pages 2274–2279. IEEE, 2009.

B. Houska, H.J. Ferreau, and M. Diehl. ACADO Toolkit – An Open Source Framework for Automatic Control and Dynamic Optimization. *Optimal Control Applications and Methods*, 32(3):298–312, 2011.

B. Houska, F. Logist, J.F. Van Impe, and M. Diehl. Robust optimization of nonlinear dynamic systems with application to a jacketed tubular reactor. *Journal of Process Control*, 22(6):1152–1160, 2012.

S.J. Julier and J.K. Uhlmann. A General Method for Approximating Nonlinear Transformations of Probability Distributions. Technical report, Robotics Research Group, Department of Engineering Science, University of Oxford, 1996.

R.E. Kalman. Lyapunov functions for the problem of lur'e in automatic control. *Proceedings of the National Academy of Sciences of the United States of America*, 49(2):201–205, 1963.

D.B. Leineweber, I. Bauer, H.G. Bock, and J.P. Schlöder. An efficient multiple shooting based reduced SQP strategy for large-scale dynamic process optimization - Part I: Theoretical Aspects. *Computer & Chemical Engineering*, 27(2):157–166, 2003a.

D.B. Leineweber, A. Schafer, H.G. Bock, and J.P. Schlöder. An efficient multiple shooting based reduced SQP strategy for large-scale dynamic process optimization - Part II: Software aspects and applications. *Computer & Chemical Engineering*, 27(2):167–174, 2003b.

F. Logist and J. Van Impe. Dynamic Optimisation / Optimal Control in the (bio)chemical indusrty, B-KUL-H06H0A Process Control in the Chemical Industry, Lecture 9, 2013.

F. Logist, P.M.M. Van Erdeghem, and J.F. Van Impe. Efficient deterministic multiple objective optimal control of (bio)chemical processes. *Chemical Engineering Science*, 64(11):2527–2538, 2009.

F. Logist, B. Houska, M. Diehl, and J.F. Van Impe. Robust multi-objective optimal control of uncertain (bio)chemical processes. *Chemical Engineering Science*, 66 (20):4670–4682, 2011.

F. Logist, M. Vallerio, B. Houska, M. Diehl, and J. Van Impe. Multi-objective optimal control of chemical processes using ACADO toolkit. *Computers & Chemical Engineering*, 37:191–199, 2012.

D.L. Ma and R.D. Braatz. Worst-Case Analysis of Finite-Time Control Policies. *Control Systems Technology, IEEE Transaction on*, 9(5):766–774, 2001.

F. Manenti, F. Logist, and J. Van Impe. Optimal Control - Industrial Applications, B-KUL-H06H0A Process Control in the Chemical Industry, 2013.

Market report 2013. EPIA - European Photovoltaic Industry Association. (retrieved in May 2014), 2014. URL `http://www.epia.org/news/publications/`.

M. Masi, V. Bertani, C. Cavallotti, and S. Carrà. Towards a multiscale approach to the growth of silicon films by chemical vapor deposition. *Materials chemistry and physics*, 66(2):229–235, 2000.

L. Masson, M. Latour, M. Rekinger, I.T. Theologitis, and M. Papoutsi. Global Market Outlook For Photovoltaics 2013 - 2017. EPIA - European Photovoltaic Industry Association, (retrieved in May 2014), 2013. URL `http://www.epia.org/news/publications/`.

A. Messac, A. Ismail-Yahaya, and C.A. Mattson. The normalized normal constraint method for generating the pareto frontier. *Structural and Multidisciplinary Optimization*, 25(2):86–98, 2003.

K.M. Miettinen. *Nonlinear Multiobjective Optimization*, volume 12. Springer, 1999.

A. Ramos, C. del Cañizo, J. Valdehita, J.C. Zamorano, and A. Luque. Radiation heat savings in polysilicon production: Validationof results through a CVD laboratory prototype. *Journal of crystal growth*, 374:5–10, 2013.

S. Recker, P. Kühl, M. Diehl, and H.G. Bock. Sigmapoint approach for robust optimization of nonlinear dynamic systems. In *Proceedings of the SIMULTECH 2012. 2nd International Conference on Simulation and Modeling Methodologies, Technologies and Applications*, pages 199–207, 2012.

J. Sanchis, M. Martinez, X. Blasco, and J.V. Salcedo. A new perspective on multiobjective optimization by enhanced normalized normal constraint method. *Structural and multidisciplinary optimization*, 36(5):537–546, 2008.

R.W.H. Sargent. Optimal control. *Journal of Computational and Applied Mathematics*, 124(1):361–371, 2000.

R.W.H. Sargent and G.R. Sullivan. The development of an efficient optimal control package. In *Optimization Techniques*, pages 158–168. Springer, 1978.

P. Schavemaker and L. van der Sluis. *Electrical power system essentials*. John Wiley and Sons, 2008.

solarbuzz. Technologies, (retrieved in may 2014), 2014. URL `http://www.solarbuzz.com/going-solar/understanding/technologies`.

B. Srinivasan, D. Bonvin, E. Visser, and S. Palanki. Dynamic optimization of batch processes: Role of measurements in handling uncertainty. *Computers & Chemical Engineering*, 27(1):27–44, 2003.

H.J. Sussmann and J.C. Willems. 300 Years of Optimal Control: From the Brachystochrone to the Maximum Principle. *Control Systems IEEE*, 17(3):32–44, 1997.

D. Telen, M. Vallerio, L. Cabianca, B. Houska, F. Logist, and J. Van Impe. Computation strategies for approximate robust optimal control of nonlinear dynamic systems under parametric uncertainty and process noise. *Submitted to Journal of Process Control*, July 2014.

M. Vallerio, D. Claessens, F. Logist, and J. Van Impe. Multi-objective and Robut Optimal Control of a CVD Reactor for Polysilicon Production. In J.J. Klemeš, P.S. Varbanov, and Y.L. Liew, editors, *Proc. of the 24th European Symposium on Computer Aided Process Engineering*, 2014.

M. Vallerio, D. Telen, L. Cabianca, D. Claessens, F. Manenti, J. Van Impe, and F. Logist. Robust multi-objective optimal control of a chemical vapor deposition reactor for polysilicon production. *Submitted to AIChe Journal*, July 2014.

V.S. Vassiliadis, R.W.H. Sargent, and C.C. Pantelides. Solution of a class of multistage dynamic optimization problems. 1. problems without path constraints. *Industrial & Engineering Chemistry Research*, 33(9):2111–2122, 1994a.

V.S. Vassiliadis, R.W.H. Sargent, and C.C. Pantelides. Solution of a class of multistage dynamic optimization problems. 2. problems with path constraints. *Industrial & Engineering Chemistry Research*, 33(9):2123–2133, 1994b.

L. Viganò, M. Vallerio, F. Manenti, N.M.N. Lima, N. Zuñiga Liñan, and G. Manenti. Model predictive control of a CVD reactor for production of polysilicon rods. In *Chemical Engineering Transactions*, volume 21, pages 523–528, 2010.

VREMCO. Voltage and power plugs in belgium, (retrieved in may 2014), 2014. URL `http://www.vremco.com/vol_pow_eng.htm`.

A. Wächter and L.T. Biegler. On the Implementation of a Primal Dual Interior Point Filter Line Search Algorithm for Large Scale Nonlinear Programming. *Mathematical Programming*, 106(1):25–57, 2006.

B.M. Weedy and B.J. Cory. *Electric Power Systems*. John Wiley and Sons, 2004.

W.L.M. Weerts, M.H.J.M. De Croon, and G.B. Marin. The kinetics of the low-pressure chemical vapor deposition of polycrystalline silicon from silane. *Journal of the Electrochemical Society*, 145(4):1318–1330, 1998.

T.J. Williams and R.E. Otto. A generalized chemical processing model for the investigation of computer control. *American Institute of Electrical Engineers, Part I: Communication and Electronics, Transactions of the*, 79(5):458–473, 1960.